CHAPTER: 6 Appendices

During the course of my PhD work, I have written one review article as a lead author on *C. auris* and also contributed to several other publications as a co-author. However, although the topics of those publications may not be directly aligned with the main themes of my thesis, I believe that they are strongly related and have consequently decided that inclusion of the six publications in the Appendix to this thesis would be appropriate. My contribution to these papers lay therein that I performed all *in vitro* biological studies and was also involved in the write-up of the articles. The goal of these studies was to evaluate the antifungal activity and mechanism of the antifungal action of different series of newly synthesised compounds against different *C. albicans* strains. The six publications are listed below and the full articles have also been included.

Appendix 1: Publications

1. **Lone SA**, Ahmad A. *Candida auris* – the growing menace to global health. Mycoses, 2019; 62(8):620-637. doi: 10.1111/myc.12904.
2. Malik MA, **Lone SA,** Wani MY, Talukdar IA, Dar OA, Ahmad A, Hashmi AA. S-benzyldithiocarbazate imine coordinated metal complexes kill *Candida albicans* by causing cellular apoptosis and necrosis. Bioorganic Chemistry, 2020;98:103771. doi: 10.1016/j.bioorg.2020.103771.
3. Dar OA, **Lone SA**, Malik MA, Aqlan FM, Wani MY, Hashmi AA, Ahmad A. Synthesis and synergistic studies of isatin based mixed ligand complexes as potential antifungal therapeutic agents. Heliyon, 2019;5(7):e02055. doi: 10.1016/j.heliyon.2019.e02055.
4. Dar OA, **Lone SA,** Malik MA, Wani MY, Hashmi AA, Ahmad A. Heteroleptic transition metal complexes of Schiff-base derived ligands exert their antifungal activity by disrupting membrane integrity. Applied Organometallic Chemistry, 2019; 33: e5128. doi.org/10.1002/aoc.5128.
5. Dar OA, **Lone SA,** Malik MA, Wani MY, Ahmad A, Hashmi AA. New transition metal complexes with a pendent indole ring: insights into the antifungal activity and mode of action. RSC Advances, 2019; 9, 15151-15157. doi.org/10.1039/C9RA02600B.
6. Malik MA, **Lone SA**, Gull P, Dar OA, Wani MY, Ahmad A, Hashmi AA. Efficacy of novel Schiff base derivatives as antifungal compounds in combination with approved drugs against *Candida albicans*. Medicinal Chemistry, 2019;15(6):648-658. doi: 10.2174/1573406415666181203115957.

Received: 28 December 2018 | Revised: 7 February 2019 | Accepted: 12 February 2019

DOI: 10.1111/myc.12904

REVIEW ARTICLE

mycoses Diagnosis, Therapy and Prophylaxis of Fungal Diseases WILEY

Candida auris—the growing menace to global health

Shabir A. Lone[1] | **Aijaz Ahmad**[1,2]

[1]Clinical Microbiology and Infectious Diseases, Faculty of Health Sciences, School of Pathology, University of the Witwatersrand, Johannesburg, South Africa

[2]Infection Control, National Health Laboratory Service, Charlotte Maxeke Johannesburg Academic Hospital, Johannesburg, South Africa

Correspondence
Aijaz Ahmad, Clinical Microbiology and Infectious Diseases, Faculty of Health Sciences, School of Pathology, University of the Witwatersrand, Johannesburg, South Africa.
Emails: Aijaz.Ahmad@wits.ac.za; Aijaz.Ahmad@nhls.ac.za

Funding information
South African Agency for Science and Technology Advancement, Grant/Award Number: RDYR180418322304; 116339; University of the Witwatersrand, Johannesburg, Grant/Award Number: 1311748

Summary

A paradigm shift of candidiasis from *Candida albicans* to non-albicans *Candida* species has fundamentally increased with the advent of *C. auris*. *C. auris*, despite being a newly emerged multidrug-resistant fungal pathogen, is associated with severe invasive infections and outbreaks with high mortality rates. Initially reported from Japan in 2009, *C. auris* have now been found in different countries on all the continents except Antarctica. Due to its capability of nosocomial transmission and forming adherent biofilms on clinically important substrates, a high number of related hospital outbreaks have been reported worldwide. As *C. auris* is a multidrug-resistant pathogen and is prone to misidentification by available conventional methods, it becomes difficult to detect and manage *C. auris* infection and also limits the therapeutic options against this deadly pathogen. The emergence of multidrug-resistant *C. auris* advocates and amplifies the vigilance of early diagnosis and appropriate treatment of fungal infections. In this review, we discussed the nine-year-old history of *C. auris*—its trends in global emergence, epidemiological relatedness, isolation, mortality, associated risk factors, virulence factors, drug resistance and susceptibility testing, diagnostic challenges, microbiological characteristics, therapeutic options and infection prevention and control associated with this pathogen.

KEYWORDS
Candida auris, candidemia, epidemiology, multidrug resistance

1 | INTRODUCTION

With ever increasing microbial drug resistance and emergence of new multidrug-resistant (MDR) species, clinicians and microbiologists are battling to control the associated morbidity and mortality rates. Among new MDR species, *C. auris* is an emerging fungal pathogen that causes severe invasive infections, with a crude mortality ranging from 30% to 72%.[1-5] *C. auris* is first isolated and described from an ear canal discharge of a patient in Japan in year 2009[6], and since then it was isolated from the 6 continents of the world.[7] After its description in 2009, first associated invasive infection was recognised from three patients in South Korea in 2011.[8] In comparison with other *Candida* species, which are thought to cause sporadic infection, *C. auris* exhibit a capability for nosocomial transmission.[9] As a result, significant clonal hospital outbreaks were reported from India, Pakistan, Colombia, Panama, Venezuela, United States, South Africa, Spain and United Kingdom.[10,50]

By 2018, cases of *C. auris* infections become widespread across the globe and had been reported from South Korea[8,11], India[12,13], Pakistan[3], Bangladesh[9], Israel[14], Kuwait[15], Oman[16,17], Malaysia[18], China[19], United Arab Emirates[20], Saudi Arabia[21], Iran[22], Singapore[23], Thailand[7], South Africa[3,24], Kenya[25], Spain[26,27], Germany[27], France[27], Austria[28], Norway[27], Belgium[29], United Kingdom[30,31], Switzerland[32], Netherlands[7], Russia[33], USA[34,35], Canada[36], Panama[37], Colombia[38], Venezuela[39] and Australia.[40] It is anticipated that *C. auris* has emerged in other countries also but has remained undetected due to its phenotypical resemblance with *Candida haemulonii*, *Candida famata*, *Candida sake*, *Saccharomyces cerevisiae* and *Rhodotorula glutinis* and is frequently misidentified by commercially available identification systems, such as Vitek-2,

API20 C-AUX and Auxacolor.[41-43] To avoid misidentification of *C. auris* more sophisticated methods, such as Matrix-assisted laser desorption/ionisation-time-of-flight mass spectrometry (MALDI-TOF MS) or molecular identification based on sequencing the internal transcribed spacer (ITS) or D1/D2 region of the 28s ribosomal DNA are used.[41-46] Recently, T2 Biosystems (Lexington, MA) developed a new rapid diagnostic T2 assay specific for the detection of *C. auris*.[47] In addition, early diagnosis of *C. auris* can initiate early and appropriate treatment therapy, which can significantly reduce the mortality rates associated with this pathogen.

The prevalence of *C. auris* and other non-albicans MDR *Candida* species was thought to be over increasing due to the misuse of currently available antifungal drugs with special emphasis on fungistatic drugs, such as fluconazole. On these basis, Antimicrobial Stewardship has been employed which clearly determines the MIC breakpoints to distinguish susceptible and resistant isolates. Despite there is lack of concrete guidelines for these MIC breakpoints in *C. auris* isolates, current distribution is based on previously used Clinical and Laboratory Standards Institute (CLSI) and/or European Committee for Antimicrobial Susceptibility Testing (EUCAST) guidelines set for other *Candida* species. The Centers for Disease Control and Prevention (CDC) and other research groups have already stated high resistance of *C. auris* against fluconazole and variable susceptibility to other azoles.[3,41,48] In addition, *C. auris* has been reported to be resistant to polyenes (approximately 50%), echinocandins (5%-10%) and nearly 50% exhibited simultaneous resistance to two classes of antifungals (azoles and polyenes).[3,41,48] Some strains of *C. auris*, unlike other species of *Candida*, demonstrated higher MICs to all three major classes of antifungal drugs (azoles, echinocandins and polyenes)[3,41,48], and thereby indicating limited treatment options against these multidrug-resistant strains.

Candida auris has been recognised as globally emerging multidrug-resistant fungal pathogen. In June 2016, CDC issued clinical alert to healthcare facilities and provided interim guidelines for clinical management, laboratory testing and infection control. Similarly, World Health Organization (WHO), Pan American Health Organization (PAHO) and South African National Institute of Communicable Diseases (NICD) also issued similar epidemiological alert in 2016.[49,50]

1.1 | Aim of the review article

Given several uncertainties related to *C. auris*, we aim to summarise and provide comprehensive update of *C. auris* published reports available to date. The review covers all important aspects of the pathogen including epidemiology, epidemiological relatedness, healthcare-associated outbreaks, clinical presentation, mortality, risk factors, pathophysiology, drug resistance and susceptibility testing, identification, microbiological characteristics, therapeutic options and infection prevention and control. Therefore, it is anticipated that this review is an excellent critique of all reported findings on this newly emerged fungal pathogen available to date.

1.2 | Study selection

We comprehensively searched and reviewed published work on *C. auris* between January 2009 to November 2018 using the most popular scientific search engines such as PubMed, Scopus and ScienceDirect. Besides these searches, we also consider the reports and updates on *C. auris* from CDC, WHO, Public Health England (PHE), NICD and the European Centres for Disease Control and Prevention (ECDC). The search words "*C. auris*" and "*Candida auris*" were used and all the publications in non-English languages and non- *C. auris* were excluded. The search was performed in duplicate by different individuals for the reproducibility. After deduplication and exclusion, 182 peer-reviewed published articles, case studies, reports and updates from CDC, PHE, WHO, NICD and ECDC up to November 2018 were included. The results were systematically grouped and presented in this review.

2 | GLOBAL EPIDEMIOLOGY AND HEALTHCARE-ASSOCIATED OUTBREAKS

The global prevalence of *C. auris* and the actual frequency of its infection are obscure. This uncertainty is related to its phenotypical resemblance with other *Candida* species and the failure of commercially available diagnostic methods for its early detection, which results in misidentification and that would underestimate the number of *C. auris* cases.[51] In a recent survey conducted by International Antifungal Surveillance Program SENTRY (JMI Laboratories), 15,271 *Candida* isolates collected from 2004 to 2015 in 152 international medical centres in different countries (Asia 41, Europe 50, Latin America 15 and North America 46) were re-tested using DNA sequencing and/or MALDI-TOF. Of all the tested isolates, only 4 isolates were re-identified as *C. auris* (2009, 2013, 2014 and 2015); however, no *C. auris* isolate was detected before 2009. Therefore, it is believed that the prevalence of *C. auris* was very rare before 2009.[3,52] In contradiction, one of the reports by Lee et al[8] a misidentified *Candida* species recovered in 1996 in South Korea was later identified as *C. auris* by molecular identification and this is so far the earliest known *C. auris* strain. In different surveillance studies in five hospitals of South Korea for the *Candida* isolates recovered between 2004 and 2006 and from Pakistan in 2008; misidentified and undetected *Candida* species were later detected as *C. auris*.[3,11] These historical isolates suggest the emergence of *C. auris* before 2009; however, rapid global emergence of *C. auris* has only been reported since 2009.

Candida auris infections are mostly involved in hospitalised patients, which depicts its emergence as an important nosocomial pathogen with significant potential of colonel transmission within hospitals.[42,53,54] The infection usually occurs few weeks posthospital admission with high mortality rates.[55] So far, healthcare-associated outbreaks of *C. auris* have been reported in numerous countries involving six of seven continents, which are briefly described below:

2.1 | Asia

Asia, being the mother of *C. auris*, has been detected in as many as 15 countries in this continent. After confirmation of *C. auris* invasive infection from South Korea in 2011[8], an outbreak from a hospital in India was reported with 15 *C. auris* isolates recovered from 15 different patients. Among these 15 isolates, 13 were earlier reported as *C. haemulonii* but were re-confirmed as *C. auris* by sequencing.[12,13,56] Subsequently, cases of *C. auris* infection from North and South Indian healthcare centres have been reported.[12,13,44,56,57] According to the national survey of ICUs in India, *C. auris* accounted for > 5% of candidemia; however, these figures go up to 30% at individual hospitals.[12,58] In a recent study on 114 *Candida* isolates collected from 2012 to 2017 from the candidemia patients in 165—bedded trauma centre in Delhi, India, 20 isolates (17.5%) were re-identified as *C. auris*. Of these 20 isolates, 15 were misidentified as *C. haemulonii* and 5 as other species. With these figures, *C. auris* was reported as the second most dominant species causing candidemia in these patients.[59]

In 2015, an outbreak in a hospital in Pakistan has been reported where the causative organism was initially reported as *Saccharomyces cerevisiae*; however, later CDC re-confirmed these isolates as *C. auris*.[3] This was the first reporting of *C. auris* cases from Pakistan and after that increased number of cases were reported from this country.

In China, the first reported case of *C. auris* infection is in 2018, isolated from the bronchoalveolar lavage fluid of a 76-year-old hospitalised women with hypertension and nephritic syndrome.[19] Simultaneously, another study reported 35 *C. auris* isolates from 15 patients from a hospital in Shenyang, China. These isolates were collected between January 2011 to October 2017 and were initially misidentified as *C. haemulonii* by Vitek but were later confirmed as *C. auris*.[60] In a recent study by Yong and his co-workers, two new cases of *C. auris* fungemia with different antifungal resistance profiles were detected from a neonatal ICU in Beijing.[61]

Although *C. auris* has been previously identified in Korea, a new case study has reported the role of *C. auris* in causing otomastoiditis.[62] In Singapore, identification of first 3 cases of *C. auris* infection in three different patients from a tertiary care hospital is recently reported.[23]

The first report of *C. auris* involved in mixed candidemia with *C. tropicalis* have been reported from Malaysia in 2018 from the blood of 63-year-old neutropenic patient.[18]

In Israel, six patients suffering from candidemia caused by *C. auris* have been reported from two hospitals in Tel Aviv.[14] These isolates were collected in a gape of one year between May 2014 and April 2015. Phylogenetic analysis based on ITS and LSU sequences showed that these collected isolates are distinct from *C. auris* isolates of East Asia, Africa and Middle East. However, in a different report travel-associated infection of *C. auris* has also been reported from Israel, where *C. auris* was isolated from a 25-year-old man transferred from South Africa with some medical conditions. Upon phylogenetic analysis, the isolate exhibits similitude to South African clade and not with Israeli clade of *C. auris*.[63]

In Kuwait, first case of *C. auris* candidemia was reported in 27-year-old women in May 2014 who was admitted to ICU for chronic renal failure.[15] A comprehensive study on emergence of *C. auris* from Kuwait on 280 clinical yeast isolates (based on the formation of pink-coloured colonies on CHROMagar *Candida*), collected between May 2014 and September 2017, reported that 158 isolates were identified and confirmed as *C. auris* from 56 patients of different clinical specimen.[64] All 158 isolates were initially misidentified as *C. haemulonii* by Vitek-2, but were re-confirmed as *C. auris* by species-specific PCR and PCR sequencing of ITS region of rDNA. In another report by Khan et al[65] invasive cases of *C. auris* including 13 cases of candidemia and four cases of other invasive infections in six different hospitals across Kuwait were reported during 2015 to 2017.

In Oman, two different studies concurrently reported separate *C. auris* fungemia cases from two different hospitals in the year 2017.[16,17] One study reported two cases of *C. auris* candidemia from two patients in a tertiary care hospital in the city of Muscat.[16] In another study, five cases of candidemia caused by *C. auris* at Sultan Qaboos University Hospital Oman, have been reported.[17] All the isolates were detected between August 2015 to February 2017 and were initially misidentified as *C. haemulonii*, but were later confirmed as *C. auris*.[1]

The first case of *C. auris* from United Arab Emirates has been recently reported in 2018 from its capital city Abu Dhabi, when this pathogen was isolated from the blood of an 84-year-old female patient with persistent candidemia.[20]

In Saudi Arabia, first three cases of *C. auris* infection have also been recently reported from two hospitals between December 2017 and February 2018. Initially, these isolates were misidentified as *C. haemulonii*, but later with the help of MALDI-TOF MS all the three isolates were confirmed as *C. auris*. Whole genome sequencing of these isolates revealed that these strains belong to the South Asian Clade.[21]

A case report recently published in Mycoses reported the first case of *C. auris* from Iran isolated from a 14-year-old female with otomycosis.[22]

2.2 | Africa

With the tropical climate of African continent and due to global warming, increasing number of immunocompromised patients and haphazard development, Africa is known as Infectious Disease continent. Surprisingly, so far *C. auris* infections have only been reported from 2 countries in the whole continent. In a recent South Africa national laboratory-based surveillance programme, the earliest confirmed case of *C. auris* infection from South Africa was in 2009.[50] This isolate was initially misidentified as *C. haemulonii*, but later in 2014 was confirmed as *C. auris*. According to this surveillance report, 1692 confirmed or probable cases of *C. auris* have been identified during a period of October 2012 to November 2016 at both public and private hospitals countrywide; however, most of the cases are in private

hospitals in Gauteng Province. Magobo et al[24] detected 4 cases of *C. auris* candidemia in South Africa between October 2012 through October 2013. Subsequently, 10 more isolates were reported in 2017 which were collected between 2012 and 2014.[3] South Africa also witnessed the outbreaks of *C. auris* infections in 2016 from different hospitals, with most cases reported in Johannesburg and Pretoria hospitals. In the same year, *C. auris* was reported as second and fourth most common cause of candidemia in South African private and public-sector hospitals, respectively. By now, *C. auris* accounts for ≈ 1 of every 10 cases of candidemia in South Africa and has now been isolated from ≥ 94 hospitals across the country.[50]

In Kenya, from a single-centre study between September 2010 and June 2013, candidemia attributed to 39% of nosocomial infections, and the most common cause was *C. haemulonii* later re-identified as *C. auris* accounting for 45 (38%) episodes followed by *C. albicans* (27%).[25]

2.3 | Europe

With the global spread of *C. auris* infection, ECDC conducted a survey in the European Union and European Economic Area countries (EU/EEA) on reported cases of *C. auris* and laboratory capacity for *C. auris* detection. This study reported a total of 620 cases of *C. auris* from six different countries [Spain (n = 388), UK (n = 221), Germany (n = 7), France (n = 2), Belgium (n = 1) and Norway (n = 1)] in a period from 2013 to 2017, including four nosocomial outbreaks in Spain and UK.[27] The first case of fungemia by *C. auris* in continental Europe occurred in Spain among four patients, hospitalised in the surgical intensive care unit between April and June 2016.[26] The same group in a separate study reported an outbreak in a Spanish National Public Health Service Hospital during April 2016-January 2017, where all the isolates were reported to have a genotypical connection with South African clade.[5] In another recent study, a single case of *C. auris* was reported from Austria in January 2018, from a 22-year-old man with an infection of external auditory canal.[28] In Switzerland, the first case of *C. auris* has been isolated from tracheal aspirates in a 74-year-old female patient with acute respiratory distress syndrome repatriated from a Spanish hospital.[32] A female patient referred from Kuwait developed a catheter-related fungemia with *C. auris* and was reported as the first case of *C. auris* infection from Belgium.[29]

In England, sporadic cases of *C. auris* infection have been identified since August 2013. The first outbreak of *C. auris* infection in England was reported in Royal Brompton Hospital, a London cardiothoracic centre, between April 2015 and July 2016. In this outbreak, fifty cases of *C. auris* infection were identified.[66] Another outbreak of *C. auris* has been reported from the United Kingdom in neurosciences intensive care unit of the Oxford University Hospitals between February 2015 and August 2017.[67] In this outbreak, a total of 70 patients have been identified as coloniser or infected with the *C. auris*. The whole genome sequencing analysis of these strains confirmed that all these isolates formed a single genetic cluster related to the *C. auris* South African clade.[67] The results from this study also concluded that reusable patient equipment including multiple axillary skin-surface temperature probes may serve as a source of hospital outbreaks.

2.4 | South America

Between March 2012 and July 2013, first *C. auris* outbreak in South America was reported in an ICU of tertiary care hospital in Maracaibo, Venezuela.[39] All these isolates were only confirmed as *C. auris* by sequencing after being initially misidentified as *C. haemulonii*. During this period, *C. auris* were reported as the sixth most common cause of fungemia in tertiary medical centre in Venezuela.[39]

Since 2012, sporadic cases of *C. auris* infection have been reported from various cities of Colombia.[38,68,69] In 2016, an outbreak by *C. auris* was reported in a paediatric intensive care unit in Cartagena, and five cases of disseminated *C. auris* infection were reported. These isolates were previously identified as *C. albicans*, *C. guillermondii* and *Rhodotorula rubra*.[49] Colombian Instituto Nacional de Salud (INS) Surveillance Programme for *C. auris*, recently confirmed and reported 123 *C. auris* cases in Colombia, during February 2015-May 2017. Most of these isolates were previously misidentified and reported as *C. haemulonii* while as confirmed as *C. auris* upon reidentification by MALDI-TOF.[69]

2.5 | North America

In North America, the first seven cases of *C. auris* infection were detected in USA occurring during May 2013-August 2016 (one in 2013, one in 2015 and five in 2016). Six of seven cases were identified through retrospective review of microbiology records from reporting hospitals and reference laboratories.[34] As of 30 November 2018, 493 confirmed and 30 probable cases of *C. auris* infection in the USA have been reported by CDC (CDC 2018). Most of the *C. auris* cases in USA have been reported from the New York City (n = 265), New Jersey (n = 99) and Chicago (n = 108). In a separate report, it has been observed that most of the *C. auris* strains in the USA have been linked to other countries of the world.[70] A molecular epidemiological survey used WGS on 133 *C. auris* cases (73 clinical and 60 screening cases) collected from the ten US states between May 2013 and August 2017. In this survey, it has been reported that all the isolates from the USA were genetically related to one of the four major clades (South America, Africa, East Asian and South Asian), suggesting *C. auris* have been introduced several times in to the USA.[71]

In May 2017, first case of multidrug-resistant *C. auris* has been reported in Canada.[36] In Central America, 14 isolates of *C. auris* from nine hospitalised patients were reported in a hospital in Panama City, Panama.[37] These isolates initially identified as *C. haemulonii* by Vitek-2 automated system were later confirmed as *C. auris* by molecular methods.

2.6 | Australia

Australian continent is the latest to join the list of other continents where *C. auris* infections have been detected. Until the end of 2018, no published data of *C. auris* infection in this continent were

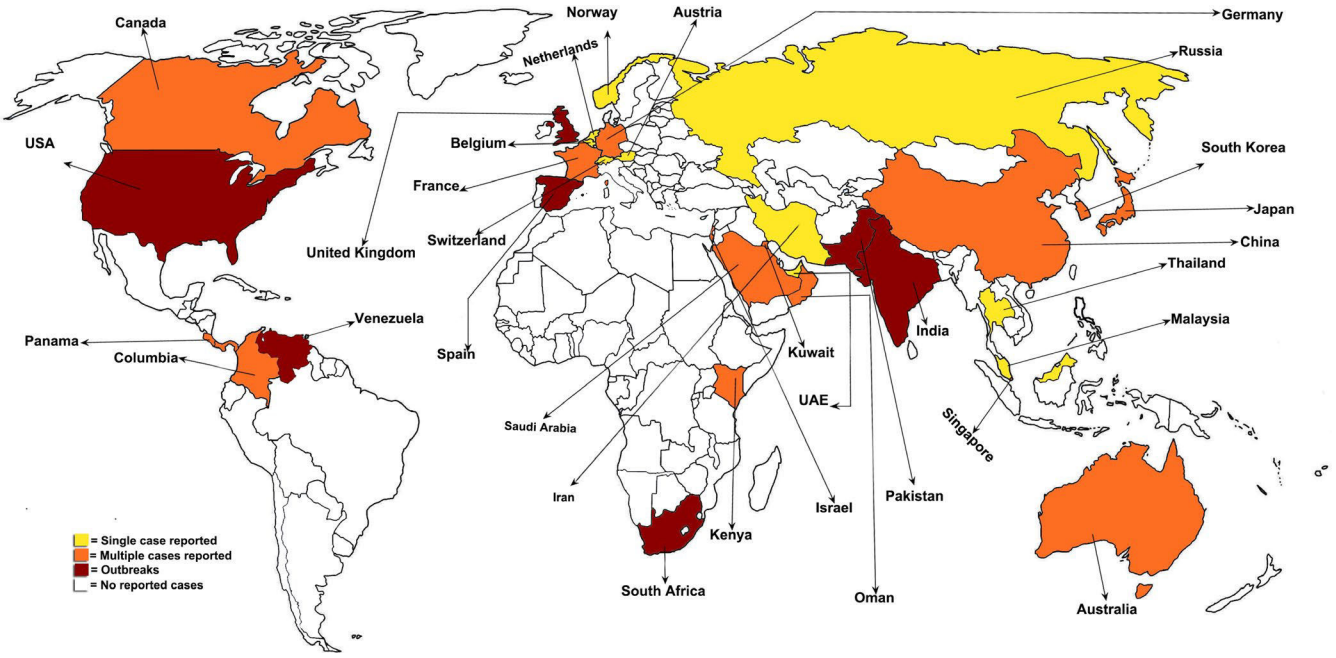

FIGURE 1 Global distribution of *Candida auris* from 2009 to 2018 in 6 continents. Different colour coding highlights single case, multiple cases and outbreaks

reported. However, in a recent report by Heath et al, travel-associated case of *C. auris* infection has been reported from Australia in a 65-year-old male patient with a history of ICU treatment in Kenya in 2012. The patient was diagnosed with chronic *C. auris* sternal osteomyelitis in 2015 in Australia, and the *C. auris* isolate was related to South African clade III.[40]

It is possible that *C. auris* has emerged in other countries also but remain undetected due to lack of special modern laboratory identification techniques, especially in the developing countries. Figure 1 outlines the global prevalence of multidrug-resistant *C. auris* from 2009 to 2018. In this figure, we also highlighted the outbreaks as well as single and multiple cases reported from these countries so far (Figure 1).

3 | EPIDEMIOLOGICAL RELATEDNESS

To determine the genetic relatedness of *C. auris* isolates, whole genome sequencing of 47 *C. auris* isolates comprised exclusively from Pakistan (16), India (15), South Africa (10), Venezuela (5), and Japan (1) during 2012-2015 was performed.[3] The estimated genome size of *C. auris* isolates is 12.3-12.5 Mb like other *Candida* species with a G+C content of 44.53%-44.8%.[72-74] Phylogenetic analysis of isolates recognises four distinct *C. auris* clades that cluster geographically.[3] These clades are East Asia, South Asia, South America and South Africa and differ by tens of thousands of single-nucleotide polymorphisms (SNPs) between the geographic regions. However, within the clades, high degree of relatedness was observed. With different clades from different geographical areas, it is suggested that emergence of *C. auris* in each geographical region is independent and not spread from a single source.[3] A very small percentage of SNPs differences were identified within clusters, for example < 70 SNPs differentiated any two isolates from the South Africa clade while as < 16 SNPs differentiated from South American clade. From South Asian clade, <60 SNPs differentiated 34 of 36 isolates. The only big difference was identified in two isolates from Pakistan, which vary from the rest of the South Asian clades by > 600 SNPs. Furthermore, from a single hospital in Pakistan, two smaller clusters were identified consisted of nearly identical strains (<2 SNPs difference).[3] However, the data also indicate that clonal isolates of *C. auris* are spread over large distance within countries and continents.

In an another study conducted on 104 isolates of *C. auris* collected from there different countries: India (n = 90), South Africa (N = 6) and Brazil (n = 5) along with control strains from Japan (n = 1) and Korea (n = 2) reported the population structure and genetic diversity in *C. auris* using multilocus sequence typing (MLST), MALDI-TOF MS and amplified fragment length polymorphism (AFLP) fingerprinting.[75] M13 PCR fingerprinting and AFLP were identified as the most accurate analytical methods for strain typing and geographical clustering.[44,75] AFLP grouped *C. auris* isolates in to Indian and Latin American cluster. South African isolates were randomly distributed among the clusters.[75] In United Kingdom, rDNA sequencing of 24 *C. auris* isolates from 14 different hospitals, separated the isolates in three different clades belonging to India/Malaysia/Kuwait, Japan/Korea and South Africa.[31]

4 | MICROBIOLOGICAL AND BIOCHEMICAL CHARACTERISTICS

Candida auris is phylogenetically related to *C. haemulonii* in the Metschnikowiaceae clade of *Candida* family.[6] *C. auris* as other

TABLE 1 Misidentification of *Candida auris* by different traditional biochemical yeast identification methods

Identification method	Misidentify *Candida auris* as
API 20C AUX	*Rhodotorula glutinis*
	Candida sake
	Saccharomyces cerevisiae
BD Phoenix	*Candida haemulonii*
	Candida catenulata
Vitek- 2[a]	*Candida haemulonii*
	Candida duobushaemulonii
	Candida famata
	Candida lusitaniae
MicroScan	*Candida famata*
	Candida guilliermondii
	Candida lusitaniae
	Candida parapsilosis
	Candida catenulata
	Candida albicans
	Candida tropicalis
RapID Yeast Plus	*Candida parapsilosis*

Note: This table is based on data from various publications [2,8,12,26,37,38,42,45,57,60,64,77,114].

[a]Update Vitek-2 software (version 8.01) should be able to accurately identify *C. auris* from the rest of the closely related species.

Candida species can grow in different culture media. Up on microscopic examination, the cells are ovoid, ellipsoidal to elongate in shape with a size of 2.0-3.0 × 2.5-5.0 μm and appears in single, pairs or in aggregates.[6,14,30] Unlike other *Candida* species, *C. auris* does not form hyphae, chlamydospore and are germ tube negative.[8,12,76] However, occasional pseudohyphae formation has been found in *C. auris*, suggesting it might be strain or condition specific.[30] It develops pale purple to pink colonies on CHROMagar and grows at 37-42°C, whereas *C. haemulonii* isolates do not grow at 42°C.[14] On Sabouraud dextrose agar (SDA), *C. auris* forms dull white to cream coloured smooth colonies, and on malt extract agar, it grows as butyrous to viscous, white to grey, smooth and glistening colonies.[6,8] *C. auris* cells treated by Gram stain appears as single or paired ovoid to elongated budding yeast cells.[77]

Biochemical features of *C. auris* for the utilisation of nitrogen and carbon sources are distinct from other *Candida* species. It ferments glucose, trehalose (weak), sucrose (weak), but does not ferment maltose, lactose, galactose or raffinose.[6] It assimilates glucose, maltose, D-trehalose, sucrose, D-melezitose, D-raffinase, soluble starch, galactitol, D-mannitol, citrate and sorbitol for carbon source.[1,6] It has been reported that some strains are also able to assimilate N-acetyl-D-glucosamine for carbon source.[12,13,75] The non-assimilated carbon sources are D-galactose, L-sorbose, D-arabinose, D-xylose, melibiose, ribose, lactose, D-cellobiose, L-arabinose, L-rhamnose, D-glucosamine, methanol, glycerol, ethanol, erythritol, salicin, succinate, inositol, α-methyl-D-glucoside, xylitol, hexadecane, DL-lactate, D-gluconate, 2-keto-D-gluconate and N-acetyl-D-glucosamine.[1,6] For the nitrogen sources, ammonium sulphate, cadaverine and L-lysine are utilised but does not utilise sodium nitrate, potassium nitrate and ethylamine.[1,6] *C. auris* does not grow in medium containing 0.1%-0.01% cycloheximide.[6,13,56,58]

These distinct microbiological and biochemical features are important as they can play an important role to develop new media, methods and/or kits for the early and accurate identification of this pathogen.

5 | IDENTIFICATION

For appropriate treatment of any infectious disease, rapid and correct identification of the causing pathogen is important. Same is true for *C. auris*, where timely diagnosis can lead to appropriate antifungal treatment and thereby can help in preventing healthcare-associated outbreaks. Species level identification of *Candida* can help in the appropriate treatment and implementation of effective infection control measures.[78] However, in *C. auris* diagnosis correct identification is a major challenge, as most of the laboratories worldwide use commercially available biochemical-based yeast identification systems such as API- 20C AUX, VITEK-2 YST, BD-Phoenix, MicroScan and Auxacolor (Table 1). These identification systems frequently misidentify *C. auris* with other closely related *Candida* species, because of lack of *C. auris* in their databases.[12,41,42] Depending upon the method used for identification, *C. auris* is frequently misidentify as *Rhodotorula glutinis*, *Candida sake* or *Saccharomyces cerevisiae* by API-20C AUX (BioMeÂrieux), as *C. haemulonii* or *C. famata* by VITEK-2YST VITEK (BioMeÂrieux), as *C. haemulonii* (except for one as *C. catenulata*) by BD-Phoenix (BD Diagnostics), as *C. famata*, *C. lusitaniae* and *C. guilliermondii* or *C. parapsilosis* by MicroScan (Beckman Coulter), and as *Saccharomyces cerevisiae* by Auxacolor (Bio-Rad).[12,42,45] However, an updated Vitek-2 software (version 8.01) should be able to accurately identify *C. auris* from the rest of the closely related species[10] (Table 1).

To facilitate reliable and accurate identification of *C. auris* with 100% sensitivity and specificity VITEK MS (BioMeÂrieux) and Bruker Biotyper (Bruker-Daltonics), MALDI-TOF MS devices using an updated "research-use only" databases can be used.[41,44,75] Molecular methods, such as sequencing of the ITS and D1/D2 regions of the 28S ribosomal DNA, PCR, real-time PCR and AFLP, can also reliably identify and confirm *C. auris*.[41,51,75] PCR assays based on the unique GPI protein encoding and *ITS2* genes have claimed accurate identification of *C. auris*.[79,80] Recently, GPS MONODOSE dtec-qPCR kit (Alicante, Spain) for the detection of *C. auris* have been introduced with many advantages compared to other PCR methods. This kit is user friendly and detects the target in less than an hour.[81]

5.1 | Clinical symptoms and course of infections

Candida auris infection has almost similar clinical presentation as that of the other *Candida* infections.[82] It has been reported to be isolated from multiple body sites with associated clinical conditions,

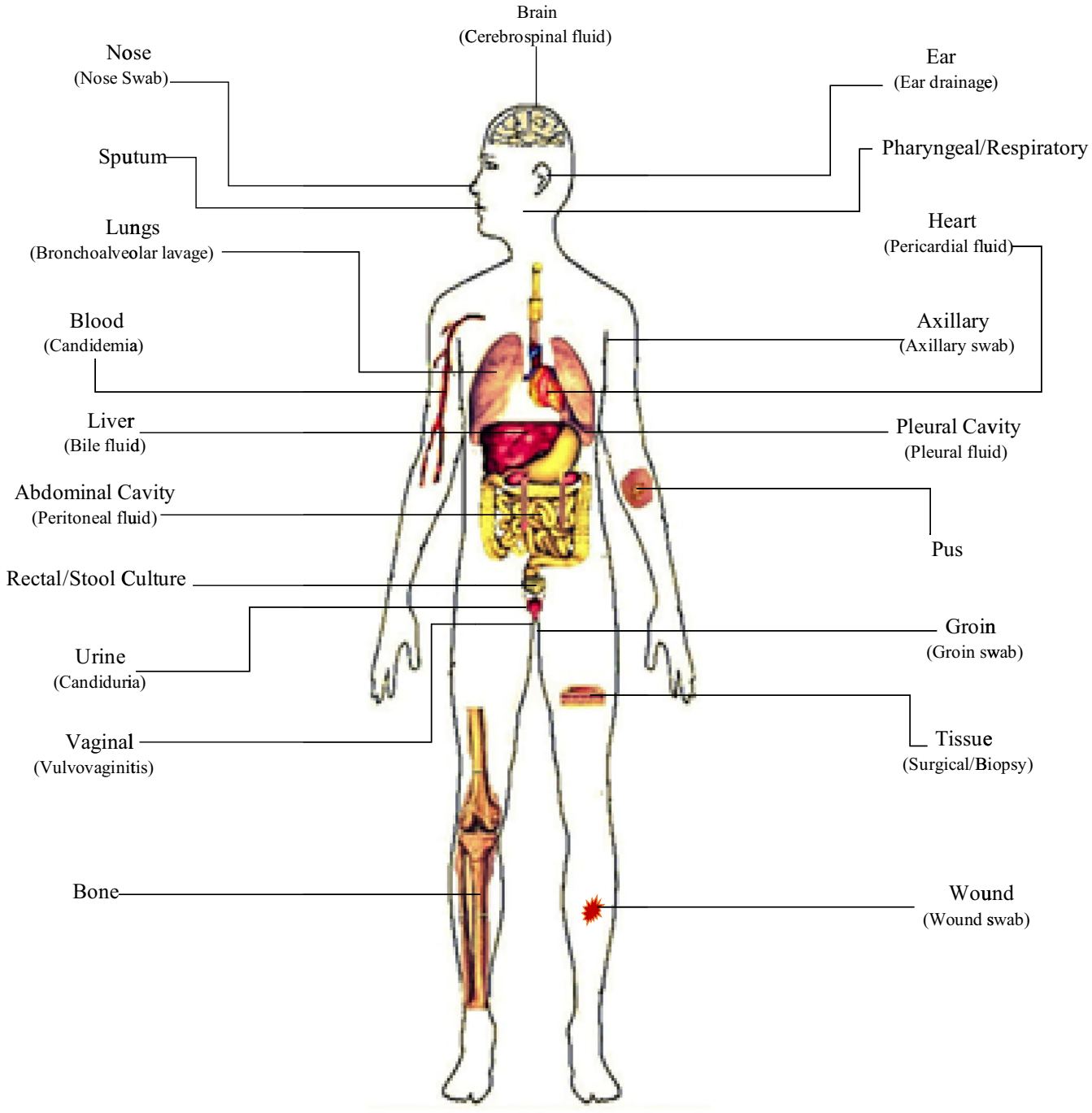

FIGURE 2 Schematic highlighting areas of the human body with distinct anatomical sites of *Candida auris* infection and colonisation

as shown in Figure 2.[56] It was first isolated from the external ear canal of a patient in Japan in 2009, followed by the first report of *C. auris* invasive infection in South Korea in 2011.[6,8] Blood stream infection (fungemia) caused by *C. auris* has been reported almost from all the continents except Antarctica. *C. auris* has been identified and reported as a cause of vulvovaginitis (from vaginal sample) and pericarditis (from last stage liver disease patient) and both these cases were reported from India.[57,83] In another recent study from India, *C. auris* nosocomial cerebrospinal fluid shunt infection was reported in a 58-year-old patient.[84] First donor-derived *C. auris* infection in a lung transplant recipient was also reported in USA in 2017.[76] In Cardio-thoracic Center outbreak in London, persistent presence of *C. auris* has been reported around patient bed-space areas, also a nose swab sample from a healthcare worker was reported positive for *C. auris*.[66] Isolation of *C. auris* has also been reported from urinary tract infections, surgical and burn wound infections, skin abscesses related to insertion catheter, bone infections, meningitis and has been isolated from respiratory tract samples.[13,38,42,56,58] The isolation of *C. auris* from urine, respiratory tract samples, wound and external ear is difficult to differentiate weather these are clinically

invasive disease or just colonisation at those sites.[56] It has been reported that *C. auris* infected patients can be colonised at multiple anatomic sites which includes the groin, axilla, rectum, nose and oropharynx[85] (Figure 2). It has also been documented that colonisation by *C. auris* persists for 1 to 3 months after initial infection.[34]

In addition, *C. auris* were also isolated from samples collected from the bed rails, bedside tables, chairs, mattress, floor around bed sites, windowsills, radiators, equipment monitors and keypads.[34,66] The reason for the survival of *C. auris* on abiotic surfaces is related to the characteristic of this pathogen to survive on plastic surfaces for 14 days, on steel surfaces and contaminated bedding for up to one week.[86-88]

6 | MORTALITY

Invasive infections caused by any species of *Candida* can be fatal; however, the mortality rate associated with *C. auris* infections is comparatively higher than other species. The crude mortality rate from *C. auris* infections has been documented ranging from 30% to 72%.[1-5] Better survival likelihood was seen in the paediatric population and in patients with immediate source control, although majority of infections affect adults.[8,39] Despite these figures, it has not yet been proven whether patients with invasive *C. auris* infections are more likely to die than patients infected with other *Candida* species.[56] An investigation, conducted by CDC on 54 *C. auris* infection cases in five countries, has reported 59% mortality rate, while as only 28% fatality has been reported from *C. auris* outbreak in a Venezuelan hospital involving 18 patients. However, in an outbreak in UK, no death case was reported from 22 involved *C. auris* infection patients. The variation in mortality data is due to the other several underlying medical conditions in these patients, confounding the attributable mortality due to *C. auris*.[12]

6.1 | Risk factors

There are no marked differences between the reported risk factors associated with *C. auris* and other *Candida* species infections.[56] The major *C. auris*-associated risk factors are prolonged hospitalisation, abdominal surgery, diabetes mellitus, admission to intensive care units, severe underlying disease and immunosuppression (such as haematological malignancy, solid tumours, bone marrow transplantation, HIV), chronic kidney disease, use of central venous and urinary catheters, recent surgery, corticosteroid therapy, parenteral nutrition, neutropenia, prior exposure to broad spectrum antibiotics and antifungal therapy.[3,8,13,14,16-18,26,34,38,39,58,66,70,76] *C. auris* has also been reported to cause infections in patients of all ages, from infants to the elderly people.[89]

6.2 | Pathophysiology

The pathogenicity of *C. albicans* and other *Candida* species is well studied; however, the exact cause of pathogenicity in *C. auris* is still being investigated. Pathogenicity of *C. auris* was compared with the other important *Candida* species such as *C. haemulonii*, *C. glabrata* and *C. albicans* in a murine model. The highest pathogenic potential was found with *C. albicans* followed by *C. auris*, *C. glabrata* and *C. haemulonii*.[90] Numerous virulence attributes of *C. auris* resemble with *C. albicans* which includes enzyme secretion, tissue invasion, nutrient acquisition, iron acquisition, histidine kinase—2 component system, multidrug efflux, genes and pathways involved in cell wall modelling and nutrient acquisition.[72-74] Study performed on an isolate of *C. auris* from a case of vulvoginitis showed phospholipase, proteinase and haemolysin activity.[83] In another study, conducted on 16 different *C. auris* isolates collected from different geographical regions showed that phospholipases and proteinases production are strain dependent.[91] Most strains of *C. auris* form biofilms, but lack of biofilm formation in some strains has also been reported.[12,72,91-93]

In vitro studies of *C. auris* isolates showed that isolates can be phenotypically divided into aggregating and non-aggregating strains.[14,30,93] The aggregative strain has the capability to form large aggregates of cells and cannot be physically disrupted, even by vortexing or by detergent treatment.[30] This property of aggregating strain may also promote the survival of *C. auris* isolates in hospital environments. In a study using *Galleria mellonella* infection model, the non-aggregating isolates exhibited more pathogenicity than aggregating isolates and have comparable pathogenicity to *C. albicans*.[30] It has also been reported that non-aggregating strains can be more pathogenic than *C. albicans*.[93] Moreover, non-aggregating isolates formed large number of individual budding yeast cells which exhibited strong biofilm forming ability in comparison with aggregating isolates of *C. auris*.[30,92] Unlike *C. albicans*, where morphological transition from non-pathogenic yeast form to pathogenic hyphae form has been identified as initial step of pathogenesis, no morphological transition has been observed in *C. auris* isolates. In different studies, it has been reported that *C. auris* isolates do not produce hyphae or only produce pseudohyphae under certain conditions.[30,76] However, in a recent study by Yue and his coworkers, a novel phenotypic switching system in *C. auris* has been reported which transits cells in three different cell types—typical yeast, filamentation-competent (FC) yeast and filamentous cells.[94]

C. auris exhibited high thermotolerance (up to 42°C) and has salt tolerant properties, which can promote its survival and pathogenicity.[6,30] A study reported that *C. auris* biofilms were thinner showing only 50% thickness compared to *C. albicans* biofilm, however, and had strong biofilm forming capacity than *C. glabrata*.[2,91] Caspofungin showed no inhibitory activity against biofilms formed by *C. auris*.[91] To fully understand the pathophysiology of *C. auris*, further research is needed to identify other virulence factors and their role in the pathogenesis of *C. auris*.

7 | DRUG RESISTANCE AND SUSCEPTIBILITY TESTING

C. auris isolates has demonstrated multidrug-resistant properties worldwide, which has not been seen in other *Candida* species

before.[56] A collaborative study undertaken by the CDC released a clinical report based on 54 *C. auris* isolates collected from five different countries, which showed that 50 (93%) isolates were resistant to fluconazole, 19 (35%) to amphotericin B and 4 (7%) isolates to echinocandins. Overall, 22 (41%) isolates were resistant to two antifungal classes (MDR), and two (4%) isolates were resistant to three antifungal classes (azoles, echinocandins and polyenes) which make them XDR.[3] A comprehensive study from Kuwait on 56 *C. auris* isolates showed 100% resistance to fluconazole, 72% to voriconazole, 23% to amphotericin B and 20% were resistant to fluconazole, voriconazole, amphotericin and only one isolate was resistant to caspofungin and micafungin.[65] It has been reported from US, that 86% of the first 35 *C. auris* cases were resistant to fluconazole, 43% and 3% were resistant to amphotericin B and echinocandins, respectively.[70] Another study reported drug resistance profiles of London outbreak isolates, which showed high level resistance to fluconazole (MIC ≥ 256 mg/L), variable susceptibility to amphotericin B (MIC = 0.5-2 mg/L) and majority of the isolates showed susceptibility to echinocandins (MIC = 0.06-0.25 mg/L) and 5-flucytosine (MIC < 0.06-0.12 mg/L).[66] Recently, antifungal susceptibility testing was performed on 350 isolates of *C. auris* from 10 hospitals in India over a period of 8 years (2009-2017) exhibited 90% of *C. auris* isolates were resistant to fluconazole (MIC 32-≥64 mg/L), 2.3% to voriconazole (MIC 16 mg/L), 8% to amphotericin B (MIC ≥ 2 mg/L) and 2% to echinocandins (MIC ≥ 8 mg/L).[95] A mouse model testing of all the three antifungal classes against nine *C. auris* strains showed that micafungin had higher fungicidal potential and is more effective than other antifungals.[96] A detailed MIC ranges of different *C. auris* isolates from different countries against all the major classes of antifungal drugs are summarised in Table 2.

Drug resistance mechanisms in *C. auris* are not clear yet; however, some studies reported that these mechanisms resemble with other resistant species of *Candida*.[53,77] Resistance of *C. auris* to azoles is assumed to occur due to upregulation of efflux pumps as that in *C. haemulonii* and *C. glabrata*[14,72]; however, it has been reported that *C. auris* in comparison *C. haemulonii* and *C. glabrata* demonstrates higher ABC-type efflux pump activity.[14] In another study, it has also been reported that the efflux pump-related genes including ATP-binding cassette (ABC) and major facilitator superfamily (MFS) transporters were upregulated in *C. auris* biofilm formation, which played a major role in azole drug resistance in this pathogen.[97] The draft genome of *C. auris* divulged that *C. auris* possess single copies of ERG3, ERG11, FKS1, FKS2 and FKS3 genes, and these genes in *C. auris* showed 78% to 85% similarity with *C. albicans* and *C. glabrata* genes.[73,74] It is also reported that a significant portion of *C. auris* genome encodes ABC and MFS transporter families along with drug transporters that could be the reason of multidrug resistance in this pathogen.[72,74] Upon comparison of *C. auris* and *C. albicans* ERG11 amino acid sequences, for the detection of azole-resistant mutations, it has been reported that the alterations in codons responsible for azole resistance in *C. albicans* are also present in *C. auris*.[3] In a recent study, it was reported that mutations in *ERG11* of *C. auris* leading to Y123F and K143R substitutions result in reduced azole susceptibility.[98] However, these substitutions are specific to geographic clades.[3] Besides role of gene mutations in azole resistance, it is evident that mutations in some genes lead to amphotericin B resistance in *C. auris*. In Colombia, four novel nonsynonymous mutations associated significantly with amphotericin B resistance were found in isolates of *C. auris*.[99] There are also reports associated with the misuse and overuse of antifungal drugs resulting in mutation of genes in *C. auris*, inducing multidrug resistance (MDR). However, there is still scope of further studies on complete genomic analysis to identify other mechanisms of multidrug resistance in this pathogen.

To better understand the drug resistance patterns and for effective patient therapy against different pathogenic microorganisms, antimicrobial susceptibility testing is an essential guide. Two major institutes, CLSI and EUCAST, have established MIC breakpoints for most of the antifungal drugs used to treat candidiasis. However, to date no such data have been reported for *C. auris* and thereby susceptibility testing for *C. auris* isolates is highly recommended by CDC. By then, for the case of clinicians to treat this pathogen, CDC provided provisional MIC breakpoints which are based on breakpoints used in other *Candida* species and on the expert opinions. CDC interim MIC breakpoints (in μg/ml) for *C. auris* include—fluconazole (≥32), amphotericin B (≥2), echinocandins (≥4 for anidulafungin and micafungin; ≥2 for caspofungin), for voriconazole and other second-generation trizoles, fluconazole resistance can be considered surrogate marker.[85]

For antifungal susceptibility testing, most commonly used methods are CLSI-BMD, VITEK-2 and Etest method.[56] The other frequently used method to check antifungal susceptibility of *C. auris* is Sensititre YeastOne™.[5] Comparison of these commonly used antifungal susceptibility methods against *C. auris* has shown differences in MIC interpretations.[75] All the methods uniformly shown higher MICs for fluconazole. There are variations in MICs of amphotericin B, which are reported high with Vitek-2 and low with Sensititre YeastOne method. The reports of antifungal susceptibility by Sensititre YeastOne method revealed high MIC values for fluconazole, however, and very low MIC values for other azoles.[5] Falsely elevated MIC of caspofungin was reported by CLSI-BMD method, reduced to 12% using Etest. Several reports also showed inter-laboratory variation in caspofungin susceptibility with both CLSI-BMD and EUCAST methods.[41,73] Several authors recommend CLSI-BMD and Etest method for antifungal susceptibility testing of *C. auris*.[56,100] To prevent fatal consequences and inappropriate treatments due to false susceptibility testing, use of more than one method to check resistance profiles of *C. auris* is highly suggested.[13,26,34,38,41,83]

8 | THERAPEUTIC OPTIONS

With an increasing case of *C. auris* infections, it becomes essential to have a broad range of therapeutic strategies against these infections. Unlike other *Candida* species, there are no concrete documented therapeutic options for *C. auris* infections and therefore it is advised that case-by-case treatment options should be followed.

In addition, CDC highly recommended the consultation of infectious disease specialist when clinicians are treating *C. auris* patients. Although *C. auris* exhibit multidrug resistance, most of the isolates are responding to echinocandins. Therefore, echinocandins are recommended initial treatment of invasive *C. auris* infections; however, prior susceptibility testing is still required.[42] A collective first- and second-line recommendations were issued by CDC with different drug dosages for adults and infants.[85]

For neonates, the initial therapy for treatment is 1 mg/kg/day of amphotericin B deoxycholate; however, if the patient is unresponsive to this initial therapy, 5 mg/kg/day of liposomal amphotericin B could be considered. Use of echinocandins for this age group could be considered only in exceptional circumstances, where central nervous system is involved. Echinocandin drugs are recommended as per dosage as first-line treatment for *C. auris* infections in adults and children ≥ 2 months of age (except anidulafungin which is not approved for use in children). Switching to a liposomal amphotericin B (5 mg/kg/day) in adults and children ≥ 2 months of age could be considered if the patient is clinically unresponsive to echinocandin therapy or has persistent fungemia for more than 5 days. However, liposomal amphotericin B has also been reported effective against *C. auris* and is used in combination therapies with an echinocandin drug.[15,26,34,76,93] An *in vitro* combinations of azoles and echinocandins drugs have also been found effective treatment against *C. auris* infections.[101] In an another study by Eldesouky, a synergistic combination of sulfamethoxazole with voriconazole and itraconazole against azole-resistant *C. auris* infections was reported.[102] Antifungal treatment is not recommended for *C. auris* cultures from non-invasive sites, when the evidence suggests colonisation rather than infection.[103,104] Despite the management of *C. auris* infection is similar to other *Candida* infections, the choice of antifungal drug treatment varies to larger extend. Importantly, it has been documented that *C. auris* rapidly develop antifungal resistance and therefore patients on treatment should be carefully monitored with follow-up cultures and susceptibility testing.

There are numerous studies reporting the efficacy of natural products, semi-synthetic and synthetic compounds, nanoparticles and peptides against *C. albicans* and other non-albicans *Candida* species; however, very limited or nothing is reported against *C. auris*. Recent studies reported SCY-078 and VT-1598 are novel antifungal compounds and are currently in the pipeline for drug development, which exhibit potent antifungal activity against *C. auris* and other pathogenic fungal species.[91,103,105] SCY-078 is the first orally bioavailable 1,3-β-D-glucan synthesis inhibitor, which demonstrated potent antifungal and antibiofilm activity against *C. auris* via growth inhibition.[91] Fungal Cyp51 (lanosterol 14α-demethylase) inhibitor VT-1598 is a tetrazole-based drug, that prevents the conversion of lanosterol to ergosterol results in disruption of ergosterol biosynthetic pathway.[103] A novel antifungal agent APX001 (formerly E1211) exhibited potent antifungal activity against *C. auris* and other drug resistant fungal species by targeting fungal enzyme *Gwt1* which catalyses the glycosylphosphatidylinositol anchored wall transfer protein 1 (GPI) biosynthesis pathway.[106] CD101 is a novel echinocandin with enhanced safety and stability, allowing intravenous administration once weekly, furthermore CD101 possesses potent antifungal activity against *C. auris*.[107,108] All these novel compounds could be an important antifungal drug for the treatment of MDR species, such as *C. auris*. The other for granted approach to test against *C. auris* is the drug combinations. Drug combinations have gained a lot of interest among microbiologists and clinicians to treat several communicable as well as non-communicable diseases, including that caused by MDR pathogens. There are several evidences which can warrant to study the combination of different antifungal drugs as well as the combination of antifungal drugs with natural products, peptides and nanoparticles to test against *C. auris* infections. From our laboratory results, we combined different antifungal drugs with different monoterpene phenols and observed that MICs of these antifungals decreased by several folds (unpublished data). These preliminary results will lead a foundation to study natural products as a chemosensitising agents to combat *C. auris* infections.

9 | INFECTION PREVENTION AND CONTROL

Candida auris, being a multidrug-resistant pathogen, is associated with nosocomial transmission and clonal hospital outbreaks. Therefore, above and over treatment options, infection prevention and control (IPC) measures are very important in limiting the spread of *C. auris*. The initial IPC measure is to isolate patients infected, colonised or suspected with *C. auris* in private single-patient rooms and while handling these patients follow both Standard Precautions and Contact Precautions as recommended by CDC, ECDC, PHE and COTHI—South Africa.[40,85] Healthcare personnel should strictly follow Contact Precautions when caring patients infected or colonised with *C. auris* to reduce the spread of infection, which includes strict adherence to hand hygiene following standard hand hygiene practices and proper use of Personal Protective Equipment (PPE).[42,85] So far, it has been reported that 3% (4/45) healthcare workers are colonised with *C. auris* on their hands.[88] Therefore, it is highly suggested to strictly follow PHE recommendations of handwashing with soap and alcohol sanitisers before and after caring patients with *C. auris* infection.[1] More care is required when healthcare personnel handle patients with high risks such as wound dressing, assisting patients with bathing, toileting, etc.[85] In addition, there are strict guidelines suggesting that any equipment used in sharing should be cleaned and disinfected after every single use. When transferring patients to other healthcare facilities, the staff at the receiving facility should be notified about the patient's *C. auris* infection or colonisation status and the level of precautions recommended.

The CDC guidelines recommended that residents in nursing homes must also be put on Standard and Contact Precautions. The CDC guidelines recommend continued infection control precautions for as long as the patient is infected or colonised with *C. auris*.

TABLE 2 Summarised antifungal resistance profile data of *Candida auris* isolates based on various susceptibility methods from different countries between 2009 and 2018

Country	No. of isolates tested/ years	Method of susceptibility	MIC range (μg/mL)	
			FLU	ITC
South Africa	4 (2012-13)	CLSI BMD (M27- A3)	64->256	0.06-0.25
India	90 (2010-14)	CLSI BMD (M27- A3)	4->64	<0.03-2
	74 (2011-12)	CLSI BMD (M27- A3)	43	3
	15 (2011-13)	CLSI BMD (M27- A3)	64	0.06-0.25
	12 (2009-11)	CLSI BMD (M27- A3)	16-64	0.125-0.25
	5 (2012-14)	CLSI BMD (M27- A3)	16-64	_
	4 (2013)	CLSI BMD (M27- A3)	>64	0.03-0.125
	2 (2011)	Not mentioned	64	_
	1(NS)	CLSI BMD (M27- A2)	≤16	≥2
	350 (2009-17)	CLSI BMD (M27- A3/S4	1-≥64	0.03-16
	123 (2010-15)	CLSI BMD M27- A3/S4)(India)	4->64	0.032-2
		EUCAST (E. Def 7.3)(Denmark)	0.05–>64	≤0.008-1
	20 (2012-17)	CLSI BMD (M27- A3/S4) (India)	0.125-32	0.03-0.125
Pakistan (19) India (19) South Africa (10) Venezuela (5) Japan (1)	54 (2012-15)	CLSI BMD (M27- S4)	4-256	0.125-2
Kuwait	1 (2014)	E-test (BioMérieux, Marcy l'Etoile, France)	>256	_
	56 (2014-17)	E-test (bioMérieux, Marcy l'Etoile, France)	128-≥256	_
	17 (2015-17)	E-test (bioMérieux, Marcy l'Etoile, France)	≥256	_
Oman	5 (2016-17)	Colorimetric microdilution Panel (YeastOne® Se-nsititre® TREK Diagnostic Systems Ltd., East Grinstead, UK)	128->256	0.12-0.25
	2	CLSI BMD (M27- A3)	≥64	0.125-0.031
	1 (2016)			
	1 (2017)			
Israel	6	CLSI BMD (M27 - A3)	32-64	0.5
	4 (2014)			
	1 (2015)			
	1 (2014-15)			
Saudi Arabia	3 (2017-18)	YeastOne microdilution broth method (TREK Diagnostics, OH, USA)	64-256	0.03-0.25
Singapore	F 3 (2018)	Sensititre™ YeastOne®microdilution panel (TREK Diagnostic Systems Ltd, Thermo Scientific)	≥256	0.12-0.25
Malaysia	1 (2018)	E-test(AB Biodisk, Solna, Sweden)	>256	4
South Korea	20	CLSI BMD, except AMB by E-test, (AB BIODISK)	2-128	0.125-4
	15 (2006)			
	5 (2007-10)			
	3	CLSI BMD (M27- A3)	2-128	0.125-2
	1 (1999)			
	2 (2009)			
Japan	1 (2009)	Not mentioned	2	0.063
China	1 (2018)	Sensititre YeastOneTM methodology (Thermo Scientific, Inc., Cleveland, OH, USA)	2	0.03
	15 (2011- 17)	Sensititre YeastOne colorimetric microdilution method(Thermo Fisher scientific, Oxoid, USA)	32	0.12
Canada	5 (2017)	CLSI BMD (M27- A3)	128	_

VRC	ISA	POS	AMB	CAS	MFG	AFG	FC	References
0.25-2	_	0.015-0.06	0.5-1	0.03-0.25	0.06-0.12	0.06-0.25	0.06-0.12	26
<0.03-16	<0.015-4	<0.015-8	0.125-8	0.125-8	<0.015-8	<0.015-8	<0.125->64	41,42
2	_	_	10	7	_	_	_	4,61
0.5-4	0.06-0.5	0.015-0.125	0.25-1	0.25-1	0.06-0.125	0.125-0.25	0.25-64	14
0.125-1	<0.015-0.25	0.06-0.25	0.25-1	0.125-0.25	0.06-0.125	0.125-0.5	0.125	13
_	_	_	Apr-16	0.25	_	_	1	74
0.06-0.125	_	≤0.015	0.125- 0.5	1	0.06	0.125-0.25	0.125-4	82
2	_	_	16	_	_	_	1	109
≤0.5	_	_	≤0.5	_	_	_	_	81
0.03-16	≤0.016-4	≤0.016-8	0.125-8	0.125-16	≤0.016-16	≤0.016-8	0.125-≥ 64	56
0.032-16	0.015-4	0.015-8	0.015-8	_	0.015-8	0.015-8	_	97
≤0.008-4	≤0.008-2	≤0.008 -0.5	0.25-1	_	0.002-4	0.002-2	_	
0.03-0.5	_	0.03-0.02	0.06-0.5	0.06-1	0.015	0.015-0.03	0.125-8	62
0.03-16	_	0.06-1	0.38-4	0.03-16	0.06-4	0.125-16	0.125-128	3
0.38	_	_	0.064	0.064	_	_	_	17
0.064-6	_	_	0.047-3	0.012-4	0.006-4	_	_	65
0.064-6	_	_	0.064-3	0.012-1	0.006-0.5	_	0.002-0.016	65
0.15-2	_	0.06-0.12	1-2	0.08-0.12	0.06-0.12	0.12	0.06-8	19
0.125-1	<0.016 -0.125	<0.016 -0.063	1-2	_	0.063 -0.125	0.031 -0.125	_	18
0.5-1	_	0.12-0.5	1-2	0.5	0.12-0.25	0.03	0.25-1	16
0.12-1	_	0.016-0.25	0.5-2	0.12	0.12	_	≤ 0.06-0.25	23
1-2	_	0.06	1-2	0.12-≥8	0.06-0.25	0.12-0.5	≤0.06-0.25	24
>32	_	_	3	>32	_	0.75	_	20
0.03-2	_	_	0.38-1.5	0.125-0.25	0.03	_	_	12,90,110
0.03-1	_	_	0.5-1	0.06	0.03	_	_	8
0.031	_	_	_	_	_	_	0.5	6
0.02	_	0.02	0.25	0.06	0.06	0.12	<0.06	21
0.25	_	0.25	0.5	0.25	0.12	0.03	4	63
_	_	_	2	_	0.5	_	_	37

(Continues)

TABLE 2 (Continued)

Country	No. of isolates tested/ years	Method of susceptibility	MIC range (μg/mL)	
			FLU	ITC
Colombia	17 (2016)	VITEK cards	16->64	_
United Kingdom	53	CLSI BMD (M27- A3)	8-> 64	_
	3 (2013)			
	1 (2014)			
	7 (2015)			
	4 (2016)			
	7 (2014 –16)			
	50 (2015-16)	Colorimetric microdilution Panel (YeastOne® Sensititre® TREK Diagnostic Systems Ltd., East Grinstead, UK)	>256	_
	4	CLSI BMD (M27- A3)	>32	_
Germany	2 (NS)	CLSI BMD (M27- A3)	> 64	0.5
Spain	8 (2016)	Colorimetric microdilution Panel (YeastOne®Sensititre® TREK Diagnostic Systems, USA)	>256	S
Austria	1 (2018)	EUCAST (microdilution method), Micronaut (Merlin Diagnostica, Bornheim, Germany).Etest (bioMérieux)	0.25-0.5	≤ 0.03
United States(US, tested strains collected from Japan (1) India (11) South Korea (2) Germany (2)	224 (2016-17)		>32 = 30	_
	Clinical-104Colonised-120			
	7		R = 5	_
	1 (2013)			
	1 (2015)			
	5 (2016)			
	16	CLSI BMD (M27- A3)	1->64	<0.063-1
	1 (2017)	Colorimetric microdilution Panel (YeastOne®Se-nsitire® TREK Diagnostic Systems, Cleveland, Ohio)	4	_
United Arab Emirates	1 (2017)	_	_	_
Venezuela	18 (2012-13)	CLSI BMD (M27- A3/S4)	>64	_

Note: AFG, anidulafungin; AMB, amphotericin B; CAS, caspofungin; CLSI-BMD, clinical and laboratory standards institute broth microdilution method; eucast, european Committee on Antimicrobial Susceptibility Testing; FC, flucytosine; FLU, fluconazole; ISA, isavuconazole; ITC, itraconazole; MFG, micafungin; MIC, minimum inhibition concentration; POS, posaconazole; VRC, voriconazole.

As the colonisation period of *C. auris* is unclear, periodic reassessment (every 1-3 months, depending upon the patient symptoms) for the existence of colonisation by *C. auris* can assist to notify the period of infection control measures. In addition, weekly testing of axilla and groin swabs, along with sites which were reported positive for *C. auris* on previous cultures, is used for the assessment of colonisation.[85] It is recommended at least two negative assessments should be performed one week apart to discontinue infection control precautions. While reassessing these patients, it should be noted that patient must not use any antifungal active against *C. auris*. Rigorous daily and terminal cleaning of patient rooms are also recommended, as patients may shed *C. auris* from their skin and other body sites for which can survive from weeks to months.[66,85,88]

Although there are no concrete evidences of any disinfectant killing *C. auris*, CDC guidelines recommend the disinfectant should be effective against *Clostridium difficile* spores. Several studies suggested use of high strength chlorine-based agents (Chlorohexidine 0.2% to 4%), hydrogen peroxide vapour, ultra violet light and phenol are effective for environmental cleaning.[34,66,88,109,110] *C. auris*, however, exhibit the tolerance against sodium hypochlorite and peracetic acid in a surface depend manner.[111] For decolonisation of skin, 2% chlorhexidine gluconate containing wipes or aqueous 4% chlorhexidine can be used.[66] Oral nystatin is effective in decolonising oropharynx.[66] In an *in vitro* study, efficacy of chlorhexidine, iodine povidone, chlorine and vaporised hydrogen peroxide exhibits effective killing of *C. auris* isolates. Inhibition of isolates was seen by chlorhexidine gluconate, iodine povidone and chlorine at a concentration of 0.125%-1.5%, 0.07%-1.25% and 1000 ppm, respectively. H_2O_2 vapour demonstrates 96.6%-100% effective killing of *C. auris*.[112] For oral decolonisation, 0.2% chlorhexidine mouthwash has been used, also chlorhexidine-impregnated protective discs

VRC	ISA	POS	AMB	CAS	MFG	AFG	FC	References
< 0.12-2	_	_	8-> 16	< 0.25-0.5	< 0.06 -0.25	_	_	[39]
0.06-2	_	< 0.03-1	0.5 -1	_	_	0.03-0.5	< 0.125-0.25	[30,31]
_	_	_	0.5-2	0.06-0.25	0.06-0.25	0.06-0.25	< 0.06-0.12	[9]
Jan-32	_	_	0.25-0.5	2-> 32	0.06-0.5	_	_	[111]
0.125-0.5	0.031	0.25-0.5	4	0.5	0.25	0.25	0.5	[89]
2	S	S	S	S	_	S	_	[28]
≤0.008 -0.016	0.002	≤0.008 -0.032	0.5-1.0	0.032 -0.125	0.064 -0.125	0.012-0.125	≤ 0.064	[68]
_	_	_	>2 = 15	>4 = 1	>4 = 1	>4 = 1	_	CDC 2017, [72]
_	_	_	R = 1	R = 1	R = 1	R = 1	_	[84]
0.063-2	0.004-0.25	0.25-1	0.5-8	_	_	_	0.5-1	[89]
0.03	_	_	2	0.12	0.12	_	0.12	[77]
0.016-1	_	_	0.02-1	0.016-0.25	_	_	_	[22]
4	_	_	01-Feb	_	_	0.125	0.5	[10]

for central vascular catheter exit sites have been found effective to reduce line-associated *C. auris* bloodstream infections.[48,50,66] For decolonisation of *C. auris* in sink drainage systems, ozonated water has been effectively used.[113] Compared to planktonic cells, *C. auris* biofilms showed reduced sensitivity to commonly used disinfectants such as povidone iodine, chlorhexidine and hydrogen peroxide.[97]

Prompt initiation of infection control interventions to control nosocomial *C. auris* outbreaks is essential to establish the source of the outbreak and to prevent further transmission of infection. Although there are limited data regarding the effectiveness of infection control interventions to control nosocomial *C. auris* outbreaks, control measures such as rapid identification of carriers, isolation of infected patients and use of recommended disinfectants for decolonisation of positive patients and their indwelling device sites should be considered.

10 | CONCLUSION AND FUTURE PROSPECTIVE

Epidemiological studies have already confirmed that *C. auris* infections are spread all around the globe. *C. auris* infections are more prevalent in developed and developing countries than under developed countries, and the underlying reason is that the efficient diagnostic tools are still beyond the reach of many microbiology laboratories in these countries. The initial requirement to deal with this pathogen is to urgently initiate consistent, sensitive and precise detection regimes. Such regimes will allow us to detect these infections at large scale and routine use and continue to build upon the fundamental knowledge of effective and well in time therapeutic treatments of *C. auris* infections in critically ill and high-risk patients. Despite the introduction of several high throughput techniques such as MALDI-TOF MS, PCR and WGS,

these techniques are expensive and time-consuming. Therefore, there is an urgent need to develop new, cost-effective and easily accessible technique or kit for early detection of this pathogen. With these features, it can be easily accessible to the different mycology laboratories worldwide. Treatment options for drug resistant *Candida* species were already limited and the increasing prevalence of *C. auris* enhances the challenges to deal with this deadly fungal pathogen. It is worth to mention that there are no or poorly defined treatment guidelines to treat *C. auris* patients. Despite the epidemiology of this pathogen gained a lot of attention for past few years, there is a greater need to develop and test new antifungals against *C. auris*. Immediate action of testing natural compounds, semi-synthetic compounds, synthetic compounds, nanoparticles, peptides against *C. auris* is a prompt requirement. These compounds have already been reported to possess antifungal activities against *Candida* and other fungal pathogens. In conclusion, it is becoming necessary to understand and recognise the *C. auris* associated problems and to implement the infection control measures, early detection and appropriate therapy for the spread and cure of the *C. auris* infections.

ACKNOWLEDGMENTS

AA acknowledges financial support from National Research Foundation Research Development Grant for Y-Rated Researchers (RDYR180418322304; Grant No: 116339). SAL is thankful for Wits Postgraduate PhD Merit Award (1311748). Authors are also thankful to P. Molefe, for the preparation of art work.

COMPETING INTERESTS

We declare no competing interests.

AUTHOR CONTRIBUTIONS

AA conceived the idea; SAL collected the data; SAL and AA analysed the data; SAL led the writing.

ORCID

Shabir A. Lone https://orcid.org/0000-0003-1850-9625
Aijaz Ahmad https://orcid.org/0000-0003-2845-0727

REFERENCES

1. Osei SJ. *Candida auris*: a systematic review and meta-analysis of current updates on an emerging multidrug-resistant pathogen. *Microbiologyopen*. 2018;7:e00578.
2. Jeffery-Smith A, Taori SK, Schelenz S, et al. *Candida auris*: a Review of the Literature. *Clin Microbiol Rev*. 2018;31:pii: e00029-17.
3. Lockhart SR, Etienne KA, Vallabhaneni S, et al. Simultaneous emergence of multidrug-resistant *Candida auris* on 3 continents Confirmed by whole-genome sequencing and epidemiological analyses. *Clin Infect Dis*. 2017;64:134-140.
4. Chakrabarti A, Sood P, Rudramurthy SM, et al. Incidence, characteristics and outcome of ICU-acquired candidemia in India. *Intensive Care Med*. 2015;41:285-295.
5. Ruiz-Gaitán A, Moret AM, Tasias-Pitarch M, et al. An outbreak due to *Candida auris* with prolonged colonisation and candidaemia in a tertiary care European hospital. *Mycoses*. 2018;61:498-505.
6. Satoh K, Makimura K, Hasumi Y, et al. *Candida auris* sp. nov., a novel ascomycetous yeast isolated from the external ear canal of an inpatient in a Japanese hospital. *Microbiol Immunol*. 2009;53:41-44.
7. Saris K, Meis JF, Voss A. *Candida auris*. *Curr Opin Infect Dis*. 2018;31:334-340.
8. Lee WG, Shin JH, Uh Y, et al. First three reported cases of nosocomial fungemia caused by *Candida auris*. *J Clin Microbiol*. 2011;49:3139-3142.
9. Currie B. Candida auris: globally emerging public health problem. *IDSE Infectious Disease Special Edition*. Spring; 2017:53-57.
10. Forsberg K, Woodworth K, Walters M, et al. *Candida auris*: the recent emergence of a multidrug-resistant fungal pathogen. *Med Mycol*. 2019;57:1-12.
11. Kim MN, Shin JH, Sung H, et al. *Candida haemulonii* and closely related species at 5 university hospitals in Korea: identification, antifungal susceptibility, and clinical features. *Clin Infect Dis*. 2009;48:e57-e61.
12. Chowdhary A, Sharma C, Duggal S, et al. New Clonal Strain of *Candida auris*, Delhi, India. *Emerg Infect Dis*. 2013;19:1670-1673.
13. Chowdhary A, Anil Kumar V, Sharma C, et al. Multidrug-resistant endemic clonal strain of *Candida auris* in India. *Eur J Clin Microbiol Infect Dis*. 2014;33:919-926.
14. Ben-Ami R, Berman J, Novikov A, et al. Multidrug-Resistant, *Candida haemulonii* and *C. auris*, Tel Aviv, Israel. *Emerg Infect Dis*. 2017;23:195-203.
15. Emara M, Ahmad S, Khan Z, et al. *Candida auris* candidemia in Kuwait, 2014. *Emerg Infect Dis*. 2015;21:1091-1092.
16. Mohsin J, Hagen F, Al-Balushi ZAM, et al. The first cases of *Candida auris* candidaemia in Oman. *Mycoses*. 2017;60:569-575.
17. Al-Siyabi T, Al Busaidi I, Balkhair A, et al. First report of *Candida auris* in Oman: clinical and microbiological description of five candidemia cases. *J Infect*. 2017;75:373-376.
18. Mohd Tap R, Lim TC, Kamarudin NA, et al. A fatal case of *Candida auris* and *Candida tropicalis* candidemia in neutropenic patient. *Mycopathologia*. 2018;183:559-564.
19. Wang X, Bing J, Zheng Q, et al. The first isolate of *Candida auris* in China: clinical and biological aspects. *Emerg Microbes Infect*. 2018;7:93.
20. Alatoom A, Sartawi M, Lawlor K, et al. Persistent candidemia despite appropriate fungal therapy: first case of *Candida auris* from the United Arab Emirates. *Int J Infect Dis*. 2018;70:36-37.
21. Abdalhamid B, Almaghrabi R, Althawadi S, Omrani A. First report of *Candida auris* infections from Saudi Arabia. *J Infect Public Health*. 2018;11:598-599.
22. Abastabar M, Haghani I, Ahangarkani F, et al. *Candida auris* otomycosis in Iran and review of recent literature. *Mycoses*. 2019;62:101-105.
23. Tan YE, Tan AL. Arrival of *Candida auris* fungus in Singapore: report of the first 3 cases. *Ann Acad Med Singapore*. 2018;47:260-262.
24. Magobo RE, Corcoran C, Seetharam S, Govender NP. *Candida auris*-associated candidemia, South Africa. *Emerg Infect Dis*. 2014;20:1250-1252.
25. Okinda N, Kagotho E, Castanheira M, et al. Candidemia at a referral hospital in sub-saharan Africa: emergence of Candida auris as a major pathogen. 2014; Poster ECCMID; Barcelona.
26. Ruiz Gaitan AC, Moret A, Lopez Hontangas JL, et al. Nosocomial fungemia by *Candida auris*: first four reported cases in continental Europe. *Rev Iberoam Micol*. 2017;34:23-27.
27. Kohlenberg A, Struelens MJ, Monnet DL, et al. *Candida auris*: epidemiological situation, laboratory capacity and preparedness in

European Union and European Economic Area countries, 2013 to 2017. *Euro Surveill*. 2018;23:13.
28. Pekard-Amenitsch S, Schriebl A, Posawetz W, Willinger B, Kölli B, Buzina W. Isolation of *Candida auris* from ear of otherwise healthy patient, Austria, 2018. *Emerg Infect Dis*. 2018;24:1596-1597.
29. Dewaele K, Frans J, Smismans A, Ho E, Tollens T, Lagrou K. First case of *Candida auris* infection in Belgium in a surgical patient from Kuwait. *Acta Clin Belg*. 2018;1-8.
30. Borman AM, Szekely A, Johnson EM. Comparative pathogenicity of United Kingdom isolates of the emerging pathogen *Candida auris* and other key pathogenic Candida species. *mSphere*. 2016;1:pii: e00189-16.
31. Borman AM, Szekely A, Johnson EM. Isolates of the emerging pathogen *Candida auris* present in the UK have several geographic origins. *Med Mycol*. 2017;55:563-567.
32. Riat A, Neofytos D, Coste A, et al. First case of *Candida auris* in Switzerland: discussion about preventive strategies. *Swiss Med Wkly*. 2018;148:w14622.
33. Vasilyeva N, Kruglov A, Pchelin I, et al. P0311 the first Russian case of candidaemia due to Candida auris. 2018; 28th European Congress of Clinical Microbiology and Infectious Diseases. Madrid, Spain.
34. Vallabhaneni S, Kallen A, Tsay S, et al. Investigation of the first seven reported cases of *Candida auris*, a globally emerging invasive, multidrug-resistant fungus-United States, May 2013-August 2016. *Am J Transplant*. 2017;17:296-299.
35. McCarthy M. Hospital transmitted *Candida auris* infections confirmed in the US. *BMJ*. 2016;355:i5978.
36. Schwartz IS, Hammond GW. First reported case of multidrug-resistant *Candida auris* in Canada. *Can Commun Dis Rep*. 2017;43:150-153.
37. Araúz AB, Caceres DH, Santiago E, et al. Isolation of *Candida auris* from 9 patients in Central America: importance of accurate diagnosis and susceptibility testing. *Mycoses*. 2018;61:44-47.
38. Morales-Lopez SE, Parra-Giraldo CM, Ceballos-Garzon A, et al. Invasive infections with multidrug-resistant yeast *Candida auris*, Colombia. *Emerg Infect Dis*. 2017;23:162-164.
39. Calvo B, Melo AS, Perozo-Mena A, et al. First report of *Candida auris* in America: clinical and microbiological aspects of 18 episodes of candidemia. *J Infect*. 2016;73:369-374.
40. Heath CH, Dyer JR, Pang S, Coombs GW, Gardam DJ. *Candida auris* sternal osteomyelitis in a man from Kenya visiting Australia, 2015. *Emerg Infect Dis*. 2019;25:192-194.
41. Kathuria S, Singh PK, Sharma C, et al. Multidrug-Resistant *Candida auris* misidentified as *Candida haemulonii*: characterization by Matrix-Assisted Laser Desorption Ionization-Time of Flight Mass spectrometry and DNA sequencing and its antifungal susceptibility profile variability by Vitek 2, CLSI broth microdilution, and E-test method. *J Clin Microbiol*. 2015;53:1823-1830.
42. Chowdhary A, Voss A, Meis JF. Multidrug-resistant *Candida auris*: 'new kid on the block' in hospital-associated infections? *J Hosp Infect*. 2016;94:209-212.
43. Kim TH, Kweon OJ, Kim HR, Lee MK. Identification of uncommon *Candida* species using commercial identification systems. *J Microbiol Biotechnol*. 2016;26:2206-2213.
44. Girard V, Mailler S, Chetry M, et al. Identification and typing of the emerging pathogen *Candida auris* by matrix-assisted laser desorption ionisation time of flight mass spectrometry. *Mycoses*. 2016;59:535-538.
45. Mizusawa M, Miller H, Green R, et al. Can multidrug-resistant *Candida auris* be reliably identified in clinical microbiology laboratories? *J Clin Microbiol*. 2017;55:638-640.
46. Bao JR, Master RN, Azad KN, et al. Rapid, accurate identification of *Candida auris* by using a novel matrix-assisted laser desorption ionization-time of flight mass spectrometry(MALDI-TOF MS) database (library). *J Clin Microbiol*. 2018;56:pii: e01700–17.
47. Sexton DJ, Bentz ML, Welsh RM, Litvintseva AP. Evaluation of a new T2 magnetic resonance assay for rapid detection of emergent fungal pathogen *Candida auris* on clinical skin swab samples. *Mycoses*. 2018;61:786-790.
48. Clancy CJ, Nguyen MH. Emergence of *Candida auris*: an international call to arms. *Clin Infect Dis*. 2017;64:141-143.
49. Sears D, Schwartz BS. *Candida auris*: an emerging multidrug resistant pathogen. *Int J Infect Dis*. 2017;63:95-98.
50. Govender NP, Magobo RE, Mpembe R, et al. *Candida auris* in South Africa, 2012-2016. *Emerg Infect Dis*. 2018;24:2036-2040.
51. Kordalewska M, Zhao Y, Lockhart SR, Chowdhary A, Berrio I, Perlin DS. Rapid and accurate molecular identification of the emerging multidrug-resistant pathogen *Candida auris*. *J Clin Microbiol*. 2017;55:2445-2452.
52. Pfaller MA, Woosley LN, Messer SA, Jones RN, Castanheira M. Significance of molecular identification and antifungal susceptibility of clinically significant yeasts and moulds in a global antifungal surveillance programme. *Mycopathologia*. 2012;174:259-271.
53. Chowdhary A, Sharma C, Meis JF. *Candida auris*: a rapidly emerging cause of hospital-acquired multidrug-resistant fungal infections globally. *PLoS Pathog*. 2017;13:e1006290.
54. Das S, Tigga R, Rai G, et al. *Candida auris* colonization in an immunocompetent patient: a new threat in medical ICU. *Med Mycol Case Rep*. 2018;21:54-56.
55. Cortegiani A, Misseri G, Fasciana F, Giammanco A, Giarratano A, Chowdhary A. Epidemiology, clinical characteristics, resistance, and treatment of infections by *Candida auris*. *J Intensive Care*. 2018;6:69.
56. Sarma S, Upadhyay S. Current perspective on emergence, diagnosis and drug resistance in *Candida auris*. *Infect Drug Resist*. 2017;10:155-165.
57. Khillan V, Rathore N, Kathuria S, Chowdhary A. A rare case of breakthrough fungal pericarditis due to fluconazole-resistant *Candida auris* in a patient with chronic liver disease. *JMM Case Reports*. 2014;1.
58. Rudramurthy SM, Chakrabarti A, Paul RA, et al. *Candida auris* candidaemia in Indian ICUs: analysis of risk factors. *J Antimicrob Chemother*. 2017;72:1794-1801.
59. Mathur P, Hasan F, Singh PK, Malhotra R, Walia K, Chowdhary A. Five-year profile of candidaemia at an Indian trauma centre: high rates of *Candida auris* blood stream infections. *Mycoses*. 2018;61:674-680.
60. Tian S, Rong C, Nian H, et al. First cases and risk factors of super yeast *Candida auris* infection or colonization from Shenyang, China. *Emerg Microbes Infect*. 2018;7:128.
61. Chen Y, Zhao J, Han L, et al. Emergency of fungemia cases caused by fluconazole-resistant *Candida auris* in Beijing, China. *J Infect*. 2018;77:561-571.
62. Choi HI, An J, Hwang JJ, Moon SY, Son JS. Otomastoiditis caused by *Candida auris*: case report and literature review. *Mycoses*. 2017;60:488-492.
63. Belkin A, Gazit Z, Keller N, et al. *Candida auris* Infection Leading to Nosocomial Transmission, Israel, 2017. *Emerg Infect Dis*. 2018;24:801-804.
64. Khan Z, Ahmad S, Al-Sweih N, Joseph L, Alfouzan W, Asadzadeh M. Increasing prevalence, molecular characterization and antifungal drug susceptibility of serial *Candida auris* isolates in Kuwait. *PLoS ONE*. 2018;13:e0195743.
65. Khan Z, Ahmad S, Benwan K, et al. Invasive *Candida auris* infections in Kuwait hospitals: epidemiology, antifungal treatment and outcome. *Infection*. 2018;46:641-650.
66. Schelenz S, Hagen F, Rhodes JL, et al. First hospital outbreak of the globally emerging *Candida auris* in a European hospital. *Antimicrob Resist Infect Control*. 2016;5:35.

67. Eyre DW, Sheppard AE, Madder H, et al. A *Candida auris* outbreak and its control in an intensive care setting. *N Engl J Med*. 2018;379:1322-1331.
68. Parra-Giraldo CM, Valderrama SL, Cortes-Fraile G, et al. First report of sporadic cases of *Candida auris* in Colombia. *Int J Infect Dis*. 2018;69:63-67.
69. Escandón P, Cáceres DH, Espinosa-Bode A, et al. Notes from the Field: surveillance for *Candida auris* - Colombia, September 2016-May 2017. *MMWR Morb Mortal Wkly Rep*. 2018;67:459-460.
70. Tsay S, Welsh RM, Adams EH, et al. Notes from the Field: ongoing transmission of *Candida auris* in health care facilities - United States, June 2016-May 2017. *MMWR Morb Mortal Wkly Rep*. 2017;66:514-515.
71. Chow NA, Gade L, Tsay SV, et al. Multiple introductions and subsequent transmission of multidrug-resistant *Candida auris* in the USA: a molecular epidemiological survey. *Lancet Infect Dis*. 2018;18:1377-1384.
72. Chatterjee S, Alampalli SV, Nageshan RK, Chettiar ST, Joshi S, Tatu US. Draft genome of a commonly misdiagnosed multidrug resistant pathogen *Candida auris*. *BMC Genom*. 2015;16:686.
73. Sharma C, Kumar N, Meis JF, Pandey R, Chowdhary A. Draft genome sequence of a fluconazole-resistant *Candida auris* strain from a candidemia patient in India. *Genome Announc*. 2015;3:pii: e00722-15.
74. Sharma C, Kumar N, Pandey R, Meis JF, Chowdhary A. Whole genome sequencing of emerging multidrug resistant *Candida auris* isolates in India demonstrates low genetic variation. *New Microbes New Infect*. 2016;13:77-82.
75. Prakash A, Sharma C, Singh A, et al. Evidence of genotypic diversity among *Candida auris* isolates by multilocus sequence typing, matrix-assisted laser desorption ionization time-of-flight mass spectrometry and amplified fragment length polymorphism. *Clin Microbiol Infect*. 2016;22(277):e1-e9.
76. Azar MM, Turbett SE, Fishman JA, Pierce VM. Donor-derived transmission of *Candida auris* during lung transplantation. *Clin Infect Dis*. 2017;65:1040-1042.
77. Navalkele BD, Revankar S, Chandrasekar P. *Candida auris*: a worrisome, globally emerging pathogen. *Expert Rev Anti Infect Ther*. 2017;15:819-827.
78. Lockhart SR, Jackson BR, Vallabhaneni S, Ostrosky-Zeichner L, Pappas PG, Chiller T. Thinking beyond the common *Candida* Species: need for species-level identification of *Candida* due to the emergence of multidrug-resistant *Candida auris*. *J Clin Microbiol*. 2017;55:3324-3327.
79. Ruiz-Gaitán AC, Fernández-Pereira J, Valentin E, et al. Molecular identification of *Candida auris* by PCR amplification of species-specific GPI protein-encoding genes. *Int J Med Microbiol*. 2018;308:812-818.
80. Leach L, Zhu Y, Chaturvedi S. Development and validation of a real-time PCR assay for rapid detection of *Candida auris* from surveillance samples. *J Clin Microbiol*. 2018;56:pii: e01223-17.
81. Martínez-Murcia A, Navarro A, Bru G, Chowdhary A, Hagen F, Meis JF. Internal validation of GPS™ MONODOSE CanAur dtec-qPCR kit following the UNE/EN ISO/IEC 17025:2005 for detection of the emerging yeast *Candida auris*. *Mycoses*. 2018;61:877-884.
82. Ku TSN, Walraven CJ, Lee SA. *Candida auris*: disinfectants and implications for infection control. *Front Microbiol*. 2018;l 9:726.
83. Kumar D, Banerjee T, Pratap CB, Tilak R. Itraconazole-resistant *Candida auris* with phospholipase, proteinase and hemolysin activity from a case of vulvovaginitis. *J Infect Dev Ctries*. 2015;9:435-437.
84. Singhal T, Kumar A, Borade P, Shah S, Soman R. Successful treatment of *C. auris* shunt infection with intraventricular caspofungin. *Med Mycol Case Rep*. 2018;22:35-37.
85. Tsay S, Kallen A, Jackson BR, Chiller TM, Vallabhaneni S. Approach to the Investigation and Management of Patients with *Candida auris*, an Emerging Multidrug-Resistant Yeast. *Clin Infect Dis*. 2018;66:306-311.
86. Welsh RM, Bentz ML, Shams A, et al. Survival, Persistence, and Isolation of the Emerging Multidrug-Resistant Pathogenic Yeast Candida auris on a Plastic Health Care Surface. *J Clin Microbiol*. 2017;55:2996-3005.
87. Piedrahita CT, Cadnum JL, Jencson AL, Shaikh AA, Ghannoum MA, Donskey CJ. Environmental surfaces in healthcare facilities are a potential source for transmission of *Candida auris* and other Candida Species. *Infect Control Hosp Epidemiol*. 2017;38:1107-1109.
88. Biswal M, Rudramurthy SM, Jain N, et al. Controlling a possible outbreak of *Candida auris* infection: lessons learnt from multiple interventions. *J Hosp Infect*. 2017;97:363-370.
89. de Cássia Orlandi Sardi J, Silva DR, Soares Mendes-Giannini MJ, Rosalen PL. *Candida auris*: epidemiology, risk factors, virulence, resistance, and therapeutic options. *Microb Pathog*. 2018;125:116-121.
90. Fakhim H, Vaezi A, Dannaoui E, et al. Comparative virulence of *Candida auris* with *Candida haemulonii*, *Candida glabrata* and *Candida albicans* in a murine model. *Mycoses*. 2018;61:377-382.
91. Larkin E, Hager C, Chandra J, et al. The emerging pathogen *Candida auris*: growth phenotype, virulence factors, activity of antifungals, and effect of SCY-078, a novel glucan synthesis inhibitor, on growth morphology and biofilm formation. *Antimicrob Agents Chemother*. 2017;61:pii: e02396-16.
92. Oh BJ, Shin JH, Kim MN, et al. Biofilm formation and genotyping of *Candida haemulonii*, *Candida pseudohaemulonii*, and a proposed new species (*Candida auris*) isolates from Korea. *Med Mycol*. 2011;49:98-102.
93. Sherry L, Ramage G, Kean R, et al. Biofilm-forming capability of highly virulent, multidrug-resistant *Candida auris*. *Emerg Infect Dis*. 2017;23:328-331.
94. Yue H, Bing J, Zheng Q, et al. Filamentation in *Candida auris*, an emerging fungal pathogen of humans: passage through the mammalian body induces a heritable phenotypic switch. *Emerg Microbes Infect*. 2018;7:188.
95. Chowdhary A, Prakash A, Sharma C, et al. A multicentre study of antifungal susceptibility patterns among 350 *Candida auris* isolates (2009-17) in India: role of the ERG11 and FKS1 genes in azole and echinocandin resistance. *J Antimicrob Chemother*. 2018;73:891-899.
96. Lepak AJ, Zhao M, Berkow EL, Lockhart SR, Andes DR. Pharmacodynamic optimization for treatment of invasive *Candida auris* infection. *Antimicrob Agents Chemother*. 2017;61:pii: e00791-17.
97. Kean R, Delaney C, Sherry L, et al. Transcriptome assembly and profiling of *Candida auris* reveals novel insights into biofilm-mediated resistance. *mSphere*. 2018;3:pii: e00334-18.
98. Healey KR, Kordalewska M, Jiménez Ortigosa C, et al. Limited ERG11 mutations identified in isolates of *Candida auris* directly contribute to reduced azole susceptibility. *Antimicrob Agents Chemother*. 2018;62:pii: e01427-18.
99. Escandón P, Chow NA, Caceres DH, et al. Molecular epidemiology of *Candida auris* in Colombia reveals a highly related, countrywide colonization with regional patterns in amphotericin B resistance. *Clin Infect Dis*. 2019;68:15-21.
100. Arendrup MC, Prakash A, Meletiadis J, Sharma C, Chowdhary A. Comparison of EUCAST and CLSI reference microdilution MICs of right antifungal compounds for *Candida auris* and associated tentative epidemiological cut off values. *Antimicrob Agents Chemother*. 2017;61:e00485-17.

101. Fakhim H, Chowdhary A, Prakash A, et al. In vitro interactions of echinocandins with triazoles against multidrug-resistant *Candida auris*. *Antimicrob Agents Chemother*. 2017;61:pii: e01056-17.
102. Eldesouky HE, Li X, Abutaleb NS, Mohammad H, Seleem MN. Synergistic interactions of sulfamethoxazole and azole antifungal drugs against emerging multidrug-resistant *Candida auris*. *Int J Antimicrob Agents*. 2018;52:754-761.
103. Berkow EL, Angulo D, Lockhart SR. *In vitro* activity of a novel glucan synthase inhibitor, SCY-078, against clinical isolates of *Candida auris*. *Antimicrob Agents Chemother*. 2017;61:e00435-17.
104. Todd B. Clinical alert: *Candida auris*. *Am J Nurs*. 2017;117:53-55.
105. Wiederhold NP, Lockhart SR, Najvar LK, et al. The fungal Cyp51 specific inhibitor VT-1598 demonstrates *in vitro* and *in vivo* activity against *Candida auris*. *Antimicrob Agents Chemother*. 2018;63:pii: AAC.02233-18.
106. Hager CL, Larkin EL, Long L. Zohra Abidi F, Shaw KJ, Ghannoum MA. *In vitro* and *in vivo* evaluation of the antifungal activity of APX001A/APX001 against *Candida auris*. *Antimicrob Agents Chemother*. 2018;62:pii: e02319-17.
107. Berkow EL, Lockhart SR. Activity of CD101, a long-acting echinocandin, against clinical isolates of *Candida auris*. *Diagn Microbiol Infect Dis*. 2018;90:196-197.
108. Hager CL, Larkin EL, Long LA, Ghannoum MA. Evaluation of the efficacy of rezafungin, a novel echinocandin, in the treatment of disseminated *Candida auris* infection using an immunocompromised mouse model. *J Antimicrob Chemother*. 2018;73:2085-2088.
109. Boyce JM. Modern technologies for improving cleaning and disinfection of environmental surfaces in hospitals. *Antimicrob Resist Infect Control*. 2016;5:10.
110. Cadnum JL, Shaikh AA, Piedrahita CT, et al. Relative resistance of the emerging fungal pathogen *Candida auris* and Other Candida species to Killing by ultraviolet light. *Infect Control Hosp Epidemiol*. 2018;39:94-96.
111. Kean R, Sherry L, Townsend E, et al. Surface disinfection challenges for *Candida auris*: an in-vitro study. *J Hosp Infect*. 2018;98:433-436.
112. Abdolrasouli A, Armstrong-James D, Ryan L, Schelenz S. In vitro efficacy of disinfectants utilised for skin decolonisation and environmental decontamination during a hospital outbreak with *Candida auris*. *Mycoses*. 2017;60:758-763.
113. Livingston S, Cadnum JL, Gestrich S, Jencson AL, Donskey CJ. Efficacy of automated disinfection with ozonated water in reducing sink drainage system colonization with Pseudomonas species and *Candida auris*. *Infect Control Hosp Epidemiol*. 2018;39:1497-1498.
114. Snayd M, Dias F, Ryan RW, Clout D, Banach DB. Misidentification of *Candida auris* by RapID Yeast Plus, a commercial, biochemical enzyme-based manual rapid identification system. *J Clin Microbiol*. 2018;56:pii: e00080-18.

How to cite this article: Lone SA, Ahmad A. *Candida auris*—the growing menace to global health. *Mycoses*. 2019;62:620–637. https://doi.org/10.1111/myc.12904

Bioorganic Chemistry 98 (2020) 103771

Contents lists available at ScienceDirect

Bioorganic Chemistry

journal homepage: www.elsevier.com/locate/bioorg

S-benzyldithiocarbazate imine coordinated metal complexes kill *Candida albicans* by causing cellular apoptosis and necrosis

Manzoor Ahmad Malik[a], Shabir Ahmad Lone[b], Mohmmad Younus Wani[c], Md. Ikbal Ahmed Talukdar[a], Ovas Ahmad Dar[a], Aijaz Ahmad[b,d,*], Athar Adil Hashmi[a,*]

[a] Bioinorganic Chemistry Lab. Department of Chemistry, Jamia Millia Islamia, New Delhi 110025, India
[b] Clinical Microbiology and Infectious Diseases, School of Pathology, Faculty of Health Sciences, University of the Witwatersrand, Johannesburg, South Africa
[c] University of Jeddah, College of Science, Department of Chemistry, Jeddah 21589, Saudi Arabia
[d] Division of Infection Control, Charlotte Maxeke Johannesburg Academic Hospital, National Health Laboratory Service, Johannesburg, South Africa

ARTICLE INFO

Keywords:
Dithiocarbazate
Metal complexes
Apoptosis
Necrosis
Candida albicans

ABSTRACT

Development of new chemotherapeutic agents and strategies are urgently needed to curb and halt the growing menace caused by hard-to-treat microbes. Coordination of metals to bioactive organic ligands is now considered to be an efficient strategy for delivering bioactive compounds inside the microbial cell membranes. Metal complexes have been effectively used to treat many dreadful diseases were other treatment modalities had failed. Use of metal complexes to treat microbial infections is now conceived to be an alternative and efficient strategy. Towards this, some new homoleptic transition metal complexes, obtained by coordination of metal ions to bioactive S-benzyldithiocarbazate Schiff-base ligands were evaluated for their anti-*Candida* activity and their potential to disrupt the membrane architecture. The complexes displayed remarkable antifungal activity against a wide spectrum of fluconazole susceptible and resistant *Candida albicans* isolates, with Ni complex **(dtc3)** being highly active with minimum inhibitory concentration (MIC) values ranging from 1 to 32 μg/mL. Cell viability assay confirmed the fungicidal activity of these metal complexes, especially the complex **dtc3**. These metal complexes kill *Candida albicans* by inducing cellular apoptosis and necrosis thereby causing phosphatidylserine externalization as revealed by Annexin V-FITC and propidium iodide staining assays.

1. Introduction

Microbial infections have crumbled our society without any boundaries of rich and poor. The unrelenting rise of microbial infections has emerged as a serious global concern intimidating the effective prevention and treatment of an ever-increasing range of infections [1–3]. Enormous effort is being invested in the development of effective antimicrobial agents to eliminate this rising clinical concern. In addition, the development of resistance to current antimicrobial agents has resulted in high rates of morbidity and mortality [4–6]. Among the various therapeutic approaches to wipe out microbial menace, development of metal containing chemotherapeutic agents is now conceived to be an efficient strategy to disrupt the microbial membrane architecture and the microbial biofilms which are considered as defence armour of the microbes against any antibiotics. Also because of the range of coordination geometries, metal complexes provide more stereochemical variability than is possible for organic molecules and the coordination of ligands to metal ions often introduces new elements of chirality which may be important for biological molecule recognition and interaction [7]. The metal complexes can also be highly positively charged that could aid their interaction with negatively charged biological molecules such as DNA, RNA, several types of phospholipids, and some regions of membrane proteins. It has been reported that silver, gold, platinum, copper and other transition metal complexes interact with different cellular targets and display efficient antimicrobial properties [8–15]. Another crucial determinant of the antimicrobial property appears to be the cellular uptake. It is generally accepted that most hydrophobic antibiotics cross the membrane by energy independent passive diffusion, but some lipophilic antibiotics cross the cell membrane by active transport. Since metal complexes contain hydrophobic as well as lipophilic regions, these allow the complexes to interact with the membrane components differently, thus causing disruption of the membrane architecture [16]. Also, because of the different microbial microenvironment, metal complexes could

* Corresponding authors at: Clinical Microbiology and Infectious Diseases, School of Pathology, Faculty of Health Sciences, University of the Witwatersrand, Johannesburg, South Africa (A. Ahmad).
E-mail addresses: aijaz.ahmad@wits.ac.za (A. Ahmad), ahashmi@jmi.ac.in (A.A. Hashmi).

https://doi.org/10.1016/j.bioorg.2020.103771
Received 22 November 2019; Received in revised form 24 January 2020; Accepted 16 March 2020
Available online 17 March 2020
0045-2068/

undergo redox reactions and ligand exchange outside or inside the microbial membranes therefore targeting the solvent exposed [4Fe-4S] clusters of proteins, undergoing thiol mediated reductions, and inducing ROS-mediated cellular damage [17].

S-benzyldithiocarbazate structural moiety is considered to be of great relevance and importance for designing flexible ligands and their metal complexes with diverse range of biological activities [18,19]. In addition, due to the limited number of currently available antifungal drugs and the increasing incidences of invasive fungal infections in immunocompromised patients such as HIV, cancer, tuberculosis etc. drug resistance become a major challenge for clinicians to provide an appropriate antifungal therapy. Based on these facts, there is an urgent need for novel antifungal molecules that could be employed to overcome antifungal drug resistance. In this work, we report the synthesis of new transition metal complexes, derived from an s-benzyldithiocarbazate Schiff base ligand with interesting antifungal activities. The antifungal potential of these complexes was studied against a panel of different susceptible and resistant *Candida albicans*. An attempt was also made to delineate the mechanism of action of these active complexes by studying the mode of cell death by Annexin V and PI staining methods.

2. Experimental

2.1. Chemistry

2.1.1. Materials and physical measurements

1,3-Benzodioxole-5-carboxaldehyde, $Cu(OAc)_2{\cdot}H_2O$, $Co(OAc)_2{\cdot}4H_2O$ and $Ni(OAc)_2{\cdot}4H_2O$ were purchased from Merck. Ethanol was distilled prior to use. IR spectra (4000–400 cm^{-1}) were obtained as KBr pellets using an FT-IR 8400-Shimadzu spectrophotometer. ^1H NMR (400 MHz) and ^{13}C NMR (200 MHz) spectra were recorded on a JEOL JNM-A400 spectrometer in DMSO with TMS as internal standard. Mass spectra were obtained on a JEOL-JMS-D300 mass spectrometer. Molar conductance measurements were obtained with a heavy-duty conductivity meter (Extech Instruments, USA, model No. 407303) and magnetic susceptibilities were measured at room temperature (20 °C). The UV–Vis spectra were recorded on a Perkin Elmer Lambda 40 UV–Vis spectrophotometer between 200 and 800 nm with 10^{-5} M solutions in DMSO. Melting points were measured on a melting point apparatus, Gallenkamp, England. XRD studies were carried out using XPERT-PRO, X-ray diffractometer. Morphological evaluation of the synthesized compounds was done by SEM analysis. Thermal stability of the complexes was performed in a nitrogen environment on a Thermogravimetric analyzer Exstar 6300.

2.1.2. Preparation of the Schiff baseligand (sbl)

A previously reported procedure was followed to synthesize dithicarbazate [18], according to which hydrazine hydrate (2.50 g, 0.05 mol, 99%) was added to an absolute ethanol solution of KOH (2.81 g, 0.05 mol) and the mixture was stirred at 0 °C. Carbon disulphide (3.81 g, 0.05 mol) was added dropwise with constant stirring over 1 h. Then benzyl chloride (8.25 g, 0.05 mol) was added dropwise with vigorous stirring at 0 °C, over an additional hour. A white precipitate of S-benzyldithiocarbazate was formed and collected. Finally, a solution of 1,3-Benzodioxole-5-carboxaldehyde (6.81 g, 0.05 mol) in methanol was added to the obtained S-benzyldithiocarbazate and refluxed for an hour. The mixture was filtered while hot and the filtrate was cooled, giving a light-yellow precipitate of the desired Schiff base product which was dried in a vacuum desiccator over anhydrous $CaCl_2$. The physical and spectroscopic data of **sbl** are as follows:

Color: Light yellow, yield: 79%; m. p. (185–190 °C). Anal. Calcd for$C_{16}H_{14}N_2O_2S_2$: C, 58.16%; H, 4.27%; N, 8.48%; S, 19.41. Found: C, 58.72%; H, 4.32%; N, 8.61%; S, 19.26. IR data (KBr pellets, cm^{-1}): ν(N−H) 3124 m, ν(C−H) 2918 m, ν(C═N) 1600 s, ν (C═C) 1492 s, ν(C═S) 1091 m, ν(N−N) 1033 s, ν(CSS) 921 m (Fig. S3). ^1H NMR (500 MHz, DMSO-d_6, ppm) δ: 13.26(s, 1H, NH), 8.15(s, 1H, CH═N), 7.68(d, 2H, C-4,6), 6.93(d, 2H, C-3,7), 4.49(2H, −SCH_2), 6.08(2H, −OCH_2O−). ^{13}C NMR (100 MHz, $CDCl_3$, ppm) δ: 196.31(C═S), 146.90(CH═N), 137.41(C-g), 124.67(C-h), 109.13(C-f), 102.21(C-d), 105.71(C-e), 37.94(C-c). UV–Vis spectrum [DMSO, λ_{max} nm]: 256, 275, 328, 376.

2.1.3. Synthesis of the metal complexes: dtc1-dtc3

To a solution of sbl (0.078 g, 0.25 mmol) in (1:1) methanol/dichloromethane (20 mL) was added a solution of $Cu(OAc)_2{\cdot}H_2O$ (0.031 g, 0.125 mmol) in methanol (10 mL). The resulting mixture was stirred at room temperature for 4 h. The dark-brown precipitate that formed was filtered off, washed with ethanol, methanol, diethylether and dried in a desiccator over anhydrous calcium chloride.

The corresponding Co(II) and Ni(II) complexes were prepared by a similar procedure as described for Co(II) complex, using $Co(OAc)_2{\cdot}4H_2O$ and $Ni(OAc)_2{\cdot}4H_2O$, respectively. Brick-red and light greenish precipitate of $Co(sbl)_2$ and $Ni(sbl)_2$ was obtained. Physical and spectroscopic data for the complexes are given below.

2.1.3.1. dtc1. Dark brown, yield: 74%; m. p. (210–220 °C). Selected IR data (KBr pellets, cm^{-1}): ν(C═N) 1572 m, ν(N−N) 1027 s, ν(CSS) 834 m (Fig. S4). UV–Vis spectrum [DMSO, λ_{max} nm]: 279, 365, 439, 568. ESI MS Calc. for $C_{32}H_{26}N_4O_4S_4Cu$: 721.01; found (M+1): 721.57. Molar conductivity (1.0×10^{-5} M; DMSO, $\Omega^{-1}cm^2mol^{-1}$): 13.8.

2.1.3.2. dtc2. Brick red, yield: 66%; m. p. (227–230 °C). Selected IR data (KBr pellets, cm^{-1}): ν(C═N) 1574 s, ν(N−N) 1032 s, ν(CSS) 827 m (Fig. S5). UV–Vis spectrum [DMSO, λ_{max} nm]: 282, 321, 383, 703. ESI MS Calc. for $C_{32}H_{26}N_4O_4S_4Co$: 717.01; found (M+1): 717.04. Molar conductivity (1.0×10^{-5} M; DMSO, $\Omega^{-1}cm^2mol^{-1}$): 10.3.

2.1.3.3. dtc3. Light green, yield: 71%; m. p. (215–220 °C). Selected IR data (KBr pellets, cm^{-1}): ν(C═N) 1569 s, ν(N−N) 1032 s, ν(CSS) 827 m (Fig. S6). UV–Vis spectrum [DMSO, λ_{max} nm]: 281, 354, 413, 515. ESI MS Calc. for $C_{32}H_{26}N_4O_4S_4Ni$: 716.01; found (M+1): 716.01. Molar conductivity (1.0×10^{-5} M; DMSO, $\Omega^{-1}cm^2mol^{-1}$): 14.6.

2.2. Microbiology

2.2.1. Candida strains and culture conditions

Candida albicans strains including fluconazole susceptible (n = 9), fluconazole resistant (n = 5) and a control laboratory strain *C. albicans* SC5314 (ATCC MYA- 2876) were used. These clinical isolates were collected previously from HIV and cancer patients visiting different clinics at Charlotte Maxeke Johannesburg Academic Hospital and were stored at −80 °C in the Department of Clinical Microbiology and Infectious Diseases, University of the Witwatersrand, Johannesburg. The ethical clearance number M000402 obtained from Human Research Ethics Committee, University of the Witwatersrand was used to collect these isolates. As the isolates were stored in glycerol stocks at −80 °C for long time, identification and drug susceptibility was done prior to the start of this study. Rapid tests for presumptive identification of *C. albicans* from clinical isolates was carried out using the germ tube assay and the API® 20 C AUX test kit (Biomerieux, France). All the isolates were also screened for flucoazole (FLC) susceptibility by determining minimum inhibitory concentrations, following CLSI guidelines. FLC was tested and the isolates having an MIC values ≤ 2 μg/mL for FLC were considered FLC susceptible, MIC values 4 μg/mL for FLC were considered FLC susceptible dose dependent, while as the isolates having MIC ≥ 8 μg/mL were categorized as FLC resistant, following the CLSI Interpretive Guidelines for *In vitro* Susceptibility Testing of *Candida* species.

2.2.2. Antifungal susceptibility testing

Minimum Inhibitory Concentrations (MIC) and Minimum Fungicidal Concentrations (MFC) of the test compounds **sbl** and **dtc1-**

dtc3 against *C. albicans* isolates were determined by following Clinical and Laboratory Standards Institute (CLSI) guidelines M27-A3 [20]. Briefly, two-fold dilutions of test compounds (100 μL) were prepared in 96-well flat-bottom microtiter plates, followed addition of 100 μL culture inoculum (1×10^6 cells/mL) and incubated at 37 °C for 24 h. In every set of experiment fluconazole and 1% DMSO were used as positive and negative controls respectively. The MIC's were determined as the lowest concentration of the test compound that resulted in complete inhibition of growth. To determine MFC, each well without visible growth was sub-cultured onto agar plates and incubated at 37 °C for 24 h. Concentration of test compound in the first well with no growth on agar plate was taken as the MFC value.

2.2.3. Cell viability assay

Muse Count and Viability kit (EMD Millipore, USA) was used for cell viability assay following the manufacturer's instructions. Cells were differentiated in to viable and non-viable cells based on their permeability to the dyes present in the reagent. Briefly, *C. albicans* cells were treated with MIC values of test entities followed incubation at 37 °C for 3 h. Cell suspension (1×10^7 cells/mL) were prepared in saline, then 380 μL of viability reagent was added to 20 μL of prepared cell suspension and incubated at room temperature for 5 min. After incubation sample analysis was done by using MUSE cell analyser (EMD Millipore, Germany). Heat killed cells and untreated cells were used positive and negative controls respectively.

2.2.4. Annexin V and PI staining

To determine the mode of cell death by the test compounds, apoptosis was studied. FITC Annexin V Apoptosis Detection Kit I (BD Biosciences, CA, USA) was used following the manufacturer's instructions. *C. albicans* cells were exposed to MIC value of test compounds **sbl, dtc1-dtc3** for 3 h at 37 °C. After incubation protoplasts of *C. albicans* cells were prepared as described in our previous study [21], then resuspended in annexin V binding buffer at a concentration of 1×10^6 cells/mL. This prepared solution (100 μL) was taken into a new tube and then FITC annexin V (5 μL) and Propidium iodide (5 μL) were added followed by incubation in the dark at room temperature for 15 min. After incubation annexin V binding buffer (400 μL) was added to each tube and analysed by flow cytometry BD LSRFortessa cell analyser (Becton Dickinson, USA). Untreated cells and cells exposed to 2.5 mM H_2O_2 were used as negative and positive controls respectively. The cells in four different quadrants were analysed and interpreted as Q1: necrosis (Annexin V-/PI+); Q2: late apoptosis (Annexin V+/PI+); Q3: early apoptosis (Annexin V+/PI-) and Q4: viable cells (Annexin V-/PI-). FlowJo_V10 software was used to analyse the final data.

2.2.5. Haemolytic assay

Haemolytic assay was used to determine the cytotoxic effect of the test compounds following method described by Ahmad et al. 2009 with modifications. Briefly, 10 mL of Horse blood (NHLS, Johannesburg, South Africa) was centrifuged at 2000 rpm for 10 min. The obtained cell pellet was washed twice with chilled PBS, followed by preparation of 10% RBC suspension in the same solution. The 10% suspension was further diluted to 1:10 in PBS. From this suspension aliquot of 100 μL was taken and added to varying concentrations (1/2 MIC, MIC and 2 MIC) of test entities. Tubes were incubated at 37 °C for 1 h, followed by centrifugation at 2000 rpm for 10 min. After centrifugation supernatant (200 μL) was transferred to a flat-bottomed 96-well plate and absorbance was read spectrophotometrically at 450 nm using iMark microplate reader (Bio-Rad laboratories, CA, USA). Triton X-100 and PBS were used as positive and negative controls respectively. The percentage of haemolysis was calculated by the following equation:

$$\%Haemolysis = \left[\frac{A450\ of\ test\ compound\ treated\ sample - A450\ of\ buffer\ treated\ sample}{A450\ of\ 1\%\ triton\ X - A450\ of\ buffer\ treated\ sample} \right] \times 100\%$$

2.2.6. Statistical analysis

The statistical analysis was performed using Dunnett's multiple comparisons of a Two-way ANOVA test by GraphPad Prism 8.1 software. All the experiments were performed independently in triplicate (n = 3), and data were presented as mean ± standard deviation (SD). p value ****p < 0.0001 was considered as statistically significant.

3. Results and discussion

Metal complexes **(dtc1-dtc3)** with a bidentate NS ligand obtained via the condensation reaction between the respective S-benzyl dithiocarbazate and 1,3-Benzodioxole-5-carboxaldehyde in equimolar amounts was prepared as described previously [18]. (Scheme 1). The physico-analytical data of **sbl** and complexes **(dtc1-dtc3)** are provided in the experimental section.

Reaction of S-benzyldithiocarbazate with 1,3-Benzodioxole-5-carboxaldehyde was carried out in methanolic solution at 60 °C to recover a light-yellow precipitate of **sbl**. Based on the ligand structure, different reaction conditions were chosen to optimize the yield and purity of the complexes. The structures of the complexes dtc1-dtc3 were proposed on the basis of the bidentate nature of ligand **(sbl)**, established by infrared spectroscopy, mass spectrometry and elemental analysis. The mass spectra ofthe complexes (Figs. S7–S9) reported in the experimental section agreed with the molecular mass of the complexes thereby confirming 2:1 ligand to metal stoichiometry in the complexes. The purity of the ligand **(sbl)** was also evaluated using Reversed Phase-High Performance Liquid Chromatography (RP-HPLC) on a C8 column. A mixture of ACN and H_2O (20:80) was used as a mobile phase to elute the compound **(sbl)**. The chromatogram obtained after evaluation using RP-HPLC with a single peak shown in Fig. S10 confirms the purity of **sbl**. Furthermore, the ^1H NMR spectrum of **sbl** (Fig. 1) displayed peaks at ca. 8.15 ppm (−C=N−), 13.26 ppm (−NH−), 4.49 ppm (−CH_2−), 6.08 ppm (−CH_2−) and 7.21–7.43 ppm (aromatic protons). To confirm

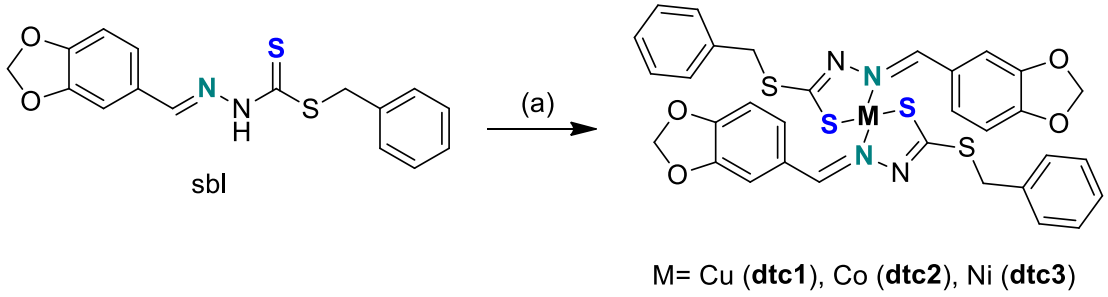

Scheme 1. Synthesis of dithiocarbazate Schiff base ligand-based metal complexes. *Reaction conditions:* (a) MeOH/CH_3CN, 1:1, r.t., 4–8 h.

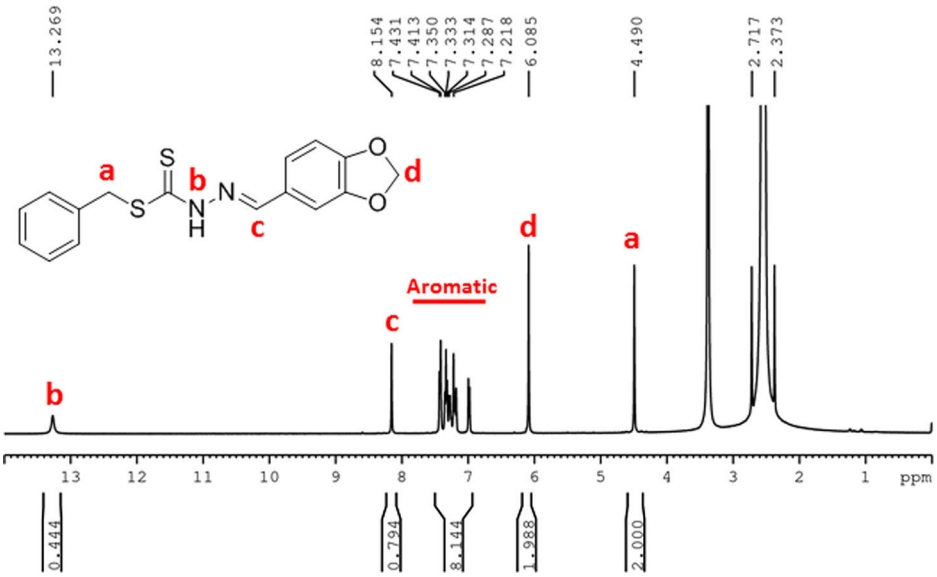

Fig. 1. ^{1}H NMR spectrum of the ligand **sbl**.

the formation of the ligand and its complexes and to better characterize them, few other techniques like FT-IR, UV–Visible, SEM, and XRD were employed. The FT-IR spectra of the **sbl** exhibited characteristic bands at ca. 3124 cm^{-1} (νNH), 2918 cm^{-1} (νCH$_2$), 1600 cm^{-1} (νC═N), 1091 cm^{-1} (νC═S) and 1033 cm^{-1} (νN–N), respectively. Upon complex formation, the band due to the azomethine ν(C═N) vibration experienced a downward shift of ca. 26–31 cm^{-1} validating its coordination to the metal ions. The disappearance of ν(C═S) at ca. 1091 cm^{-1} and the splitting of asymmetric ν(CSS) of the free ligand at ca. 990–923 cm^{-1} in the spectra of the complexes strongly backed the evidence of coordination via the thiolate sulphur atoms. Furthermore, in the complexes **dtc1-dtc3** new bands were found in the regions 544–574 cm^{-1}, attributed to υ(M–O) stretching vibrations and the bands present at 440–475 cm^{-1} in complexes have been ascribed to υ(M–N) stretching vibrations.

The electronic spectra of the ligand **(sbl)** and complexes **dtc1-dtc3** (Fig. S12) were recorded in DMSO in the region 200–800 nm. The spectra of the ligand **(sbl)** exhibited two bands at ca. 256 nm and 275 nm, attributed to the π-π* transitions in aromatic rings andtheiminic (–C═N–) group, respectively. Other bands at 328 nm and 376 nm are allotted to π-π* and n-π* transitions of thedithiocarbazate group. For all the complexes, the spectrum displayed strong bands at ca. 280 and 345 nm (sh) corresponding to the intra-ligand π- π* and n- π * electronic transitions. The spectrum of the **dtc1** complex exhibited a d–d transition band at 568 nm due to $^{2}B_{1g}\rightarrow{}^{2}E_{g}$ corresponding to a square planar geometry with a magnetic moment value of 1.82 BM due to a single unpaired electron [22]. The electronic absorption spectra of the Co(II), d^7, complex **(dtc2)** displayed a d–d band in the visible region at ca. 703 nm due to $^{1}B_{1g}\rightarrow{}^{1}A_{1g}$indicating a distorted square planar geometry for the complex also supported by the observed effective magnetic moment of 2.61BM [23]. The UV–Vis spectrum of **dtc3** complex displays absorption peaks at 281 nm, 354 nm and 515 nm. The bands at 281 nm and 354 nm corresponds to π- π* and n- π* electronic transitions, while the absorption band at 515 nm is assigned a d–d transition due to $^{1}B_{1g}\rightarrow{}^{1}A_{1g}$characteristic of low-spin square planar diamagnetic **dtc3** complexes [24,25].

The room temperature molar conductance values of the complexes **(dtc1-dtc3)** were obtained in 10^{-5} M DMSO solutions. The low molar conductivity values 13.8 $\Omega^{-1}cm^{2}mol^{-1}$, 10.3 $\Omega^{-1}cm^{2}mol^{-1}$ and 14.6 $\Omega^{-1}cm^{2}mol^{-1}$ for complexes **dtc1, dtc2** and **dtc3** respectively, are indicative of the non-electrolytic nature of all the complexes [26].

Thermo grams of **dtc1-dtc3** complexes were recorded in the temperature range of 40–800 °C. The results obtained are in close agreement with the theoretical formula of the compounds as suggested by the analytical data. The obtained thermo grams revealed that all the complexes were stable up to a temperature of about 210–230 °C exhibiting a two-step decomposition in each complex. All the complexes did not show any loss of hydrated or coordinated water molecules, which is in accordance with the predicted structures of the complexes. In the **dtc1** complex the first decomposition occurred in the temperature range of 210–430 °C may be ascribed to the loss of $C_{16}H_{14}N_2O_2S_2$ group and the second decomposition observed in the range of 430–760 °C may be assigned to the removal of other $C_{16}H_{14}N_2O_2S_2$ group, thereby confirming the loss of one part of the ligand in the first step and the remaining ligand molecule in the second step with Cu metal as the residue. The **dtc2** and **dtc3** complexes showed similar decomposition patterns like that of **dtc1** complex with slight deviations in the recorded thermo grams. Residues of (Co, Ni) metal were recovered in all the cases. A characteristic TGA diagram of the complexes is given in Fig. S13.

Single crystal X-Ray diffraction is a more precise technique that furnishes complete information about the structure of the compounds. But despite of our several efforts of recrystallization, none of the compounds was obtained in the crystalline form. Therefore, powder XRD of the ligand and the complexes was performed to describe the structure of the synthesized compounds. The powder XRD pattern of the ligand **(sbl)**, **dtc1, dtc2** and **dtc3** complexes recorded in the range of 2θ = 10–80° are shown in Fig. 2. From the XRD data, the ligand **(sbl)** and complexes, display sharp crystalline peaks confirming their crystalline nature. The average crystallite size of the synthesized compounds was calculated using Scherrer equation [27]. The ligand and complexes have an average crystallite size of 31.23, 13.25, 25.70 and 17.21 nm, respectively, suggesting that the compounds are polycrystalline.

SEM analysis was performed to determine the surface morphology of the ligand **(sbl)** and its complexes **dtc1-dtc3**. The SEM images given in Fig. 3 clearly indicate that the compounds exhibited different morphological structures. The ligand **sbl** shows irregularly shaped particles while as the complexes exhibit rod like, grass like and fibre/needle like morphologies. The different surface morphologies of metal complexes from that of the ligand further confirm the interaction of the metal ions with the ligand molecule. The average grain size (17–36 nm) obtained from SEM analysis confirm that the complexes are polycrystalline in nature which is well in accordance with XRD analysis.

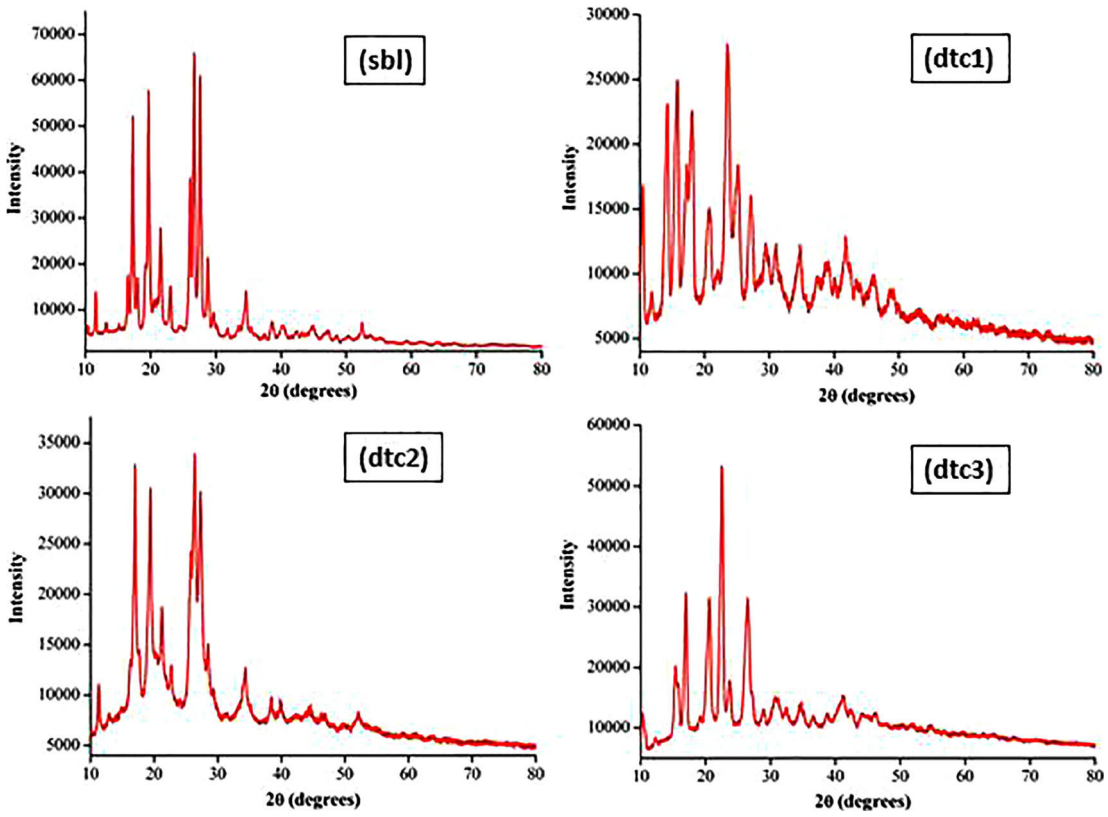

Fig. 2. Powder XRD patterns of ligand **sbl** and its complexes**dtc1, dtc2** and **dtc3**.

4. Biological activity

4.1. Antifungal activity

The *in vitro* susceptibility of *C. albicans* isolates (n = 15) against the test compounds **(sbl** and complexes **dtc1-dtc3)**, were evaluated by determining MIC and MFC values and the results are summarized in Table 1. From the results, it is evident that all the three metal complexes **dtc1-dtc3** exhibited enhanced antifungal activity than the ligand **(sbl)**. The mean range of MIC and MFC values for all test compounds against different FLC susceptible *C. albicans* strains were 1 – ≥ 512 μg/mL and 4 – 1024 μg/mL respectively. These figures for different FLC resistant *C. albicans* strains were in the range of 16 – 512 μg/mL and 32 – 1024 μg/mL respectively. The highest antifungal activity was observed for the

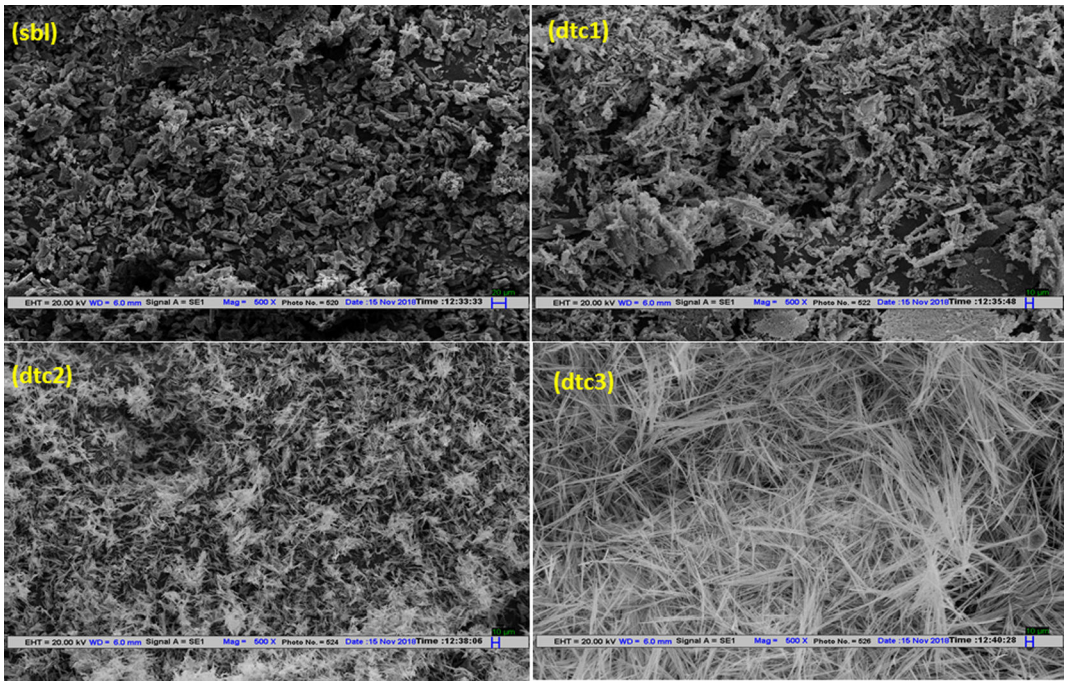

Fig. 3. SEM images of ligand **(sbl)** and complexes **dtc1, dtc2** and **dtc3**.

Table 1
Mean minimum inhibitory concentrations and minimum fungicidal concentrations of Schiff base ligand and its derivatives against different *C. albicans*.

Candida strains			sbl	dtc1	dtc2	dtc3	FLC
FLC Susceptible strains (n = 10)	**SC5314**	**MIC**	256	64	4	0.5	0.125
		MFC	512	128	16	1	
	4554	**MIC**	512	128	4	0.5	0.125
		MFC	1024	512	16	1	
	4180	**MIC**	512	64	4	1	0.25
		MFC	1024	128	16	4	
	4251	**MIC**	512	128	8	1	0.125
		MFC	1024	1024	32	4	
	4563	**MIC**	256	64	8	1	0.25
		MFC	512	128	32	4	
	4175	**MIC**	512	128	16	0.5	0.25
		MFC	1024	512	64	4	
	4179	**MIC**	1024	128	8	0.5	0.5
		MFC	2048	512	32	2	
	4576	**MIC**	1024	64	4	2	0.125
		MFC	2048	128	16	8	
	2281	**MIC**	512	256	16	2	0.25
		MFC	1024	1024	64	8	
	2367	**MIC**	256	256	8	1	0.5
		MFC	512	1024	32	4	
FLC Resistant strains (n = 5)	**4106**	**MIC**	512	256	32	8	16
		MFC	–	512	64	16	
	4135	**MIC**	512	256	32	8	32
		MFC	–	512	64	16	
	4085	**MIC**	1024	512	64	16	16
		MFC	–	1024	128	32	
	4324	**MIC**	2048	1024	128	32	64
		MFC	–	2048	256	64	
	4122	**MIC**	1024	512	64	16	32
		MFC	–	1024	128	32	

nickel (II) metal complex **dtc3** with MIC and MFC range of 0.5 – 32 μg/mL and 1 – 64 μg/mL respectively, followed by **dtc2** (MIC 4 – 128 μg/mL and MFC 16 – 256 μg/mL), and **dtc1** (MIC 64 – 1024 μg/mL and MFC 128 – 2048 μg/mL). The ligand showed the least antifungal effect with MIC and MFC values of 256 – 2048 μg/mL and 512 – > 2048 μg/mL respectively. These results indicated that metalation of dithiocarbazate derived Schiff base compounds significantly improved their antifungal activity.

4.2. Cell viability

The cell viability of *C. albicans* SC5314 at MIC values of different test entities are presented in Fig. 4. The results demonstrated these test compounds considerably decreased the cell viability when compared to untreated control cells. After treatment, the ligand**sbl** showed only 23% ± 2.5% cell death, while there was a drastic increase in percentage of cell death after treatment with metal complexes **dtc1-dtc3**. Ni complex **(dtc3)** exhibited highest percentage of cell death 80% ± 8.5% followed by Co **(dtc2)** 70% ± 7.5% and Cu **(dtc1)** with 47% ± 7.5%. The negative (untreated) and positive (heat killed) controls exhibited 2% ± 1.5% and 95% ± 2.5% cell death respectively. These results revealed that after metalation test compounds showed improved antifungal activity with fungicidal nature. The viability results reflect the same pattern as observed in the MIC determination, which also advocates the reliability of this technique to be used in antifungal studies. To further differentiate the results between the cells and debris and/or non-nucleated cells, cell size index was also done in the same assay and it was confirmed that the results are due to live and dead cells (Fig. 4).

4.3. Annexin V and PI staining

Annexin V-FITC and Propidium iodide double staining was performed to observe the apoptotic effect of the test compounds against *C. albicans* SC5314. The annexin V detects phosphatidylserine (PS) externalization and PI stains necrotic and dead cells. *C. albicans* cells after exposed to MIC values of test compounds showed varying degree of apoptosis represented in Fig. 5 and summarized in Fig. 6. Among the test compounds, the Ni metal complex **dtc3** was the most active which induced early apoptosis (17% ± 4.2%), late apoptosis (38% ± 2.6%) and necrosis (20% ± 2.5%). Co and Cu metal complexes **dtc2** and **dtc1** induced early apoptosis (6% ± 3.5%), late apoptosis (34% ± 3.6%), necrosis (23% ± 1.5%) and early apoptosis (11% ± 1.2%), late apoptosis (27% ± 2.5%) and necrosis (13% ± 2.0%), respectively. In contrary, the ligand **sbl** showed only 2% ± 1.0%, 9% ± 3.6% and 5% ± 2.3% of early apoptosis, late apoptosis and necrosis respectively. Negative control (untreated sample) exhibited early apoptosis (2% ± 1.0%), late apoptosis (1% ± 1.5%) and necrosis (1% ± 1.0%) and positive control (H_2O_2 exposed sample) showed early apoptosis (32% ± 2.5%), late apoptosis (25% ± 3.0%) and necrosis (2% ± 1.5%). From the results it was observed that all these test compounds can induce apoptosis in *C. albicans* cells mainly through late apoptosis and necrotic pathways.

4.4. Haemolytic activity

To determine the cytotoxicity of these test compounds, haemolytic assay using horse red blood cells was performed. When compared to positive control (Triton X-100), which causes 100% lysis these test compounds exhibited significantly less haemolysis. PBS was used as a negative control which showed no lysis of RBCs. Metal complexes **(dtc1-dtc3)** showed cell haemolysis in the range of 4–6%, 8–12% and 12–23% at 1/2 MIC, MIC and 2 MIC values respectively while as the ligand **sbl** exhibited 7% ± 3%, 12% ± 3.5% and 27% ± 5.5% cell haemolysis at 1/2 MIC, MIC and 2 MIC values, respectively. Further, results also indicated that the haemolytic activity of these compounds is concentration dependent. Red blood cells provide a handy tool for toxicity studies of new compounds, because they are readily available, their membrane properties are well known, and their lysis is easily monitored by measuring the release of haemoglobin [28]. The comparative study of **sbl** and its complexes **(dtc1-dtc3)** with Triton-X, which is well known to cause haemolysis in RBCs, indicated that these compounds within their MIC ranges and above showed significantly less cytotoxicity (Fig. 7).

C. albicans is the most widespread opportunistic fungal pathogen in the human body, causing mucosal and systemic infections. Fungal-selective targets are insufficient due to the fact that most eukaryotes share similar metabolic pathways and essential cellular machinery with humans. Therefore, new compounds are needed to be identified or synthesized that can cause fungal programmed cell death also called as apoptosis to allow specific manipulation of cell death without costing human counterparts. Apoptosis in *C. albicans* can be induced by several external and internal factors and has been regulated at biochemical and molecular levels [29]. Flow cytometry analysis revealed that the *C. albicans* cells exposed to sub-MIC concentrations of the test compounds showed the movement of phosphatidylserine to the outer leaflet of the plasma membrane. The externalisation of phospholipids results with the binding of annexin V, which was detected by flow cytometer. It has been extensively observed that fungicidal compounds at sub-MIC values show programmed cell death [29,30]. Previous studies have shown that several stimuli including hydrogen peroxide, metal complexes, diallyl disulfide, farnesol, lactoferrin, defensins and the antifungal agents amphotericin B and caspofungin cause *Candida albicans* cells to undergo apoptosis [31–36]. Cell wall stress stemming from inhibition of (1,3)-β-D-glucan, which is essential for ergosterol biosynthesis is also a trigger for apoptosis. In our previous studies we found that metal complexes have the potential to inhibit ergosterol biosynthesis, resulting in apoptotic death of *C. albicans* [37–39]. It has also been established that metal complexes affect mitochondrial function, retard the synthesis of cytochrome *b* and c and uncouple respiration. Treatment of fungal cells

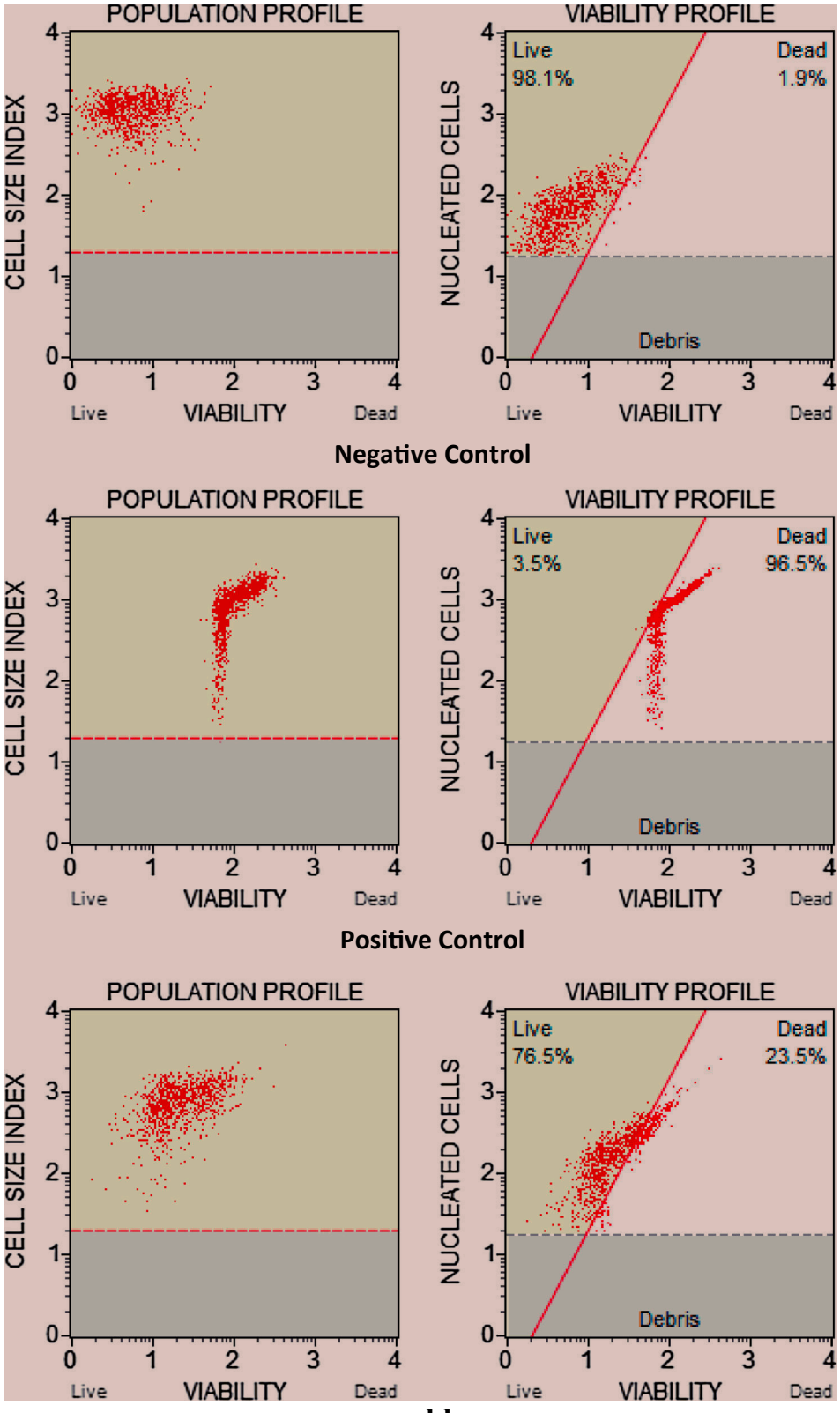

Fig. 4. Cell Viability assay for *C. albicans* SC5314: Cells at a density of 1×10^7 were exposed to MIC values of **sbl** and its derivatives. Percentage live and dead cells are shown in two different subsets. Negative and positive controls represent untreated and heat killed cells respectively. Cell size index represented that the results are due to live and dead cells and not due to the debris.

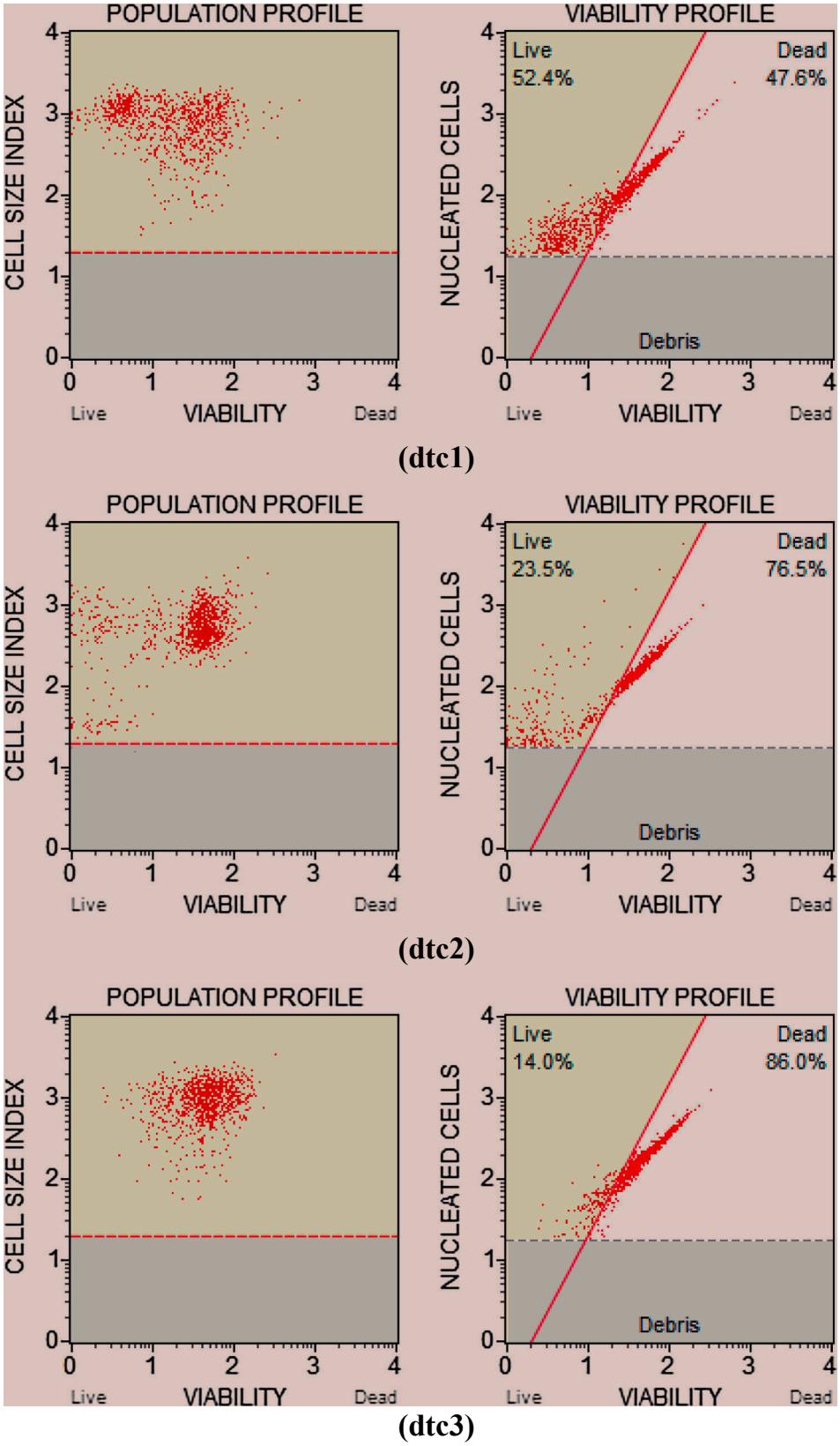

Fig. 4. (*continued*)

with Cu(II) and Ag(I) complexes results in a reduced amount of ergosterol in the cell membrane and subsequent increase in its permeability [34]. Also cells exposed to Cu(II) and Mn(II) complexes demonstrate an elevation in oxygen uptake, which goes to show that the metal complexes damage mitochondria and uncouple respiration. Ag(I) complexes have been shown to cause extensive, non-specific DNA cleavage to *C. albicans*, disrupt cell division and induce gross distortions in fungal cell morphology [34]. Since metal complexes are known to

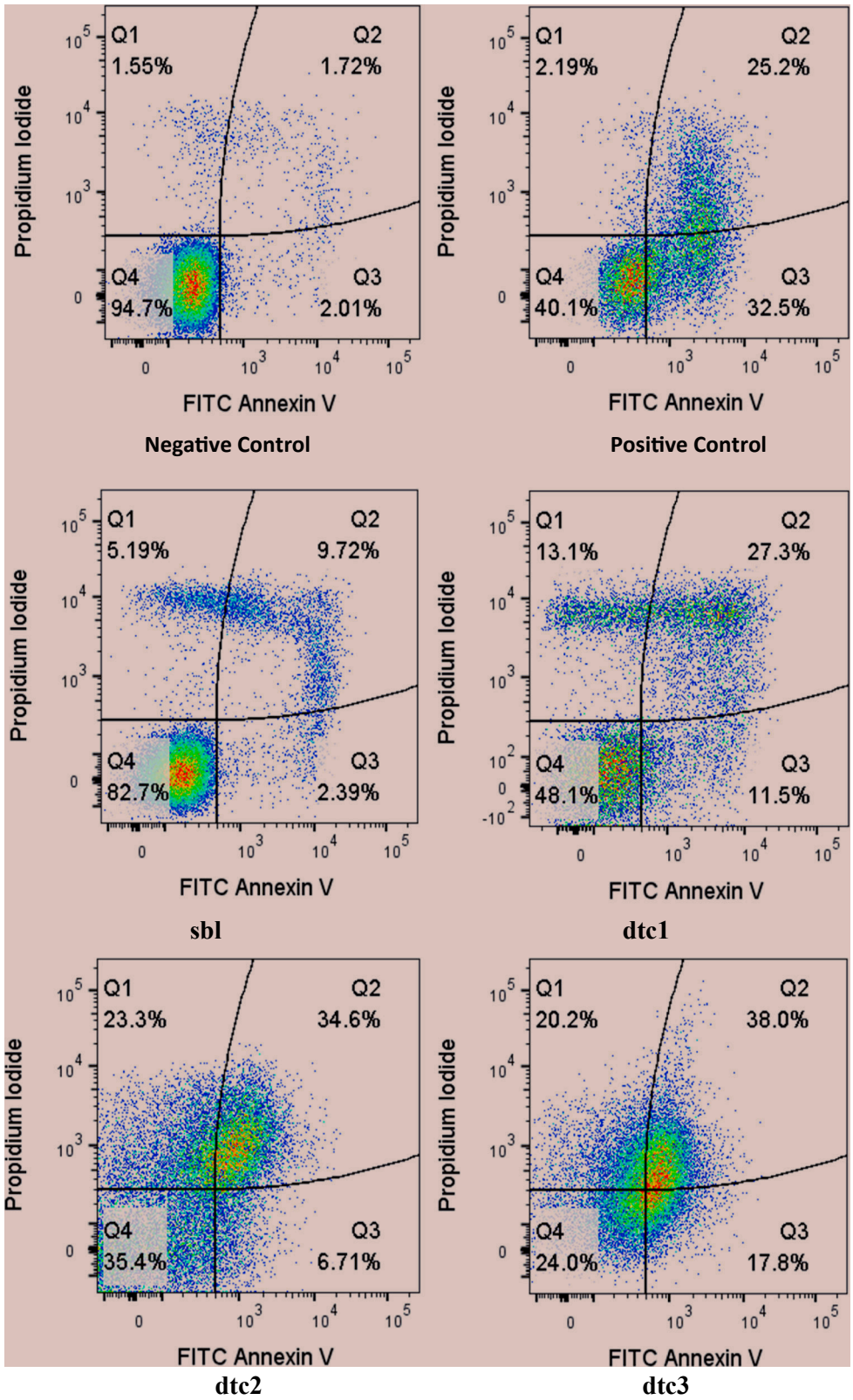

Fig. 5. Cell apoptosis measured by flowcytometry using Annexin V-FITC and PI double staining. *C. albicans* SC5314 cells were exposed to MIC values of test compounds. Untreated cells and cells exposed to H_2O_2 were used as negative and positive controls respectively. In each density plot quadrant Q1: shows necrotic cells (annexin- PI^+); Q2: late apoptotic cells ($annexin^+$ PI^+); Q3: early apoptotic cells ($annexin^+$ PI^-) and Q4: shows viable cells ($annexin^-$ PI^-).

affect mitochondrial function and it is the site for both the origin and target of ROS, mitochondria and ROS play an essential role in apoptotic processes [40,41]. During apoptosis, oxidative stress induces the mitochondrial permeability transition pore (PTP) to open, which then triggers the mitochondrial outer membrane permeabilization (MOMP) that is involved in the release of cytochrome *c* and other proapoptotic

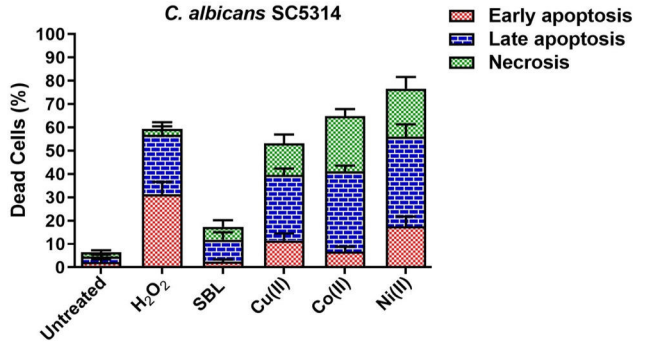

Fig. 6. Percentage of cells showing early apoptosis, late apoptosis and necrosis after being exposed to the MIC values of **sbl** and its derivatives **[Cu(II) dtc1, Co (II) dtc2 and Ni(II) dtc3]**. Untreated cells and cells exposed to H_2O_2 (250 μmol/L) were used as negative and positive controls, respectively. Data are presented from three independent experiments using the means ± S.D.

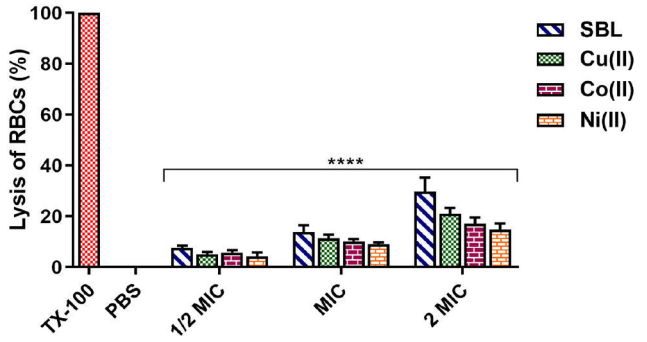

Fig. 7. Heamolytic activity of **sbl**, **Cu(II) dtc1, Co(II) dtc2 and Ni(II) dtc3** at varying concentrations showed significant difference in hemolysis of RBCs compared to positive control 1% Triton X-100 (reference for 100% haemolysis). Phosphate buffer saline was used as negative control, which showed complete absence of haemolysis. Data are presented from three independent experiments using means ± S.D. ****$p < 0.0001$.

factors, leading to subsequent metacaspase activation [42]. ROS can also directly induce apoptosis in a metacaspase-dependent manner [43].

Besides ROS, Ca^{2+} is also closely related to apoptosis [44]. Under oxidative stress, Ca^{2+} signal can lead to PTP opening and release of cytochrome *c* and other proapoptotic factors, which ultimately results in the formation of apoptotic bodies and cell death. Although there is no MCU complex (mitochondrial calcium uniporter) in yeast mitochondria, apoptotic stimuli could induce enough mitochondrial Ca^{2+} to undergo the permeability transition, which is accompanied by increased ROS and cytosolic Ca^{2+} levels. Once PTP opens, Ca^{2+} levels in the cytosol and matrix equilibrate and stabilize PTP in the open conformation, leading to matrix swelling, outer mitochondrial membrane damage, and release of proapoptotic proteins, thereby causing cell death. Several studies reported that antioxidant or mitochondrial Ca^{2+} channel inhibitors could rescue cells from natural product-induced apoptosis [45–47], indicating that oxidative stress or elevated mitochondrial Ca^{2+} might be the reasons leading to apoptosis. High antifungal activity of the complexes, especially the Ni complex **dtc3** demands further *in vivo* studies against *C. albicans* and other non-albicans *Candida* species. Low toxicity and potential to cause apoptosis and necrosis magnifies its potential to be developed as a novel antifungal drug.

5. Conclusion

Metal-based drugs have several promising advantages in comparison to organic ligands and have gained trust from the researches after the worldwide approval of the drug cisplatin. The distinct mechanism of action from conventional drugs makes them perfect alternatives to the conventional drugs where resistance has already appeared. In this direction, a series of new transition metal complexes were synthesized, characterized and evaluated for their antifungal activities. The biological profiles revealed that the complexes **(dtc1-dtc3)** were more active than the free ligand **(sbl)**. Complex **dtc3** exhibited a minimum inhibitory concentration (MIC) value ranging from 1 to 32 μg/mL. The mechanism of action appears to be due to apoptosis in *C. albicans*, causing phosphatidylserine externalization as revealed by Annexin V-FITC and propidium iodide staining assays. Furthermore, low toxicity and potential to cause apoptosis and necrosis further amplifies its potential to be developed as a novel antifungal drug.

Ethics approval

This study was approved by the Human Research Ethics Committee of University of the Witwatersrand (Johannesburg, South Africa). Existing stock cultures of *Candida albicans* used in this study were stored in the department of Clinical Microbiology and Infectious Diseases, University of the Witwatersrand, Johannesburg, South Africa.

Funding

M. A. M gratefully acknowledges Council of Scientific and Industrial Research (CSIR) New Delhi, India for the financial assistance in the form of Senior Research Fellowship (Grant No: 09/466(0215) 2K19EMR-1).

Declaration of Competing Interest

The authors declare that they have no known competing financial interests or personal relationships that could have appeared to influence the work reported in this paper.

Appendix A. Supplementary material

Supplementary data to this article can be found online at https://doi.org/10.1016/j.bioorg.2020.103771.

References

[1] www.wto.org/english/news_e/news16_e/heal_29aug16_e.pdf.
[2] N.S. Ng, P. Leverett, D.E. Hibbs, Q. Yang, J.C. Bulanadi, M.J. Wua, J.R. Aldrich-Wright, The antimicrobial properties of some copper(II) and platinum(II) 1,10-phenanthroline complexes, Dalton Trans. 9 (2013) 3196–3209.
[3] A.S. Abd-el-aziz, C. Agatemor, N. Etkin, D.P. Ovary, M. Lanteigne, K. Mcquillan, R.G. Kerr, Antimicrobial Organometallic Dendrimers with tunable activity against multidrug-resistant bacteria, Biomacromolecules 16 (2015) 3694–3703.
[4] F. Li, J.G. Collins, F.R. Keene, Ruthenium complexes as antimicrobial agents, Chem. Soc. Rev. 44 (2015) 2529–2542.
[5] J. Duan, H. Liu, P. Jeyakkumar, L. Gopala, S. Li, R. Geng, C. Zhou, Design, synthesis and biological evaluation of novel Schiff base-bridged tetrahydroprotoberberine triazoles as a new type of potential antimicrobial agents, Medchemcomm. 8 (2017) 907–916.
[6] M.A. Malik, O.A. Dar, P. Gull, M.Y. Wani, A.A. Hashmi, Heterocyclic schiff base transition metal complexes in antimicrobial and anticancer chemotherapy, Medchemcomm. 9 (2018) 409–436.
[7] F. Li, J.G. Collins, F.R. Keene, Ruthenium complexes as antimicrobial agents, Chem. Soc. Rev. 44 (2015) 2529–2542.
[8] S. Rafique, M. Idrees, A. Nasim, H. Akbar, A. Athar, Transition metal complexes as potential therapeutic agents, Biotechnol. Mol. Biol. Rev. 5 (2010) 38–45.
[9] V. Bobbarala, A Search for Antibacterial Agents, InTech Press, Rijeka, Croatia, 2012.
[10] M.D. Rhodes, P.J. Sadler, M.D. Scawen, S. Silver, Effects of gold(I) antiarthritic drugs and related compounds on Pseudomonas putida, J. Inorg. Biochem. 46 (1992) 129–142.
[11] A.D. Richards, A. Rodger, M.J. Hannon, A. Bolhuis, Antimicrobial activity of an iron triple helicate, Int. J. Antimicrob. Agents 33 (2009) 469–472.
[12] N.S. Ng, P. Leverett, D.E. Hibbs, Q. Yang, J.C. Bulanadi, M.J. Wu, J.R. Aldrich-Wright, The antimicrobial properties of some copper(ii) and platinum(ii) 1,10-phenanthroline complexes, Dalton Trans. 42 (2013) 3196–3209.

[13] M.A. Neelakantan, M. Esakkiammal, S.S. Mariappan, J. Dharmaraja, T. Jeyakumar, Synthesis, characterization and biocidal activities of some Schiff base metal complexes, Indian J. Pharm. Sci. 72 (2010) 216–222.

[14] B.S. Sekhon, Matrix metalloproteinases – an overview, J. Pharm. Educ. Res. 1 (2010) 1–20.

[15] L.J. Ming, Structure and function of metalloantibiotics, Med. Res. Rev. 23 (2003) 697–762.

[16] S.K. Nandanwar, H.J. Kim, Anticancer and antibacterial activity of transition metal complexes, Chem. Select 4 (2019) 1706–1721.

[17] J.A. Lemire, J.J. Harrison, R.J. Turner, Antimicrobial activity of metals: mechanisms, molecular targets and applications, Nat. Rev. Microbiol. 11 (2013) 371.

[18] M.L. Low, L. Maigre, P. Dorlet, R. Guillot, M.J Pagès, K.A. Crouse, C. Policar, N. Delsuc, Conjugation of a New Series of Dithiocarbazate Schiff Base Copper (II) Complexes with Vectors Selected to Enhance Antibacterial Activity Conjugation of a New Series of Dithiocarbazate Schiff Base Copper (II) Complexes with Vectors Selected to Enhance Anti- bacterial Activity, Bioconjugate Chem. 25 (2014) 2269–2284, https://doi.org/10.1021/bc5004907.

[19] M.A. Ali, A.H. Mirza, R.J. Butcher, M.T.H. Tarafder, T. Boon, A.M. Ali, Biological activity of palladium (II) and platinum (II) complexes of the acetone Schiff bases of S -methyl- and S -benzyldithiocarbazate and the X-ray crystal structure of the [Pd (asme) 2] (asme 5 anionic form of the acetone Schiff base of S -methyldithiocarbazate) complex, J. Biol. Inorg. Chem. 92 (2002) 141–148.

[20] CLSI, Performance Standards for Antifungal Susceptibility Testing of Yeasts, 1st ed. CLSI supplement M60. Clinical and Laboratory Standards Institute, Wayne, PA, 2017.

[21] A. Khan, A. Ahmad, L.A. Khan, N. Manzoor, *Ocimum sanctum* (L.) essential oil and its lead molecules induce apoptosis in *Candida albicans*, Res. Microbiol. 165 (2014) 411–419.

[22] S. Tejaswi, M.P. Kumar, A. Rambabu, N. Vamsikrishna, Shivaraj, Synthesis, structural, DNA binding and cleavage studies of Cu (II) complexes containing benzothiazole cored schiff bases, J. Fluoresc. 26 (2016) 2151–2163.

[23] A.B.P. Lever, Inorganic Electronic Spectroscopy, Elsevier, Amsterdam, 1984.

[24] R. Takjoo, R. Centore, Synthesis, X-ray structure, spectroscopic properties and DFT studies of some dithiocarbazate complexes of nickel (II), J. Mol. Struct. 1031 (2013) 180–185.

[25] C.F. Wise, D. Liu, K.J. Mayer, P.M. Crossland, Carolyn L. Harley, William R. McNamara, A nickel complex of a conjugated bisdithiocarbazate schiff base for the photocatalytic production of hydrogen, Dalton Trans. 00 (2013) 1–3.

[26] M.S. Nair, D. Arish, R.S. Joseyphus, DNA cleavage studies of some heterocyclic Schiff base metal complexes, J. Saudi Chem. Soc. 16 (2012) 83–88.

[27] C.J. Dhanaraj, I.U. Hassan, J. Johnson, J. Joseph, R.S. Joseyphus, Synthesis, spectral characterization, DNA interaction, anticancer and molecular docking studies on some transition metal complexes with bidentate ligand, J. Photochem. PhotoBio. 162 (2016) 115–124, https://doi.org/10.1016/j.jphotobiol.2016.06.032.

[28] A. Ahmad, A. Khan, N. Manzoor, L.A. Khan, Evolution of ergosterol biosynthesis inhibitors as fungicidal against, Candida 48 (2010) 35–41.

[29] D. Carmona-Gutierrez, T. Eisenberg, S. Buttner, C. Meisinger, G. Kroemer, F. Madeo, Apoptosis in yeast: triggers, pathways, subroutines, Cell Death Differ 17 (2010) 763–773.

[30] B. Almeida, A. Silva, A. Mesquita, B. Sampaio-Marques, F. Rodrigues, P. Ludovico, Drug-induced apoptosis in yeast, Biochim. Biophys Acta 1783 (2008) 1436–1448.

[31] M.E. Shirtliff, B.P. Krom, R.A. Meijering, B.M. Peters, J. Zhu, M.A. Scheper, M.L. Harris, M.A. Jabra-Rizk, Farnesol-induced apoptosis in Candida albicans, Antimicrob. Agents Chemother. 53 (2009) 2392–2401.

[32] H. Lu, Z. Zhu, L. Dong, X. Jia, X. Sun, L. Yan, Y. Chai, Y. Jiang, Y. Cao, Lack of trehalose accelerates H_2O_2-induced Candida albicans apoptosis through regulating Ca^{2+} signaling pathway and caspase activity, PLoS One 6 (2011) 15808.

[33] I.S. Hwang, J. Lee, J.H. Hwang, K.J. Kim, D.G. Lee, Silver nanoparticles induce apoptotic cell death in Candida albicans through the increase of hydroxyl radicals, FEBS J. 279 (2012) 1327–1338.

[34] A. Eshwika, B. Coyle, M. Devereux, M. McCann, K. Kavanagh, Metal complexes of 1,10-phenanthroline-5,6-dione alter the susceptibility of the yeast Candida albicans to amphotericin B and miconazole, Biometals 17 (2004) 415–422.

[35] K.M. Lemar, M.A. Aon, S. Cortassa, B. O'Rourke, C.T. Muller, D. Lloyd, Diallyl disulphide depletes glutathione in Candida albicans: oxidative stress-mediated cell death studied by two-photon microscopy, Yeast 24 (2007) 695–706.

[36] H. Nikawa, L.P. Samaranayake, J. Tenovuo, K.M. Pang, T. Hamada, The fungicidal effect of human lactoferrin on *Candida albicans* and *Candida krusei*, Arch. Oral Biol. 38 (1993) 1057–1063.

[37] O.A. Dar, S.A. Lone, M.A. Malik, M.Y. Wani, Md.I.A. Talukdar, A.S. Al-Bogami, A.A. Hashmi, A. Ahmad, Heteroleptic transition metal complexes of Schiff-base-derived ligands exert their antifungal activity by disrupting membrane integrity, Appl. Organometall. Chem. 33 (2019) 5128.

[38] O.A. Dar, S.A. Lone, M.A. Malik, M.Y. Wani, A. Ahmad, A.A. Hashmi, New transition metal complexes with a pendent indole ring: insights into the antifungal activity and mode of action, RSC Adv. 9 (2019) 15151–15157.

[39] O.A. Dar, S.A. Lone, M.A. Malik, F.M. Aqlan, M.Y. Wani, A.A. Hashmi, A. Ahmad, Synthesis and synergistic studies of isatin based mixed ligand complexes as potential antifungal therapeutic agents, Heliyon 5 (2019) 02055.

[40] A. Terman, B. Gustafsson, U.T. Brunk, The lysosomal-mitochondrial axis theory of postmitotic aging and cell death, Chem. Biol. Interact. 163 (2006) 29–37.

[41] C. Pereira, R. Silva, L. Saraiva, B. Johansson, M. Sousa, M. Côrte-Real, Mitochondria-dependent apoptosis in yeast, Biochim. Biophys. Acta. 1783 (2008) 1286–1302.

[42] H.U. Simon, A. Hajyehia, F. Levischaffer, Role of reactive oxygen species (ROS) in apoptosis induction, Apoptosis 5 (2000) 415–418.

[43] X.Z. Wu, W.Q. Chang, A.X. Cheng, L.M. Sun, H.X. Lou, Plagiochin E, an antifungal active macrocyclic bis(bibenzyl), induced apoptosis in Candida albicans through a metacaspase-dependent apoptotic pathway, Biochim. Biophys. Acta 2010 (1800) 439–447.

[44] M. Carraro, P. Bernardi, Calcium and reactive oxygen species in regulation of the mitochondrial permeability transition and of programmed cell death in yeast, Cell Calcium 60 (2016) 102–107.

[45] R. Zhang, I. Humphreys, R.P. Sahu, Y. Shi, S.K. Srivastava, In vitro and in vivo induction of apoptosis by capsaicin in pancreatic cancer cells is mediated through ROS generation and mitochondrial death pathway, Apoptosis 13 (2008) 1465–1478.

[46] D.G. Yun, D.G. Lee, Silibinin triggers yeast apoptosis related to mitochondrial Ca^{2+} influx in Candida albicans, Int. J. Biochem. Cell Biol. 80 (2016) 1–9.

[47] W. Lee, D.G. Lee, Reactive oxygen species modulate itraconazole induced apoptosis via mitochondrial disruption in *Candida albicans*, Free Radic Res. 52 (2017) 39–50.

Heliyon 5 (2019) e02055

Contents lists available at ScienceDirect

Heliyon

journal homepage: www.heliyon.com

Synthesis and synergistic studies of isatin based mixed ligand complexes as potential antifungal therapeutic agents

Ovas Ahmad Dar [a], Shabir Ahmad Lone [b], Manzoor Ahmad Malik [a], Faisal Mohammed Aqlan [c], Mohmmad Younus Wani [c], Athar Adil Hashmi [a,*], Aijaz Ahmad [b,d,**]

[a] Department of Chemistry, Jamia Millia Islamia, New Delhi 110025, India
[b] Clinical Microbiology and Infectious Diseases, School of Pathology, Faculty of Health Sciences, University of the Witwatersrand, Johannesburg, 2193, South Africa
[c] Chemistry Department, Faculty of Science, University of Jeddah, P.O. Box 80327, Jeddah 21589, Kingdom of Saudi Arabia
[d] Infection Control, Charlotte Maxeke Johannesburg Academic Hospital, National Health Laboratory Service, Johannesburg, 2193, South Africa

ARTICLE INFO

Keywords:
Inorganic chemistry
Organic chemistry
Pharmaceutical chemistry
Microbiology
Pharmaceutical science

ABSTRACT

Metal based drugs are important class of chemotherapeutic agents that have the potential to circumvent drug resistance. Increasing drug resistance, treatment failures and limited treatment options necessitates the development of new therapeutic drugs with different mechanisms of action. Towards this direction, we synthesized a series of isatin based mixed ligand complexes of [Cu(dbm)LClH$_2$O] **(mlc1)**, [Co(dbm)LCl$_2$]$^-$ **(mlc2)** and [Ni(dbm)LClH$_2$O] **(mlc3)** and evaluated their antifungal activity alone and in combination with fluconazole (FLC) against seven different *Candida albicans* isolates. The insight mechanism of antifungal action was revealed by studying apoptosis via terminal deoxynucleotidyl transferase dUTP nick-end labeling (TUNEL) assay. The study revealed that all these compounds showed antifungal activity at varying concentrations with **mlc3** as the most potent compound with minimum inhibitory concentration ranging from 0.5–8 μg/mL and minimum fungicidal concentration ranging from 4–16 μg/mL. Upon combination with FLC, most of the interactions were either synergistic (54 %) or additive (32 %) with no antagonistic combination against any of the tested isolate. The study on their mechanism of action revealed that these compounds show apoptotic effect on *C. albicans* at sub-inhibitory concentrations, suggesting that strategies to target this process may augment the current antifungal treatment modalities.

1. Introduction

Fungal infections take more than 1.3 million lives each year worldwide, nearly as many as tuberculosis. There is an urgent need for the development of new antifungal agents or strategies that could add to the current armament against fungi and augment the treatment options which have been challenged by increasing multi-drug resistance. A good strategy to design new antifungal drugs has been the complexation of bioactive compounds with transition metals. Metal complexes of sulfonamide drugs, fluoro quinolones and penicillin have already been synthesized and it was observed that metalation enhances the efficacy of the already established drugs [1, 2, 3]. Pd(II) complex of tetracycline has been reported to have potency sixteen times more than the parent compound against *E.coli HB101/pBR322*, a bacterial strain resistant to tetracycline whereas Pd(II) complex of doxycycline is two times more potent than doxycycline against resistant strain [2]. In another study Copper(II) norfloxacin complex sharply decreased the viability and proliferation rate of HL-60 cells, leading to cell death through apoptosis in a time-dependent manner [1].

Isatin possess an indole ring structure, common to many pharmaceuticals and heterocyclic natural products of biological interest [4]. Its derivatives have shown important biological activities such as antimicrobial, anticonvulsant, cysticidal, antimalarial, herbicidal, antimycobacterial, anticancer, anti-inflammatory and antiviral [5, 6]. They also exhibit anti-HIV, antihelminthic and antiprotozoal activities [7]. Dibenzoylmethane (DBM) on the other hand belongs to a small group of flavonoids known as β-hydroxychalcones [8] and is rarely found in nature. DBM and its derivatives have attracted considerable attention because of their promising biological activities [9, 10]. DBM has also been found as a possible candidate for dementia treatment [11]. Based on

* Corresponding author.
** Corresponding author.
E-mail addresses: aah_ch@yahoo.co.in (A.A. Hashmi), aijaz.ahmad@wits.ac.za (A. Ahmad).

https://doi.org/10.1016/j.heliyon.2019.e02055
Received 13 December 2018; Received in revised form 7 June 2019; Accepted 4 July 2019

our previous studies it is our premise that complexation of bioactive ligands with transition metals and combination therapy greatly improves the treatment efficacy and provides a broader treatment window that greatly helps to circumvent drug resistance [12, 13, 14]. In this study, we proposed to prepare some mixed ligand complexes of a ligand derived from isatin and DBM as a co-ligand and tested them against different FLC susceptible and resistant *C. albicans* isolates alone and in combination with FLC to obtain new antifungal agents or potentiators that could be used in combination therapy. The mechanism of action was studied by TUNEL assay.

2. Results and discussion

The mixed ligand metal complexes (**mlc1-mlc3**) were successfully synthesized by reacting equimolar amounts of Schiff base ligand (**L**) with the corresponding metal salts and dibenzoylmethane in presence of NaOH as shown in Scheme 1. The synthesized metal complexes were colored, air stable and insoluble in most of the organic solvents except DMF and DMSO. The ligand (**L**) and metal complexes (**mlc1-mlc3**) were analyzed using various physico-chemical properties like melting point, yield, color, elemental analysis and conductivity measurements. The data is shown in Table 1. It was concluded from the results that **m1c1** and **m1c3** complexes had molar conductance values of the 21.25 and 24.72 $\Omega^{-1}cm^2mol^{-1}$ respectively, indicating their non-electrolytic nature. While **m1c2** complex had the molar conductance of 86.43 $\Omega^{-1}cm^2mol^{-1}$ indicated the electrolytic nature of this complex. All the compounds were further characterized by various spectral techniques like FT-IR, NMR, UV-Vis spectra, mass spectrometry, magnetic moments and thermal studies. The analytical data of the ligand and metal complexes are in good agreement with their proposed formula.

2.1. FT-IR spectral studies

The infrared spectrum of the synthesized Schiff base ligand and metal complexes were taken in the range of 4500–400 cm^{-1} to interpret the nature of the ligands to metal ion bonding. Upon chelation the intensities of the peaks are expected to change as compared to that of the ligands and also some new peaks appeared due to chelation. The IR spectra of the Schiff base ligand, DBM and **m1c1** metal complex as an example is shown in Fig. 1.

The IR spectrum of the ligand (**L**) displayed a strong band at 1600 cm^{-1} corresponding to υ(C=N) of imine group. In complexes (**mlc1-mlc3**) the imine υ(C=N) of the ligand shifted to lower wavenumbers 1543-1586 cm^{-1} upon coordination to metal [15]. A broad band of medium intensity at 3130-3205 cm^{-1} assigned to υ(N–H) was also observed. The strong band observed in the ligand at 1727 cm^{-1} is characteristic of υ(C=O) amide [5]. In complexes this band was shifted to lower frequencies (10-12 cm^{-1}), indicating the coordination of carbonyl oxygen of the ligand to metal ions. In DBM the band present at 1665cm^{-1} correspond to υ(C=O) and in complexes this band is shifted to lower frequencies signifying the coordination of carbonyl oxygen of DBM to metal ions [16]. In DBM the band present at 1282 cm^{-1} was assigned to the phenolic C–O stretching mode. In case of complexes (**mlc1-mlc3**) this band was found at higher wavenumbers in the range of 1287–1290 cm^{-1} confirming the involvement of the enolic oxygen in coordination. The **mlc1** and **mlc3** complexes show a broad band at 3500 and 3468 cm^{-1} characteristic of υ(OH) coordinated water molecule. The IR spectra of the **mlc2** and **mlc3** complexes are shown in supplementary data.

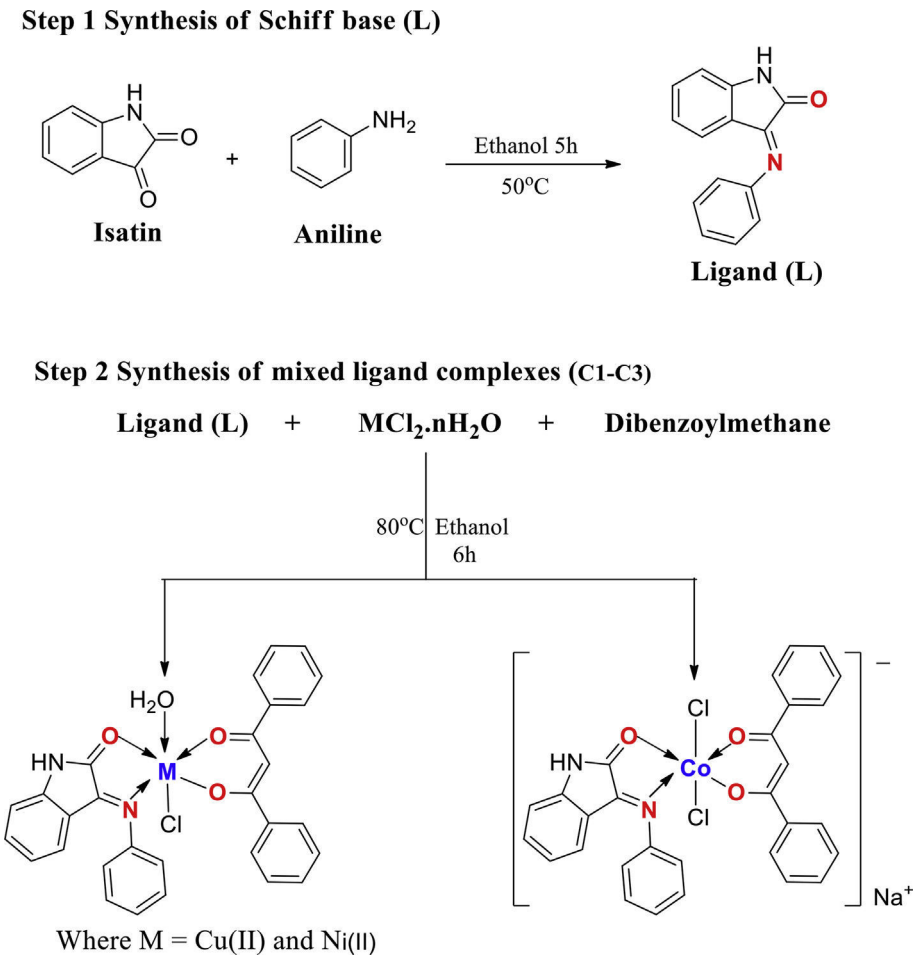

Scheme 1. Synthesis of isatin based ligand (L) and mixed ligand complexes (mlc1-mlc3).

Table 1
Physico-chemical properties of Ligand (**L**) and complexes (**mlc1-mlc3**).

Comp.	Colour	Mol. formula	Mol. Wt.	(m/z) ratio	Yield (%)	Λ_m (Ω^{-1} cm^2 mol^{-1})	Mp (°C)	μ_{eff} (BM)
L	Orange	$C_{14}H_{10}N_2O$	222.2	223.0	80	-	162	-
mlc1	Yellow Green	$[C_{29}H_{23}ClCuN_2O_4]$	562.5	563.5	70	21.25	272	1.85
mlc2	Brown	$[(C_{29}H_{21}Cl_2CoN_2O_3)Na]$	598.3	599.2	68	86.43	221	4.60
mlc3	Reddish Brown	$[C_{29}H_{23}Cl\ N_2NiO_4]$	557.6	558.7	72	24.72	215	3.10

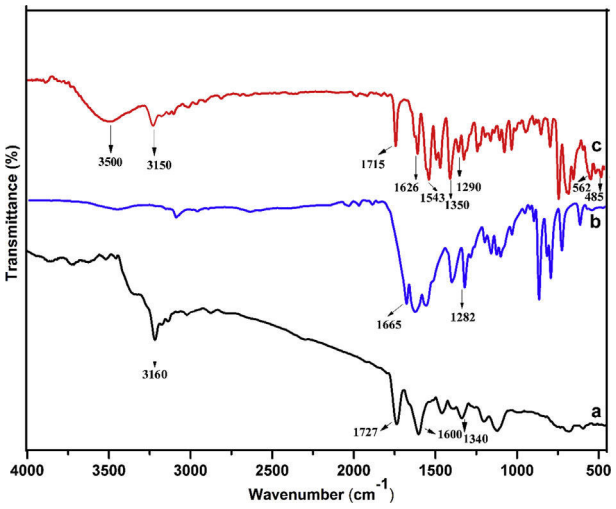

Fig. 1. FT-IR spectra of (a) ligand (L), (b) DBM and (c) mlc1 complex.

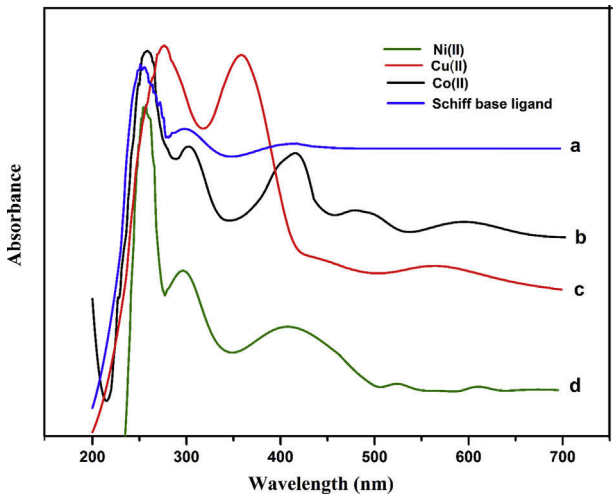

Fig. 2. UV-Vis spectra of (a) ligand (L), (b) mlc2, (c) mlc1 and (d) mlc3 complexes in 10^{-3} M DMSO solution.

The low frequency region of the spectra in complexes (**mlc1-mlc3**) showed the presence of new medium and weak intensity bands in the region of 400–600cm^{-1}, assigned to υ(M-O) and υ(M-N) stretching vibrations. The above results revealed that the two ligands coordinated to metal ions via the carbonyl oxygen of dibenzoylmethane moiety in enolic or ketonic form and the azomethine nitrogen and carbonyl oxygen of ligand (**L**).

2.2. Mass spectrometry

The mass spectra of the ligand (**L**) and metal complexes (**mlc1-mlc3**) were recorded and were found in close agreement with the molecular weights of these compounds. The mass spectra $[M + H]^+$of the ligand showed the molecular ion peak at m/z 223.0 and the mixed ligand complexes (**mlc1-mlc3**) showed molecular ion peaks at 563.5, 599.2 and 558.7 respectively. The mass spectrum is given in supplementary data.

2.3. Magnetic susceptibility and electronic spectral studies

The electronic spectra were recorded in 10^{-3}M DMSO solution in the range of 200–800 nm at room temperature using same solvent as blank. Two bands were observed in the ligand at 255 and 305 nm. The first band appearing at 255 nm is attributed to π-π* transitions of the aromatic rings and the band at 305 nm might be attributed to the n-π* transitions of the azomethine group. In complexes the n-π* transition band is observed in the range of 300–360 nm. In complexes this band undergoes shift due to the coordination of azomethine nitrogen with the metal ions as shown in Fig. 2. The complex (**mlc1**) displayed the broad asymmetric band in the range of 505–638 nm due to the combination of three bands $^2B_{1g} \rightarrow {}^2A_{1g}$ (υ_1), $^2B_{1g} \rightarrow {}^2B_{2g}$ (υ_2) and $^2B_{1g} \rightarrow {}^2E_g$ (υ_3) which are similar in energy. The broadness of the band revealed its distortion from the octahedral geometry. The magnetic moment of **mlc1** was found to be 1.85 B.M, which is an indicative of an octahedral geometry. In complex (**mlc2**) the high intensity band at 420 nm may be assigned as the L→M charge transfer transition. In this complex the low intense bands at 492 and 605 nm corresponds to $^4T_{1g}(F) \rightarrow {}^4T_{2g}(P)$ and $^4T_{1g}(F) \rightarrow {}^4A_{2g}(F)$ excitations respectively [17]. The magnetic moment of **mlc2** was found to be 4.6 B.M. The magnetic moment and electronic spectral data suggest an octahedral geometry around the Co(II) ion. The complex (**mlc3**) exhibited bands at 425, 525 and 620 nm corresponding to three spin allowed transitions as $^3A_{2g}(F) \rightarrow {}^3T_{1g}(P)$, $^3A_{2g}(F) \rightarrow {}^3T_{1g}(F)$ and $^3A_{2g}(F) \rightarrow {}^3T_{2g}(F)$ respectively. The magnetic moment for **mlc3** was found to be 3.1 B.M. The electronic spectra and magnetic moment suggest an octahedral geometry around the Ni(II) ion [15].

2.4. ^1H NMR and ^{13}C NMR spectra

The ^1H NMR of the ligand (L) and complexes (mlc1-mlc3) was recorded in $CDCl_3$ and DMSO-d6 respectively using tetramethylsilane (TMS) as internal standard. The ^1H NMR of the ligand (L) gave characteristic signal at 9.46 ppm (s, 1H) which was assigned to the NH proton [17]. In addition, the aromatic protons of the ligand appeared as multiplets in the range of 6.65–7.49 ppm (m, 9H). The ^1H NMR of the complexes (**mlc1-mlc3**) was not clear probably due to the paramagnetic nature of the complexes. The ^1H NMR and ^{13}C NMR of the ligand and complexes obtained as such is given in the supporting information (see Figs. S7-S14).

2.5. Thermogravimetric studies (TG and DTG)

The thermal analysis of the complexes was studied by using thermo gravimetric techniques within a temperature range from room temperature to 1000 °C at a heating rate of 10 °C/min. As a representative case the TG/DTG curve of complex **mlc3** is depicted in Fig. 3 The temperature intervals and the percentage loss of masses of complexes is summarized in Table 2. The thermal decomposition of the complexes **mlc1-mlc3** undergoes in three stages. The first stage is a degradation step where weight loss of 3% (Calcd. 3.2%) in the temperature range of 50–200 °C with DTG peaks at 120 °C was observed in **m1c1** complex. This weight loss is due to the liberation of one coordinated water. The **m1c1** complex in the second stage degrade at the temperature range of 200–400 °C by

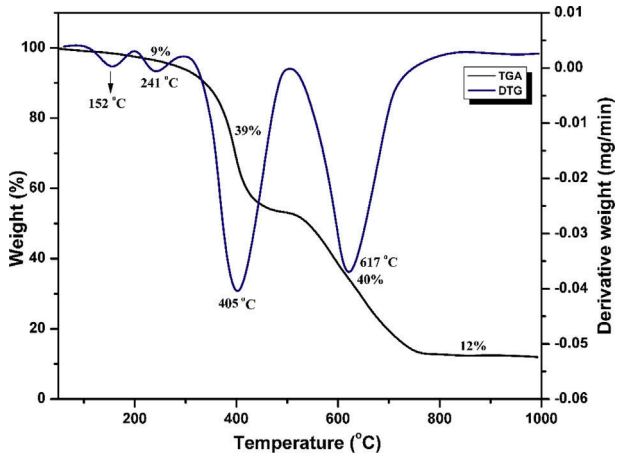

Fig. 3. TGA and DTG curves of mlc3 complex.

the simultaneous loss of coordinated chlorine atom and $C_{14}H_{10}N_2O$ moiety with the weight loss of 45% (Calcd. 45.8%) with DTG peaks observed at 210 and 396 °C. The third stage of decomposition in this complex occurred at the temperature range of 400–700 °C with the weight loss of 39% (Calcd. 39.7%) due to the loss of $C_{15}H_{12}O_2$ fragment with DTG peak observed at 590 °C. The overall weight loss observed in thiscomplex was found to be 87% (Calcd. 88.7%). The metallic residue left has the observed weight of 13% (Calcd. 11.3%).

The **m1c2** complex undergoes decomposition in three stages. The first stage occurred at the temperature range of 100–270 °C with the weight loss of 12% (Calcd. 12.28%). This weight loss corresponds to the loss of Cl_2 molecule with DTG peak observed at 242 °C. The second stage of degradation occurred at the temperature range of 270–590 °C with the weight loss of 38% (calcd. 38.49%). This weight loss corresponds to the loss of $C_{14}H_{10}N_2O$ fragment with DTG peaks observed at 378 °C. The third stage in this complex proceeded with one degradation step. This degradation step occurred within the temperature range of 590–860 °C with the weight loss of 39% (Calcd. 39.84%), which corresponds to the loss of $C_{15}H_{12}O_2$ fragment with DTG peak observed at 700 °C. The total weight loss observed was found to be 89% as against the calculated value of 89.61%. The metallic residue finally left has the observed mass of 11% as against the calculated value of 10.39%.

In **m1c3** complex the first stage of degradation occurred at the temperature range of 100–300 °C with the weight loss of 9% (calcd. 9.5%). This weight loss corresponds to the simultaneous loss of one coordinated water molecule and one coordinated chlorine atom. The DTG peaks were observed at 152 and 241 °C. The second stage of degradation occurred at the temperature range of 300–515 °C with the weight loss of 39% (calcd. 39.77%). This weight loss corresponds to the loss of $C_{14}H_{10}N_2O$ fragment with DTG peaks observed at 405 °C. The third stage proceeded with one degradation step and occurred within the temperature range of 590–860 °C with the weight loss of 40% (Calcd. 40.12%), which corresponds to the loss of $C_{15}H_{12}O_2$ fragment with DTG peak observed at 617 °C. The total weight loss observed was found to be 88% as against the calculated value of 89.39%. The metallic residue finally left has the observed mass of 12% as against the calculated value of 10.61%.

From all the physical measurements and spectroscopic techniques, the metal complex **mlc1** appears to have a distorted octahedral geometry and the complexes **mlc2** and **mlc3** have octahedral geometry. The structures of these complexes was drawn in chemdraw ultra 12.0 and energy minimized (MM2) in chem3D pro using the set functions. The energy minimized structures are shown in Fig. 4.

2.6. Biological studies

2.6.1. Minimum inhibitory concentrations and minimum fungicidal concentrations

The ligand (**L**) and its mixed ligand complexes (**mlc1-mlc3**) were evaluated *in vitro* against seven different isolates of *C. albicans* by microbroth dilution assay. All the MIC and MFC results are summarized in **Table 3**. The MIC values range from 0.5 μg/mL to 500 μg/mL while as MFC values vary from 4 μg/mL to 1000 μg/mL. The complex **mlc3** exerted highest inhibitory activity against all the tested fungal isolates with an MIC values ranging from 0.5 – 8 μg/mL while as the ligand has shown the least inhibitory activity ranging from 125 – 500 μg/mL. We did not evaluate dibenzoylmethane (DBM) because it is known to be inactive. As a positive control, FLC was used because of its common use in the treatment *Candida* infections. As expected, the MIC values for FLC against susceptible and standard laboratory strain was ranging from 0.12 μg/mL to 0.25 μg/mL while as these values range from 16 μg/mL to 32 μg/mL against FLC resistant isolates. These results are congruent with the CLSI Interpretive Guidelines for *In vitro* Susceptibility Testing of *Candida* species [18]. Furthermore, all the test compounds were prepared to different concentrations using 1% DMSO and therefore DMSO was used as negative vehicle control and was observed to have no inhibitory activity against any of the tested isolates. Based on the MIC results, order of potency of these compounds was **mlc3**>**mlc2**>**mlc1**>**L.** The MIC data revealed that the structural changes from ligand to its metal complexes produced the marked enhancement in their potency as antifungal agents. Unlike FLC, all the test compounds showed MFC values indicating their potential to kill the fungal pathogen within varying concentration ranges.

2.6.2. In vitrocombination antifungal activities

Having established the individual MIC values for **L**, **mlc1**, **mlc2**, **mlc3** and **FLC**, the MIC and FICI values of these compounds in combination with the FLC were determined in 1:1 combination by microbroth dilution assay against seven *C. albicans* isolates (See supporting information Table S1). When combined with FLC (n = 28), most of the combinations were either synergistic (54%; n = 15) or additive (32%; n = 9) and only few were indifferent (14%; n = 4) with no antagonistic interaction. Ligand **(L)** when combined with FLC showed strong synergisticinhibitory

Table 2
Thermoanalytical results (TG and DTG) of mixed ligand metal complexes.

Complex	TG range(°C)	DTG_{max}(°C)	n*	Found (calcd. %)		Assignment	Metallic residue
				Mass loss	Total mass loss		
$[C_{29}H_{23}ClCuN_2O_4]$	50–200	120	1	3.0(3.2)		Loss of one coordinated H_2O molecule	
	200–500	310,390	2	45(45.8)	87(88.7)	Loss of $\frac{1}{2}Cl_2$and $C_{14}H_{10}N_2O$	Cu
	500–800	590	1	39(39.7)		Loss of $C_{15}H_{12}O_2$	
$[(C_{29}H_{21}Cl_2CoN_2O_3)Na]$	100–270	242	1	12(12.28)		Loss of coordinated Cl_2 molecule	
	270–590	378	1	38(38.49)	89(89.61)	Loss of $C_{14}H_{10}N_2O$	Co
	590–860	700	1	39(38.84)		Loss of $C_{15}H_{12}O_2$	
$[C_{29}H_{23}Cl\ N_2NiO_4]$	100–300	152,241	2	9(9.5)		Loss of one coordinated H_2O and $\frac{1}{2}Cl_2$ molecule	
	300–515	405	1	39(39.77)	88(89.39)	Loss of and $C_{14}H_{10}N_2O$	Ni
	515–765	617	1	40(40.12)		Loss of $C_{15}H_{12}O_2$	

n* = number of decomposition.

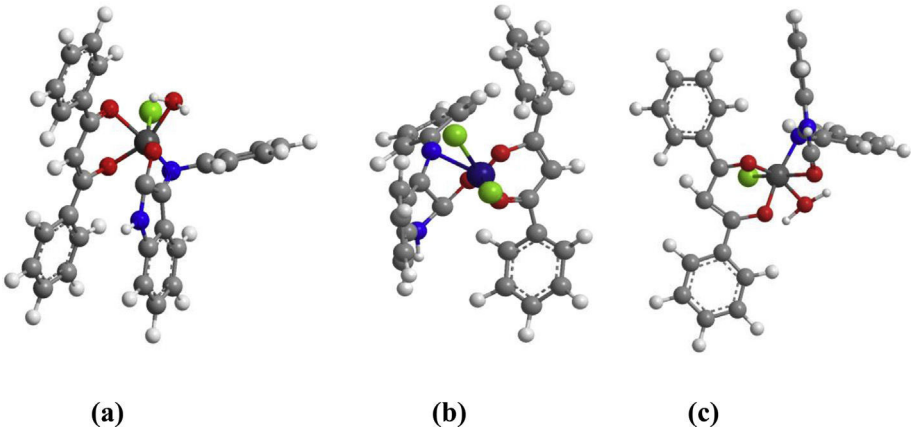

Fig. 4. Energy minimized (MM2) structures of (a) mlc1, (b) mlc2 and (c) mlc3 complexes.

Table 3
Minimum inhibitory concentrations (μg/mL) of ligand (**L**) and mixed ligand complexes (**mlc1-mlc3**) against FLC susceptible and resistant isolates.

Isolates		Ligand (L)		mlc1		mlc2		mlc3		FLC
		MIC	MFC	MIC	MFC	MIC	MFC	MIC	MFC	MIC
Lab strain	*C. albicans* SC5314	125	500	125	250	32	125	0.5	8	0.25
FLC Susceptible strains	4175	250	500	250	500	64	500	2	8	0.12
	4179	250	1000	125	500	64	125	1	4	0.25
	4180	125	500	125	500	64	125	1	4	0.25
FLC Resistant strains	4085	500	1000	250	500	125	500	8	16	16
	4122	500	1000	250	500	125	500	4	8	32
	4135	500	1000	250	500	125	500	8	16	32

effects against the majority of the tested *C. albicans* strains (6 out of 7) with FICI values ranging from 0.146–0.380 (See supporting information Table S1). Likewise, the combination of **mlc1** with FLC also exhibited good synergy against the majority of the tested *C. albicans* strains (5 out of 7), with FICI values ranging from 0.266–0.500. Interestingly, mlc3 which was the most active compound showed only one synergistic activity against one of the resistant isolates while as all other activities are either additive or indifferent. Similar findings were reported by Shrestha *et al,* where they found less potent amphiphilic tobramycin analogue C_{12} showing more synergistic inhibitory effects when combined with azoles against all strains of *C. albicans*than it's another analogue C_{14} [19]. A comparison between FLC susceptible and FLC resistant isolates indicated that resistant isolates showed more synergy (75%; n = 12) than susceptible isolates (50%; n = 12), which are congruent with our previous findings [13, 14, 20].Despite only 54% combinations were synergistic, it is important to mention that the MIC values of FLC were greatlyreduced when used with test compounds against all the tested fungal strains.These findings set up the base for further studies to use these and similar compounds as chemosensitizing agents with FLC to provide a new strategy to fight fungal infections caused by resistant strains.

2.6.3. TUNEL assay: FITC labeling

Numerous molecular level apoptotic regulators have been identified and characterized [21]. DNA damage is a well-established hallmark of late apoptosis. TUNEL assay was used as primary screening tool for apoptosis as it targets fundamental apoptotic event in yeast cells. To investigate whether the newly synthesized compounds display features of the late stages of apoptosis in *C. albicans*, we evaluated DNA fragmentation and visualized it with the help of a TUNEL assay by labeling 3′-OH ends of nicked DNA with fluorescent dUTP (TUNEL-FITC). **Fig. 5** represents *C. albicans* cells (SC5314) exposed to MIC and ½ MIC values of **m1c3**for 1 h, exhibiting a significant amount of changes in nuclear DNA and that of the ligand (**L**) and complexes **mlc1** and **mlc2** are shown in Fig. S17. In cells exposed to low concentrations of the test compounds (MIC/2), the proportion of TUNEL-positive nuclei (green fluorescence) was significantly increased compared to that of the untreated control population. Theanalyses of results revealed remarkable apoptosis for **mlc3** treated *Candida* cells with >95% apoptotic cells when treated with ½ MIC values. The other compounds also showed apoptotic activity on *C. albicans* at different ratios when cells were treated with sub-MIC values. At MIC values very, less number (<10%) of apoptotic cells were observed. Cells exposed to positive controls (2 μg/ml amphotericin B) revealed an increase in TUNEL-positive nuclei identified as green fluorescence spots.

Compounds inducing apoptosis in *Candida* at sub-MIC values is of dominant value as these compounds may then be used forthe design of new drugs with fungicidal activity at higher concentrations and programmed cell death at lower concentrations. The most used polyene - amphotericin B, is known to be fungicidal and induces apoptosis in *C. albicans* [22, 23] which could be a possible reason for low resistance levels against this drug. In contrary FLC, which is a fungistatic drug aids *Candida* to develop resistance at lower concentrations [24].

Many metal-based drugs have been demonstrated to show mechanism of action distant from conventional drugs which make them ideal candidates where resistance to conventional drugs has already emerged. The different mechanism of action of metal-based drugs could also be utilized by using them in combination with conventional drugs to target multiple pathways with limited resistance. Some previous studies have shown that treatment of *Candida* with Silver(I) complexes resulted in many morphological features of programmed cell death which was shown to be due to reduction in the ergosterol biosynthesis, a sterol essential to maintain membrane integrity [25]. Altered susceptibility to miconazole and amphotericin B mediated through alterations in the respiration rate has been observed when *Candida* cells were treated with Cu and Ag complexes [26]. In a previous study we observed that treatment of *Candida* with metal complexes disrupts their membrane integrity [20]. In this study we observed that all the metal complexes show synergistic interaction with fluconazole and one of the complexes (**mlc3**) showed

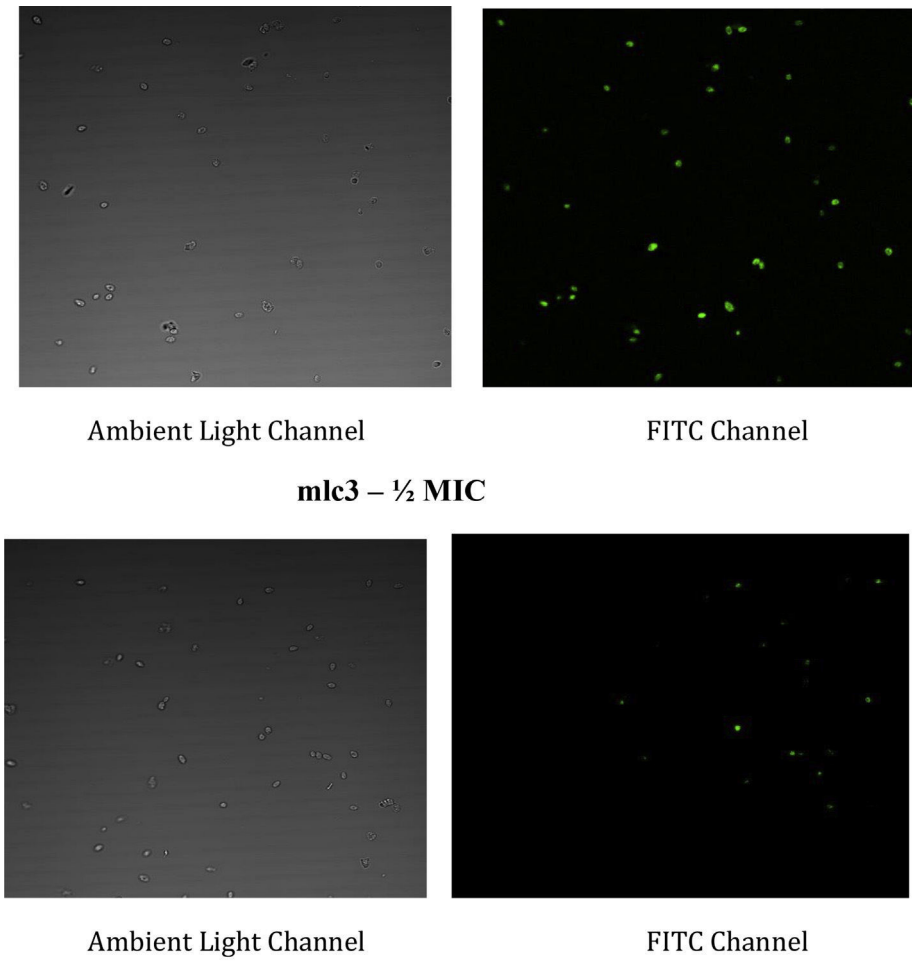

Fig. 5. Fluorescent images of *C. albicans* SC5314 cells treated with MIC and ½ MIC values of m1c3 complex. Green fluorescence emitting cells are TUNEL-FITC positive, indicating active DNA fragmentation, in cells undergoing apoptosis.

remarkable apoptosis. The different behavior of these otherwise structurally similar complexes could be due to the different nature of the metal ions in their complexes. The most ideal complex (**mlc3**) could be further studied for its detailed mechanism of action by studying the other markers of early and late apoptosis, such as Annexin V-FITC and PI labeling, cytochrome C oxidase activity, membrane potential and ergosterol biosynthesis assay. Furthermore, this complex will also be tested against other species of *Candida* including *C. auris*, which are known multidrug resistant fungal species responsible for several outbreaks worldwide.

3. Conclusions

Isatin and DBM based mixed ligand complexes were synthesized, characterized and evaluated for their antifungal properties. **mlc2** and **mlc3** complexes possess octahedral geometry whereas a distorted octahedral geometry was assigned to the complex **mlc1**, based on various physical and spectroscopic techniques. The biological results revealed that these compounds, with special emphasis to **mlc3**, have a potential to be used as antifungal drugs and significant potentiators with known antifungal azole drug, Fluconazole. The mechanism of action appears to be due to apoptosis in *C. albicans* and therefore this study paves the way for the study and role of metal based drugs as potential antifungal agents and potentiators in mediating fungal cell death by inducing apoptosis. Further investigations would result in a strategy that would lead to the development of novel antifungal agents that switch on endogenous cell suicide mechanisms and therefore bypasses the development of drug resistance.

4. Experimental

4.1. Materials and physical methods

Isatin, aniline and metal chlorides were analytical grade products from Merck. Dibenzoylmethane was purchased from Aldrich and all chemicals were used as received. Solvents used for the synthesis and analysis was reagent grade chemicals and used without further purification.

The percentages of carbon, hydrogen, nitrogen in Schiff base ligand and metal complexes were determined using Flash EA 1112 elemental analyzer (Thermo Scientific). Electrothermal melting point apparatus was used to determine the melting point of the synthesized compounds. The absorption spectra of the synthesized compounds were recorded between 200-600 nm(cm^{-1}) using UV/visible spectrophotometer (UV-260 Shimadzu, with 1cm quartz cuvettes). IR spectra of the ligand and complexes were recorded in KBr pellets on a Perkin-Elmer 283 spectrophotometer. For ^{1}H NMR and ^{13}C NMR measurements Brucker WH 300 (200MHz) and Brucker WH 270(67.93 MHz) were used using $CDCl_3$ or DMSO-d_6 as a solvent and tetramethylsilane as an internal standard. ESI-MS (AB-Sciex 2000, Applied Biosystem) was used to record mass spectra

of the synthesized ligand and complexes. Magnetic moments were measured using Sherwood scientific magnetic susceptibility balance at 25 °C. The thermogravimetric analysis (TGA/DTG) was carried out in the temperature range of 20–1000 °C in a dynamic nitrogen atmosphere with a heating rate of 10 ºC/min using NETZSCH STA 449F3 thermal analyzer.

4.2. Synthesis of schiff base ligand and its mixed ligand complexes

4.2.1. Synthesis of 3-(phenylimino)indolin-2-one ligand (L)

To a hot ethanolic solution (20 mL) of isatin (1.47 g, 10 mmol) a 10 mL ethanolic solution of aniline (0.93 g, 10 mmol) was added in the stoichiometric ratio of 1:1 respectively. The reaction mixture was stirred for 5 h at 50 °C and monitored by taking TLC at regular intervals. The resulting clear solution was then reduced to half the volume and then allowed to stay at room temperature. The orange colored crystalline product was then filtered off, washed with least amount of ethanol and diethyl ether several times and then dried in vacuo over $CaCl_2$ for further use.

Colour (Orange) Yield: 80%. Elemental Anal. Calc. for$C_{14}H_{10}N_2O$: C, 75.65; H, 4.54; N; 12.61; Found: C, 75.57; H, 4.48; N, 12.65; IR (KBr Pellet, cm^{-1}): 1600 υ(-C=N-), 1727 υ(C=O), 1340 υ(C–N), 3160 υ(N–H); ^1H NMR ($CDCl_3$, δ, ppm) 9.46 (s, 1H, NH), 6.65–7.49 (m, 9H, ArH). ^{13}C NMR (DMSO-d_6,δ(ppm)): 149.47 (C=O), 163.94 (C=N), 143.43(-C-N=C), 116.15–134.92 (Ar C's), Mass spectrum (ESI) $[M + H]^+ = 223.0$. UV -vis (DMSO): λ/nm 255, 305.

4.2.2. Synthesis of mixed ligand complexes

To a 20 mL hot ethanolic solution of dibenzoylmethane (0.45 g, 2 mmol), NaOH (2 mmol) was added. After 15 minutes to the flask was added an ethanolic solution of Schiff base ligand (0.44 g, 2 mmol) and then ethanolic solution of $[M(Cl)_2.nH_2O]$ (2 mmol) was added drop wise with constant stirring. The reaction mixture was refluxed for 5–6 h at 80 °C under nitrogen atmosphere. The reaction mixture was then cooled at room temperature. The product was filtered off, washed several times with ethanol and diethyl ether then dried in vacuum over fused calcium chloride.

*[Cu(dbm)LClH_2O]:(**mlc1**)*

Colour (Yellow green) Yield: 70%. Elemental Anal. Calc. for $[C_{29}H_{23}ClCuN_2O_4]$: C, 61.92; H, 4.12; N, 4.98; Found: C, 60.02; H, 3.97; N, 4.79; IR(KBr Pellet, cm^{-1}): 1543 υ(C=N), 1715 υ(C=O amide),1620 υ(C=O), 3150 υ(N–H), 3500 υ(OH), 1350 υ(C–N), 1290 υ(C–O), 562 υ(Cu–O), 485 υ(Cu–N); ^1H NMR (DMSO-d6, δ, ppm) 11.0 (s, 1H, NH), 6.71 (1H, –CH), 3.59 (s, 2H, H_2O), 6.34–8.18 (m, 20H, ArH); ^{13}C NMR (DMSO-d_6,δ(ppm)): 150.82 (C=O), 164.75 (C=N), 143.41 (-C-N=C), 93.2 (CH of DBM), 186.8 (C=O of DBM), 183.8 (C–O of DBM), 112.0–133.3 (Ar C's), Mass spectrum (ESI) $[M + H]^+ = 563.50$.

*[Co(dbm)LCl2]¯:(**mlc2**)*

Colour (Brown) Yield: 68%. Elemental Anal. Calc. for $[(C_{29}H_{21}Cl_2CoN_2O_3)Na]$: C, 60.44; H, 3.85; N, 4.86; Found: C,60.31; H, 3.87; N, 4.89; IR(KBr Pellet, cm^{-1}): 1586 υ(C=N), 1718 υ(C=O amide), 1640 υ(C=O), 3205 υ(N–H), 1360 υ(C–N), 1290 υ(C–O), 570 υ(Co–O), 486 υ(Co–N); ^1H NMR (DMSO-d_6, δ, ppm) 10.28 (s, 1H, NH), 6.65 (1H, –CH), 6.28–7.52 (m, 19H, ArH). ^{13}C NMR (DMSO-d_6,δ(ppm)): 151.15 (C=O), 165.32 (C=N), 138.8 (-C-N=C), 93.7 (CH of DBM), 185.8 (C=O of DBM), 184.8 (C–O of DBM), 112.0–134.1 (Ar C's), Mass spectrum (ESI) $[M + H]^+ = 599.2$.

*[Ni(dbm)LClH_2O]:(**mlc3**)*

Color (Reddish Brown) Yield: 72%. Elemental Anal. Calc. for $[C_{29}H_{23}ClN_2NiO_4]$: C, 62.46; H, 4.15; N, 5.02; Found: C, 61.39; H, 3.98; N, 4.96; IR(KBr Pellet, cm^{-1}): 1580 υ(C=N), 1722 υ(C=O amide),1648 υ(C=O), 3130 υ(N–H), 3468 υ(OH), 1348 υ(C–N), 1287 υ(C–O), 565 υ(Ni–O), 488 υ(Ni–N); ^1H NMR (DMSO-d_6, δ, ppm) 10.97 (s, 1H, NH), 6.68 (1H, –CH), 3.62 (s, 2H, H_2O), 6.32–7.60 (m, 19H, ArH). ^{13}C NMR (DMSO-d_6,δ(ppm)): 151.43 (C=O), 164.92 (C=N), 143.4 (-C-N=C), 93.1 (CH of DBM), 185.2 (C=O of DBM), 182.1 (C–O of DBM), 111.2–130.0 (Ar C's), Mass spectrum (ESI) $[M + H]^+ = 558.70$.

4.3. Microbiological analysis

4.3.1. Strains, media and chemicals

In this study, along with one laboratory strain (*Candida albicans* SC5314), three fluconazole (FLC) susceptible (4175; 4179; 4180) and three FLC resistant (4085; 4122; 4135) clinical strains of *C. albicans* were used. Clinical *Candida* strains were isolated from either HIV positive patients or patients with other immunocompromised conditions that were attending clinics at the Charlotte Maxeke Johannesburg Academic Hospital, Johannesburg, South Africa. All the strains were maintained on Sabouraud Dextrose (SD) Agar (Sigma Aldrich, USA) and prior to experiments; cells were grown in fresh SD broth.*Candida albicans* used in this study were isolated from patients under the ethical clearance number M10102 obtained from the Human Research Ethics Committee, University of the Witwatersrand. Fluconazole was purchased from Sigma Fluke (USA) and stock solution of 2 mg/mL was prepared in sterile distilled water. All other chemicals and media were purchased from Sigma Aldrich and Merck.

4.3.2. Determination of Minimum Inhibitory Concentrations and Minimum Fungicidal Concentrations

Minimum Inhibitory Concentrations (MIC) and Minimum Fungicidal Concentrations (MFC) of all the newly synthesized Schiff base ligand and its derivative complexes against all the tested *C. albicans* were determined by a serial dilution technique using Clinical and Laboratory Standards Institute (CLSI) guidelines M27-A3 [27]. Briefly, 100 μL volumes of the test compounds with a final concentration of 2000 μg/mL were added in the first row and were serially diluted. In addition, negative control (1% DMSO), sterility control (media only) and positive control (FLC) were alsoincluded in each test. After proper sealing, plates were incubated at 37 °C for 24 h. After incubation, 400 μg/mL of *p*-iodonitrotetrazolium violet solution (INT) was added to each well (40 μL). Viable microorganisms interact with INT to create a colour change from clear to a red-purple colour. Thus, the lowest dilution with no colour change was considered as the MIC for that test compound. Further, MFC was determined by sub-culturing the test dilutions from each well without colour change on SD agar plates and incubated for 24 h. The lowest concentration that showed no fungal growth was defined as the MFC value. All the experiments were done in duplicate and all the results were expressed in μg/mL.

4.3.3. Combination of test compounds with FLC

Based on the MIC values, ligand and its mixed ligand complexes (**mlc1-mlc3**)were examined for the type of combination interaction with FLC by determining the Fractional Inhibitory Concentration Index (FICI), following the method described previous [28]. In each combination set, test compounds and FLC were added into a well in 1:1 ratio. Interactions were assessed on the basis of zero-interaction theory of Loewe additivity and FICI values were calculated as follows:

$$\mathbf{FICI} = \mathbf{FICa} + \mathbf{FICb} = \frac{\mathbf{MICa\ in\ combination}}{\mathbf{MICa\ tested\ alone}} + \frac{\mathbf{MICb\ in\ combination}}{\mathbf{MICb\ tested\ alone}}$$

where MICa is the MIC of the Schiff base derivativesand MICbis the MIC of drug (FLC). Interpretations of FICI values weredone as synergy when ≤0.5, additive between 0.5 and 1.0, indifferent between 1.0 and 4.0 and antagonistic when FICI values were >4.0.

4.3.4. Apoptosis study

To study the apoptotic effect of ligand and its mixed ligand complexes (**mlc1-mlc3**) against *C. albicans*, Terminal deoxynucleotidyl transferase-mediated dUTP nick end labeling (TUNEL) assay was

performed by using *In Situ* Cell Death Detection Kit, Fluorescein (Roche Applied Science), as described previously [29]. Briefly, cells were exposed to MIC and ½ MIC values of all the test compounds followed by washing 3 times in PBS. Cells are then fixed with a fixative solution (4% paraformaldehyde in PBS pH 7.4) for 1 hour at 25 °C. After fixation protoplasts were prepared by digesting cell wall with lyticase in different washing steps in protoplast buffers pH 7.4 (buffer I - containing 1M sorbitol, 50 mM tris base, 10 mM $MgCl_2$ and 30 mM DTT; buffer II – 1M sorbitol, 50 mM tris base, 10 mM $MgCl_2$ and 1 mM DTT; buffer III – 1M sorbitol, 50 mM tris base and 10 mM $MgCl_2$. Cells were harvested and washed thrice for 5 min each with buffer I (3 mL/g cells). Cells were then incubated in buffer II (5 mL/g cells; supplemented with lyticase) for 2 h at 25 °C. Centrifuge and discard the supernatant then incubated with buffer III (5 mL/g cells) for 20 min. Again, centrifuge to remove buffer III, then washed the protoplasts once with PBS and incubated with permeabilization solution (0.1% Triton X-100 in 0.1% sodium citrate) for 2 min on ice, then again rinsed twice with PBS. Stain with 50 μL TUNEL reaction mixture and incubate for 60 min at 37 °C in a humidified atmosphere in the dark. Wash cells twice with PBS and examine by fluorescent microscope (Zeiss LSM 780 - laser scanning confocal microscope) with an excitation wavelength of 488 nm and the detection range of 515 nm. Two negative controls and a positive control should be run with each experiment.

Declarations

Author contribution statement

Mohmmad Younus Wani: Conceived and designed the experiments; Analyzed and interpreted the data; Wrote the paper.

Ovas Dar, Faisal Mohammed Aqlan: Performed the experiments; Analyzed and interpreted the data; Wrote the paper.

Shabir Lone: Performed the experiments.

Manzoor Malik: Performed the experiments; Analyzed and interpreted the data.

Athar Hashmi: Contributed reagents, materials, analysis tools or data.

Aijaz Ahmad: Conceived and designed the experiments; Analyzed and interpreted the data; Contributed reagents, materials, analysis tools or data; Wrote the paper.

Funding statement

This research did not receive any specific grant from funding agencies in the public, commercial, or not-for-profit sectors.

Competing interest statement

The authors declare no conflict of interest.

Additional information

Supplementary content related to this article has been published online at https://doi.org/10.1016/j.heliyon.2019.e02055.

References

[1] M.E. Katsarou, E.K. Efthimiadou, G. Psomas, A. Karaliota, D. Vourloumis, Novel copper(II) complex of N-propyl-norfloxacin and 1,10-phenanthroline with enhanced antileukemic and DNA nuclease activities, J. Med. Chem. 51 (2008) 470–478.

[2] W. Guerra, E. de Andrade Azevedo, A.R. de Souza Monteiro, M. Bucciarelli-Rodriguez, E. Chartone-Souza, A.M.A. Nascimento, A.P.S. Fontes, L. Le Moyec, E.C. Pereira-Maia, Synthesis, characterization, and antibacterial activity of three palladium(II) complexes of tetracyclines, J. Inorg. Biochem. 99 (2005) 2348–2354.

[3] I. Turel, L. Golic, P. Bukovec, M. Gubina, Antibacterial tests of Bismuth(III)–Quinolone (Ciprofloxacin, cf) compounds against Helicobacter pylori and some other bacteria. Crystal structure of $(cfH_2)_2[Bi_2Cl_{10}]\cdot 4H_2O$, J. Inorg. Biochem. 71 (1998) 53–60.

[4] G.S. Singh, Z.Y. Desta, Isatins as privileged molecules in design and synthesis of spiro-fused cyclic frameworks, Chem. Rev. 112 (2012) 6104–6155.

[5] H. Pervez, M. Ahmad, S. Zaib, M. Yaqub, M.M. Naseer, J. Iqbal, Synthesis, cytotoxic and urease inhibitory activities of some novel isatin-derived bis-Schiff bases and their copper(II) complexes, Medchemcomm 7 (2016) 914–923.

[6] P. Davidovich, V. Aksenova, V. Petrova, D. Tentler, D. Orlova, S. Smirnov, V. Gurzhiy, A.L. Okorokov, A. Garabadzhiu, G. Melino, N. Barlev, V. Tribulovich, Discovery of novel isatin-based p53 inducers, ACS Med. Chem. Lett. 6 (2015) 856–860.

[7] H. Torres-Gomez, E. Hernandez-Nunez, I. Leon-Rivera, J. Guerrero-Alvarez, R. Cedillo-Rivera, R. Moo-Puc, R. Argotte-Ramos, M. del Carmen Rodriguez-Gutiérrez, M.J. Chan-Bacab, G. Navarrete-Vazquez, Design, synthesis and in vitro antiprotozoal activity of benzimidazole-pentamidine hybrids, Bioorg. Med. Chem. Lett. 18 (2008) 3147–3151.

[8] E.F. Canzi, F.M. dos Santos, E.K. Meneghetti, B.H.L.N. Sales Maia, J.M. Batista, Absolute configuration of a rare dibenzoylmethane derivative from dahlstedtia glaziovii (Fabaceae), Tetrahedron Lett. 59 (2018) 135–137.

[9] M.L. Daly, C. Kerr, C.A. DeRosa, C.L. Fraser, Meta-alkoxy-substituted difluoroboron dibenzoylmethane complexes as environment-sensitive materials, ACS Appl. Mater. Interfaces 9 (2017) 32008–32017.

[10] W.H. Mahmoud, G.G. Mohamed, O.Y. El-Sayed, Coordination compounds of some transition metal ions with new Schiff base ligand derived from dibenzoyl methane. Structural characterization, thermal behavior, molecular structure, antimicrobial, anticancer activity and molecular docking studies, Appl. Organomet. Chem. 32 (2018) e4051.

[11] M. Halliday, H. Radford, K.A.M. Zents, C. Molloy, J.A. Moreno, N.C. Verity, E. Smith, C.A. Ortori, D.A. Barrett, M. Bushell, G.R. Mallucci, Repurposed drugs targeting eIF2α-P-mediated translational repression prevent neurodegeneration in mice, Brain 140 (2017) 1768–1783.

[12] M.A. Malik, O.A. Dar, P. Gull, M.Y. Wani, A.A. Hashmi, Heterocyclic Schiff base transition metal complexes in antimicrobial and anticancer chemotherapy, Medchemcomm 9 (2018) 409–436.

[13] M.Y. Wani, A. Ahmad, S. Kumar, A.J.F.N. Sobral, Flucytosine analogues obtained through Biginelli reaction as efficient combinative antifungal agents, Microb. Pathog. 105 (2017) 57–62.

[14] A. Ahmad, M.Y. Wani, M. Patel, A.J.F.N. Sobral, A.G. Duse, F.M. Aqlan, A.S. Al-Bogami, Synergistic antifungal effect of cyclized chalcone derivatives and fluconazole against *Candida albicans*, Medchemcomm 8 (2017) 2195–2207.

[15] M.A. Ali, H.J. Hj Abu Bakar, A.H. Mirza, S.J. Smith, L.R. Gahan, P.V. Bernhardt, Preparation, spectroscopic characterization and X-ray crystal and molecular structures of nickel(II), copper(II) and zinc(II) complexes of the Schiff base formed from isatin and S-methyldithiocarbazate (Hisa-sme), Polyhedron 27 (2008) 71–79.

[16] A.S. El-Tabl, F.A. El-Saied, W. Plass, A.N. Al-Hakimi, Synthesis, spectroscopic characterization and biological activity of the metal complexes of the Schiff base derived from phenylaminoacetohydrazide and dibenzoylmethane, Spectrochim. Acta Part A Mol. Biomol. Spectrosc. 71 (2008) 90–99.

[17] G.Y. Nagesh, K. Mahendra Raj, B.H.M. Mruthyunjayaswamy, Synthesis, characterization, thermal study and biological evaluation of Cu(II), Co(II), Ni(II) and Zn(II) complexes of Schiff base ligand containing thiazole moiety, J. Mol. Struct. 1079 (2015) 423–432.

[18] P. Wayne, Clinical and Laboratory Standards Institute: Reference Method for Broth Dilution Antifungal Susceptibility Testing of Yeasts; Fourth Informational Supplement, 2012 (Document M27-S4).

[19] S.K. Shrestha, M.Y. Fosso, S. Garneau-Tsodikova, A combination approach to treating fungal infections, Sci. Rep. 5 (2015) 17070.

[20] M.Y. Wani, A. Ahmad, M.A. Malik, A.J.F.N. Sobral, Mononuclear transition metal complexes containing iodo-imidazole ring endowed with potential anti-Candida activity, Med. Chem. Res. 25 (2016) 2557–2566.

[21] D. Carmona-Gutierrez, T. Eisenberg, S. Büttner, C. Meisinger, G. Kroemer, F. Madeo, Apoptosis in yeast: triggers, pathways, subroutines, Cell Death Differ. 17 (2010) 763–773.

[22] R.S. Al-Dhaheri, L.J. Douglas, Apoptosis in Candida biofilms exposed to amphotericin B, J. Med. Microbiol. 59 (2010) 149–157.

[23] A.J. Phillips, I. Sudbery, M. Ramsdale, Apoptosis induced by environmental stresses and amphotericin B in *Candida albicans*, Proc. Natl. Acad. Sci. 100 (2003) 14327–14332.

[24] D.M. Arana, C. Nombela, J. Pla, Fluconazole at subinhibitory concentrations induces the oxidative- and nitrosative-responsive genes TRR1, GRE2 and YHB1, and enhances the resistance of *Candida albicans* to phagocytes, J. Antimicrob. Chemother. 65 (2010) 54–62.

[25] B. Thati, A. Noble, R. Rowan, B.S. Creaven, M. Walsh, M. McCann, D. Egan, K. Kavanagh, Mechanism of action of coumarin and silver(I)–coumarin complexes against the pathogenic yeast *Candida albicans*, Toxicol. In Vitro 21 (2007) 801–808.

[26] A. Eshwika, B. Coyle, M. Devereux, M. McCann, K. Kavanagh, Metal complexes of 1,10-phenanthroline-5,6-dione alter the susceptibility of the yeast *Candida albicans* to Amphotericin B and Miconazole, BioMetals 17 (2004) 415–422.

[27] P. Wayne, Clinical and Laboratory Standards Institute: Reference Method for Broth Dilution Antifungal Susceptibility Testing of Yeasts; Approved Standard, 2008, p. 3. CLSI document M27-A3 and Supplement S.

[28] A. Ahmad, M.Y. Wani, A. Khan, N. Manzoor, J. Molepo, Synergistic interactions of Eugenol-tosylate and its congeners with fluconazole against *Candida albicans*, Plos one 10 (2015) e0145053.

[29] A. Kha, n, A. Ahmad, L.A. Khan, N. Manzoor, Ocimum sanctum (L.) essential oil and its lead molecules induce apoptosis in *Candida albicans*, Res. Microbiol. 165 (2014) 411–419.

Received: 15 April 2019 | Revised: 23 June 2019 | Accepted: 28 June 2019

DOI: 10.1002/aoc.5128

FULL PAPER

WILEY Applied Organometallic Chemistry

Heteroleptic transition metal complexes of Schiff-base-derived ligands exert their antifungal activity by disrupting membrane integrity

Ovas Ahmad Dar[1] | Shabir Ahmad Lone[2] | Manzoor Ahmad Malik[1] | Mohmmad Younus Wani[3] | Md Ikbal Ahmed Talukdar[1] | Abdullah Saad Al-Bogami[3] | Athar Adil Hashmi[1] | Aijaz Ahmad[2,4]

[1] Department of Chemistry, Jamia Millia Islamia, New Delhi 110025, India

[2] Clinical Microbiology and Infectious Diseases, School of Pathology, Faculty of Health Sciences, University of the Witwatersrand, Johannesburg 2193, South Africa

[3] Chemistry Department, Faculty of Science, University of Jeddah, Jeddah, Kingdom of Saudi Arabia

[4] Infection Control, Charlotte Maxeke Johannesburg Academic Hospital, National Health Laboratory Service, Johannesburg 2193, South Africa

Correspondence
Mohmmad Younus Wani, Chemistry Department, Faculty of Science, University of Jeddah, P.O. Box 80327, Jeddah 21589, Kingdom of Saudi Arabia.
Email: mwani@uj.edu.sa

Athar Adil Hashmi, Professor, Department of Chemistry, Jamia Millia Islamia (Central University). New Delhi-110025, India.
Email: aah_ch@yahoo.co.in

Aijaz Ahmad, Senior Medical Scientist, Clinical Microbiology & Infectious Diseases, University of the Witwatersrand. Johannesburg, 2193, South Africa.
Email: aijaz.ahmad@wits.ac.za

Funding information
University Research Committee Grant for 2019 - Friedel Sellschop Award, Grant/Award Number: AZMD019

Development of new treatment strategies and chemotherapeutic agents is urgently needed to combat the growing multidrug resistant species of *Candida*. In this direction, a new series of Cu (II), Co (II), Ni (II) and Zn (II) heteroleptic complexes were synthesized, characterized and evaluated for antifungal activity. Based on spectral characterization and physical measurements, an octahedral geometry was assigned to $[Co(L1)(L2)ClH_2O]$ (**C2**), $[Ni(L1)(L2)ClH_2O]$ (**C3**), $[Zn(L1)(L2)ClH_2O]$ (**C4**) complexes, while a distorted octahedral geometry was assigned to $[Cu(L1)(L2)ClH_2O]$ (**C1**) complex. All the synthesized compounds were tested for antifungal activity against 11 *Candida albicans* isolates, including fluconazole (FLC)-resistant isolates, by determining minimum inhibitory concentrations (MIC) and minimum fungicidal concentrations (MFC), following CLSI guidelines. The mechanism of their antifungal activity was assessed by studying their effect on the plasma membrane using flow cytometry and quantifying the ergosterol contents. All the test compounds showed varying levels of antifungal activity. Both the ligands showed moderate antifungal activity with a median MIC value of 100 μg/mL with no fungicidal activity. Compound **C3** was the most potent compound with median MIC and MFC values of 0.10 and 1.60 μg/mL, respectively. Flow cytometry analysis revealed that these compounds at MFC values disrupt the cell membrane, resulting in propidium iodide entering the cells. These compounds also reduced a considerable amount of ergosterol content after treating the cells with MIC and sub-MIC values. This study indicates that these compounds have high antifungal activity against *C. albicans*, and have the potential to be developed as novel antifungal drugs.

KEYWORDS
Candida albicans, ergosterol, heteroleptic complexes, membrane disruption

1 | INTRODUCTION

The growing incidences of life-threatening systematic fungal infections due to a rise in immunocompromised patient populations and the limited availability of antifungal medications necessitates the development of new antifungal drugs or treatment strategies.[1,2] Fungal diseases, which include pulmonary aspergillosis, cryptococcal meningitis, pneumocystis pneumonia, invasive candidiasis, invasive aspergillosis, disseminated histoplasmosis, fungal asthma and fungal keratitis, kill more than 1.5 million and affect over a billion people worldwide.[3,4] Different antifungal drugs belonging to either azoles or polyenes are currently being used to treat fungal infections, but emergence of drug resistance and treatment failures is a big challenge.[5–7] Among the various strategies to tackle this challenge and curb growing drug resistance and fungal infections, development of new drugs based on a different mechanism of action or drugs that target multiple pathways to evade drug resistance are currently being pursued.[8–10] Complexation of potentially bioactive organic molecules with metals results in a sharp increase in their biological activity. A metal complex usually results in enhanced efficacy compared with the ligand or the metal ion alone, by sometimes the ligands protecting or stabilizing the otherwise reactive metal ion or the metal undergoing redox events that enhance the overall efficacy of the complex, and sometimes the metal and the ligand are mutually responsible for the biological activity of the complex.[11] Coordination compounds offer many binding modes to polynucleotides, including outer-sphere non-covalent binding, metal coordination to nucleobase and phosphate backbone sites, as well as strand cleavage induced by oxidation using redox-active metal centers.[12] The accessibility of different oxidation states of metals such as Fe, Cu, Co, Ru, Mn, etc. may allow for redox chemistry resulting in strand breakage and other alterations, which result in the selective inhibition of the target cell or pathogen.[13]

A diverse range of ligands with different coordination sites have been synthesized and used as chelators for various metal ions. An important class of molecules is the Schiff base ligands; they show great chelating properties due to their azomethine and other coordinating sites or groups. They are stabile under various oxidative and reductive conditions, which make them ideal candidates for the development of new metal-based antimicrobial and anticancer agents.[14–16]

Keeping in view the imperative influence of Schiff bases in medicinal chemistry,[17] and the impact of metallodrugs as potential chemotherapeutic agents, our main rationale of this study was to explore whether the incorporation of a transition metal ion, a Schiff base derived from biologically important scaffolds in the form of heteroleptic complexes, would deliver a synergistic effect and thus act as a hopeful stratagem for development of effective chemotherapeutic agents. Literature reveals that the Schiff base ligands derived from 1,4-benzodioxane-6-amine have not been much studied, and the Schiff bases derived from 4-(dimethyl-amino)benzaldehyde show great pharmacological effects.[18–21] Therefore, in the present study some new heteroleptic complexes derived from two different bidentate Schiff base ligands have been synthesized, and their promising antifungal potential was evaluated against different fluconazole (FLC)-susceptible and -resistant *Candida albicans* isolates in a quest to find a better antifungal agent.

2 | EXPERIMENTAL

2.1 | Materials and physical methods

All the chemicals used were of reagent grade, and were used without further purification. 1,4-Benzodioxane-6-amine and 2-hydroxy-1-naphthaldehyde were purchased from Sigma-Aldrich Chemie (Germany). Ethylenediamine, metal chlorides and ethanol were purchased from Merck. 4-(dimethyl-amino)Benzaldehyde was purchased from Sd-fine.

The prepared Schiff base ligands and metal complexes were subjected to microanalyses (C, H and N) that were carried out with Elementar (Thermo Scientific). The molar conductivities of freshly prepared solutions at room temperature were measured on a Syntronics type 302 conductivity bridge equilibrated at 25 ± 0.01°C. For conductivity measurements, 1 mM solutions in dimethylsulfoxide (DMSO) were prepared. Electrothermal melting point apparatus was used to determine the melting point of the synthesized compounds. UV–Vis spectra were recorded between 200 and 800 nm using UV–Vis spectrophotometer (UV-260 Shimadzu, with 1-cm quartz cuvettes). Fourier transform-infrared (FT-IR) spectra of the Schiff base ligands and metal complexes were investigated using KBr pellets on a Perkin-Elmer 283 spectrophotometer. ^{1}H-NMR and ^{13}C-NMR measurements were recorded using Brucker WH 300 (200 MHz) and Brucker WH 270 (67.93 MHz) using DMSO-d_6 as a solvent and tetramethylsilane as an internal standard. ESI-MS (AB-Sciex 2000, Applied Biosystem) was used to record mass spectra of the synthesized ligands and complexes. The magnetic susceptibility of the investigated compounds was measured using the Faraday balance. Powder X-ray diffraction (XRD) studies of the synthesized compounds were carried out at room temperature using Rigaku, Mini Flex II powder diffractometer using CuKα

monochromatic radiation (λ = 1.5406 Å) in the range of $10° \leq 2\theta \leq 80°$. The thermogravimetric analysis (TGA/DTG) was carried out in the temperature range of 20–1000°C in a dynamic nitrogen atmosphere with a heating rate of 10°C/min using NETZSCH STA 449F3 thermal analyzer.

2.2 | Synthesis

2.2.1 | Synthesis of Schiff base ligand (L1)

The Schiff base ligand *N*,*N*′-bis(4-dimethylamino) benzylidene-ethane-1,2-diamine (**L1**) was synthesized by the condensation reaction of 4-(dimethyl-amino)benzaldehyde (0.60 g, 4 mmol) and ethylenediamine (0.13 ml, 2 mmol) dissolved in ethanol in the stoichiometric ratio of 2:1, respectively, and the reaction mixture was stirred in a round-bottom flask for 4 hr at room temperature (approximately 25°C). The reaction was monitored by taking thin-layer chromatography at regular intervals. The white precipitate obtained was separated by filtration, washed with water and diethyl ether, and dried in vacuum over $CaCl_2$ for further use. Synthetic outline of the Schiff base ligand is shown in Scheme 1.

Color: off white; yield: 82%. Elemental anal. calcd for $C_{20}H_{26}N_4$: C, 74.50; H, 8.13; N, 17.38; found: C, 73.77; H, 8.10; N, 17.40; IR (KBr pellet, cm^{-1}): 1590 υ(-HC=N-), 1344 $\upsilon(C\text{-}N)_{aromatic}$, 1162 $\upsilon(C\text{-}N)_{aliphatic}$, 1480 υ(C=C), 2915υ($-CH_2$-). ^{1}H-NMR (DMSO-$d_6$, δ, ppm): 8.65 (s, 2H, CH=N), 3.05 (s, 12H, N-$(CH_3)_4$), 3.73 (s, 4H, N-CH_2), 6.69–7.52 (m, 8H, ArH). ^{13}C-NMR (DMSO-d_6, δ, ppm): 161.70 (-HC=N-), 40.60 ($-CH_3$), 61.86 ($-CH_2$-), 111.94, 124.50, 129.54, 152.23 ($-C_6H_4$-). Mass spectrum (ESI) $[M + H]^+$ = 323.2. UV–Vis (DMSO): λ/nm 286, 328.

2.2.2 | Synthesis of Schiff base ligand (L2)

(*E*)-1-(((2,3-dihydrobenzo[1,4]dioxin-6-yl)imino)methyl) Naphthalen-2-ol (**L2**) was synthesized from the condensation of 2-hydroxy-1-naphthaldehyde (0.86 g, 5 mmol) and 1,4-benzodioxane-6-amine (0.75 g, 5 mmol) dissolved in ethanol in the molar ratio of 1:1, respectively. The reaction mixture was stirred at room temperature for 4 hr. The yellow precipitate formed was filtered, and washed thoroughly with the least amount of ethanol and diethyl ether. Finally, the residue was collected and dried in a desiccator over anhydrous calcium chloride for further use.

Color: yellow; yield: 78%. Elemental anal. calcd for $C_{19}H_{15}NO_3$: C, 74.72; H, 4.95; N; 4.59; found: C, 74.80; H, 5.05; N, 4.62. IR (KBr pellet, cm^{-1}): 1610 υ(-CH=N-), 3251 υ(OH), 1286 υ(C-O), 1257 υ(C-O-C). ^{1}H-NMR (DMSO-d_6, δ, ppm): 9.59 (s, 1H, CH=N), 4.29(s, 4H, $-OCH_2$), 13.15 (s, 1H, OH), 6.94–8.51 (m, 9H, ArH).^{13}C-NMR (DMSO-d_6, δ, ppm): 170.05 (C-OH), 155.80 (CH=N), 144.96 (C-N),143.38 (C-O), 65.05–65.09 ($-OCH_2$), 109.46–138.73 (Ar Cs). Mass spectrum (ESI) $[M + Na]^+$ = 328.09. UV–Vis (DMSO): λ/nm 272, 330.

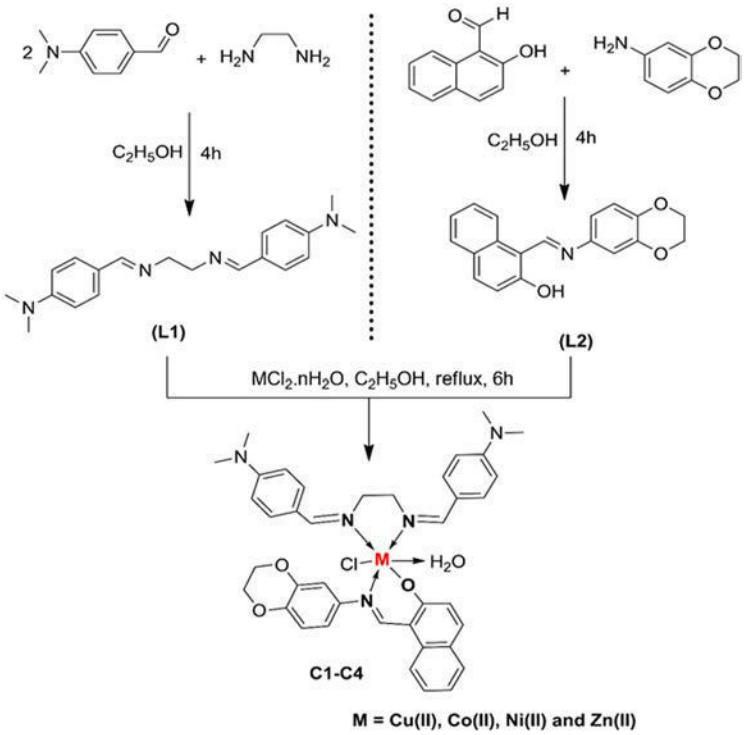

SCHEME 1 Synthesis of Schiff base ligands (**L1** and **L2**) and their heteroleptic complexes (**C1–C4**)

2.2.3 | Synthesis of heteroleptic metal complexes (C1–C4)

Ethanolic solution (15 ml) of metal salts, $[M(Cl_2)\cdot nH_2O]$ (2 mmol) was added to hot ethanolic solution (20 ml) of Schiff base ligand (**L1**) with constant stirring, and then after a few minutes an ethanolic solution of Schiff base ligand (**L2**) was added. Triethylamine was added to maintain the pH of solution. The reaction mixture was then refluxed for about 5–6 hr at 80°C. The reaction mixture was then cooled to room temperature. The precipitate formed was filtered, washed thoroughly with ethanol followed by diethyl ether to remove the unreacted compounds, and finally dried in a vacuum over fused calcium chloride in a desiccator.

$[Cu(L1)(L2)Cl\cdot H_2O]$ (C1)

Color: pale green; yield: 68%. Elemental anal. calcd for $[C_{39}H_{42}ClCuN_5O_4]$: C, 62.98; H, 5.69; N, 9.42; found: C, 63.72; H, 5.72; N, 9.47. IR (KBr pellet, cm^{-1}): 1585 υ(CH=N), 1298 $\upsilon(C\text{-}O_{phenol})$, 1359 $\upsilon(C\text{-}N)_{aromatic}$, 1178 $\upsilon(C\text{-}N)_{aliphatic}$, 1263 υ(C-O-C), 3490 υ OH), 562 υ(Cu-O), 448 υ(Cu-N). Mass spectrum (ESI) $[M + H]^+ = 742.3$.

$[Co(L1)(L2)Cl\cdot H_2O]$ (C2)

Color: black; yield: 65%. Elemental anal. calcd for $[C_{39}H_{42}ClCoN_5O_4]$: C, 63.37; H, 5.73; N, 9.47; found: C, 63.40; H, 5.79; N, 9.52. IR (KBr pellet, cm^{-1}): 1592 υ(CH=N), 1350 $\upsilon(C\text{-}N)_{aromatic,}$ 1290 $\upsilon(C\text{-}O_{phenol})$, 1263 υ(C-O-C), 1166 $\upsilon(C\text{-}N)_{aliphatic}$, 3497 υ(OH), 562 υ(Co-O), 457 υ(Co-N). Mass spectrum (ESI) $[M + H]^+ = 739.3$.

$[Ni(L1)(L2)Cl\cdot H_2O]$ (C3)

Color: brown; yield: 69%. Elemental anal. calcd for $[C_{39}H_{42}ClN_5NiO_4]$: C, 63.39; H, 5.73; N, 9.48; found: C, 63.09; H, 5.76; N, 9.57. IR (KBr pellet, cm^{-1}): 1582 υ(CH=N), 1290 $\upsilon(C\text{-}O_{phenol})$, 1347 $\upsilon(C\text{-}N)_{aromatic}$, 1165 $\upsilon(C\text{-}N)_{aliphatic}$, 1262 υ(C-O-C), 3495 υ(OH), 556 υ(Ni-O), 460 υ(Ni-N). Mass spectrum (ESI) $[M + H]^+ = 738.8$.

$[Zn(L1)(L2)Cl\cdot H_2O]$ (C4)

Color: orange yellow; yield: 70%. Elemental anal. calcd for $[C_{39}H_{42}ClN_5O_4Zn]$: C, 62.82; H, 5.68; N, 9.39; found: C, 63.12; H, 5.72; N, 9.60. IR (KBr pellet, cm^{-1}): 1590 υ(CH=N), 1302 $\upsilon(C\text{-}O_{phenol})$, 1353 $\upsilon(C\text{-}N)_{aromatic}$, 1175 $\upsilon(C\text{-}N)_{aliphatic}$, 1264 υ(C-O-C), 3497 υ(OH), 570 υ(Zn-O), 475 υ(Zn-N). ^{1}H-NMR (DMSO-d_6, δ, ppm): 8.72, (s, 2H, CH=N), 9.60 (s, 1H, CH=N), 3.14 (s, 12H, N-$(CH_3)_4$), 3.80 (s, 4H, N-CH_2),4.37 (s, 4H, -OCH_2), 6.69–7.89 (m, ArH). ^{13}C-NMR (DMSO-d_6, δ, ppm): 162.30, 156.85 (-HC=N-), 42.65 (-CH_3), 61.19 (-CH_2-), 170.15 (C-O), 145.51 (C-N), 143.44 (-O-C), 65.10 (-OCH_2), 109.47–138.57 (Ar Cs). Mass spectrum (ESI) $[M + H]^+ = 743.7$.

3 | BIOLOGICAL INVESTIGATIONS

3.1 | Strains, media and chemicals

All the strains used in this study are detailed in Table 3, which consists of eight FLC-susceptible (including one laboratory strain *C. albicans* SC5314 and seven clinical isolates) and three FLC-resistant clinical isolates. All the clinical *C. albicans* strains were collected from Charlotte Maxeke Johannesburg Academic Hospital, Johannesburg, South Africa, and were stored in glycerol stocks at−80°C in the Department of Clinical Microbiology and Infectious Diseases. All the test strains were isolated from patients under the ethical clearance number M10102 obtained from the Human Research Ethics Committee, University of the Witwatersrand. Prior to experiments, *Candida* isolates were revived by plating on Sabouraud Dextrose (SD) Agar (Sigma Aldrich, USA), followed by growing single colonies in fresh SD broth. FLC and amphotericin were purchased from Sigma Fluke (USA). All other chemicals and media were purchased from Sigma Aldrich and Merck.

TABLE 1 Physico-chemical properties of Schiff base ligands (**L1** and **L2**) and their heteroleptic complexes (**C1–C4**)

Compound	Color	Mol. formula	Mol. wt.	(m/z) ratio	Yield (%)	Λ_m (Ω^{-1} cm^2 mol^{-1})	m.p. (°C)	μ_{eff} (B.M.)
L1	Off white	$C_{20}H_{26}N_4$	322.4	323.2	82	–	190	–
L2	Yellow	$C_{19}H_{15}NO_3$	305.3	328.0	78	–	192	–
C1	Pale green	$[C_{39}H_{42}ClCuN_5O_4]$	742.2	742.3	68	26	252	1.90
C2	Black	$[C_{39}H_{42}ClCoN_5O_4]$	738.2	739.3	65	20	285	4.90
C3	Brown	$[C_{39}H_{42}ClN_5NiO_4]$	737.2	738.8	69	17	310	3.70
C4	Orange Yellow	$[C_{39}H_{42}ClN_5O_4Zn]$	743.2	743.7	70	22	290	Diamag.

TABLE 2 Thermoanalytical results (TG and DTG) of heteroleptic complexes (**C1–C4**)

Complex	TG range (°C)	DTG_{max} (°C)	*n**	Found (calcd %) Weight loss	Total weight loss	Assignment	Metallic residue
$[C_{39}H_{42}ClCu\ N_5O_4]$	100–230	148,222	2	6 (7.18)		Loss of one coordinated H_2O and $\frac{1}{2}Cl_2$ molecule	Cu
	230–490	347	1	40 (41.07)	88 (91.62)	Loss of $C_{19}H_{15}NO_3$	
	490–800	660	1	42 (43.37)		Loss of $C_{20}H_{26}N_4$	
$[C_{39}H_{42}ClCoN_5O_4]$	100–220	142,220	2	6.50 (7.24)		Loss of one coordinated H_2O and $\frac{1}{2}Cl_2$ molecule	Co
	220–480	315	1	40.50 (41.33)	89.40 (92.21)	Loss of $C_{19}H_{15}NO_3$	
	480–880	674	1	42.40 (43.64)		Loss of $C_{20}H_{26}N_4$	
$[C_{39}H_{42}ClN_5NiO_4]$	100–240	130,229	2	6 (7.22)		Loss of one coordinated H_2O and $\frac{1}{2}Cl_2$ molecule	Ni
	240–500	376	1	40 (41.37)	89 (92.39)	Loss of $C_{19}H_{15}NO_3$	
	500–920	754	1	43 (43.8)		Loss of $C_{20}H_{26}N_4$	
$[C_{39}H_{42}ClN_5O_4Zn]$	100–250	120,220	2	6 (7.18)		Loss of one coordinated H_2O and $\frac{1}{2}Cl_2$ molecule	Zn
	250–540	287	1	41 (41.03)	90 (91.56)	Loss of $C_{19}H_{15}NO_3$	
	540–790	710	1	43 (43.35)		Loss of $C_{20}H_{26}N_4$	

*n** = number of decomposition.

TABLE 3 MICs (μg/ml) of ligands (**L1**, **L2**) and the complexes (**C1–C4**) against FLC-susceptible and -resistant *Candida albicans* isolates

Strains		MICs (μg/mL) L1 MIC	L1 MFC	L2 MIC	L2 MFC	C1 MIC	C1 MFC	C2 MIC	C2 MFC	C3 MIC	C3 MFC	C4 MIC	C4 MFC	FLC MIC
	Candida albicans SC5314	100	–	100	–	6.25	12.5	0.40	3.12	0.10	1.60	12.5	25	0.25
FLC-susceptible	4175	100	–	100	–	6.25	12.5	0.40	3.12	0.10	1.60	12.5	25	0.12
	4179	100	–	50	–	12.5	12.5	3.12	6.25	0.20	3.12	50	50	0.25
	4180	100	–	100	–	6.25	12.5	0.40	3.12	0.10	1.60	12.5	25	0.25
	4251	100	–	100	–	6.25	12.5	0.40	3.12	0.10	1.60	12.5	50	0.25
	4554	100	–	50	–	6.25	12.5	0.40	3.12	0.10	1.60	12.5	50	0.25
	4563	100	–	100	–	6.25	12.5	1.60	3.12	0.20	1.60	12.5	25	0.25
	4576	100	–	100	–	6.25	12.5	0.40	3.12	0.10	1.60	12.5	25	0.25
FLC-resistant strains	4085	100	–	100	–	12.5	50	1.60	6.25	0.20	3.12	25	50	16
	4122	100	–	100	–	12.5	50	3.12	6.25	0.40	3.12	50	50	32
	4135	100	–	100	–	12.5	50	1.60	6.25	0.20	3.12	25	50	32

FLC, fluconazole; MIC, minimum inhibitory concentration.

3.2 | Antifungal susceptibility tests

3.2.1 | Determination of minimum inhibitory concentrations and minimum fungicidal concentrations

To determine the antifungal activity of newly synthesized Schiff base ligands (**L1** and **L2**) and their four complexes (**C1–C4**), minimum inhibitory concentrations (MICs) were determined against tested FLC-susceptible and FLC-resistant *C. albicans* isolates by serial micro-broth dilution assay following Clinical and Laboratory Standards Institute (CLSI)-recommended guidelines M27-A3,[22] with modifications. The initial concentrations of all the newly synthesized compounds were 400 μg/mL, in order to achieve the concentrations of 100, 50, 25, 12.5, 6.25, 3.12, 1.60, 0.8, 0.4, 0.2, 0.1 and 0.05 μg/mL in a 96-well plate after serial dilution. The positive control FLC (1000 μg/mL) and the negative vehicle control (1% DMSO) were also included in every set of experiments. Media and culture controls were included to confirm the sterility and viability, respectively. Further, minimum fungicidal concentration (MFC) was determined by subculturing the test dilutions from each well without color change on SD

agar plates and incubated for 24 hr. The lowest concentration that showed no fungal growth on the agar plate was defined as the MFC value. All the experiments were done in triplicate, and all the results were expressed in μg/mL.

3.2.2 | Sterol quantification

To study the effect of newly synthesized compounds on the ergosterol biosynthesis pathway, total intracellular sterols were extracted and quantified using a spectrophotometer, as reported previously.[23] One FLC-susceptible and one -resistant isolate of *C. albicans* cells were treated with MIC and ½ MIC values of both the ligands and their four derivatives. In all the tests, there is a negative control (without test compound) and positive control (2 μg/mL FLC). All the sterol samples were scanned spectrophotometrically between 240 and 300 nm, using a spectrophotometer. The presence of ergosterol and the late sterol intermediate 24(28) DHE in the extracted sample resulted in a characteristic four-peaked curve. The absence of detectable ergosterol in extracts was indicated by a flat line. Ergosterol content was calculated as a percentage of the wet weight of the cell, using the following equations:

$$\%\text{ergosterol} + \%24(28)\ \text{DHE} = [(A_{281.5}/290) \times F]/\text{pellet weight}$$
$$\%24(28)\ \text{DHE} = [(A_{230}/518) \times F]/\text{pellet weight}$$
$$\%\text{ergosterol} = [\%\text{ergosterol} + \%24(28)\ \text{DHE}] - \%24(28)\ \text{DHE}$$

where F is the factor for dilution in ethanol, and 290 and 518 are the E values (in percentages per centimeter) determined for crystalline ergosterol and 24(28) DHE, respectively.

3.2.3 | Effect on membrane permeability

Based on the MIC results, all the active compounds (**C1**, **C2**, **C3** and **C4**) except the ligands were tested to study the effect on membrane integrity, by doing flow cytometry using propidium iodide (PI). PI is a fluorescent dye with a characteristic to enter into necrotic cells with disintegrated membranes. Mid-exponentially grown *C. albicans* cells were exposed to MFC values of the test entities for 2 hr. After the exposure time, cells were harvested and resuspended in phosphate-buffered saline. To this solution, 1 mL of PI was added with a final concentration of 1 mg/mL of PI. All the samples were incubated at 35°C for 15 min in the dark at room temperature. In every set of experiments, negative (untreated cells) and positive (2 μg/mL amphotericin B-treated cells) controls were included. Unstained cells were always included as autofluorescence controls. Cell-associated fluorescence was measured using a flow cytometry BD LSRFortessa cell analyzer (Becton Dickinson, USA). The results were analyzed using FlowJo software version 10.0. For data analysis, quadrants were adjusted, analyzed and interpreted as reported earlier.[24]

4 | RESULTS AND DISCUSSION

The heteroleptic complexes (**C1–C4**) were successfully prepared by reacting equimolar amounts of Schiff base ligands (**L1** and **L2**) with the corresponding metal salts in the presence of triethylamine. The metal complexes were neutral, colored, air-stable, and insoluble in water and common organic solvents but remarkably soluble in DMF and DMSO. Synthesis and the final structures of the ligands and their complexes were verified by different physical and spectroscopic techniques. The different physico-chemical properties of Schiff base ligands (**L1** and **L2**) and metal complexes (**C1–C4**) are shown in Table 1. The molar conductivity (Λm) of the complexes was carried out using DMSO (10^{-3} M) at 25°C. The results obtained were in the range of 17–26 $\Omega^{-1}cm^2m^{-1}$, which showed their non-electrolytic nature.

4.1 | Magnetic susceptibility and electronic spectral studies

The geometry of the synthesized heteroleptic complexes was obtained from the electronic spectral data and magnetic susceptibility measurements. The electronic absorption spectra of the ligands (**L1** and **L2**) and their complexes (**C1–C4**) were recorded in 10^{-3} M DMSO solution in the range of 200–800 nm using the same solvent as blank. The UV–Vis spectrum of **L1** displayed two absorption bands at 286 and 328 nm, and **L2** also showed two absorption bands at 272 and 330 nm corresponding to π-π* and *n*-π* transitions, respectively. In complexes, these bands were shifted towards lower or higher wavelengths signifying the coordination of ligands to metal ions, as shown in Figure 1. The addition of metal ion to ligands produced characteristic changes in the visible absorption spectrum of the ligands, signifying the complex formation. In complexes, a band appeared in the region 352–424 nm corresponding to charge transfer from ligand to metal. In complex **C1** the absorption band appearing at 398 nm can be attributed to charge transfer from ligand to metal. The broad asymmetric band in **C1** appearing at 681 nm corresponded to a combination of three bands $^2B_{1g} \rightarrow {}^2A_{1g}$ (υ_1), $^2B_{1g} \rightarrow {}^2B_{2g}$ (υ_2) and $^2B_{1g} \rightarrow {}^2E_g$ (υ_3), which are similar in energy. The broadness of the band showed its distortion from the octahedral geometry and provided the indication for Jahn Teller distortion.[25,26] The magnetic moment of this

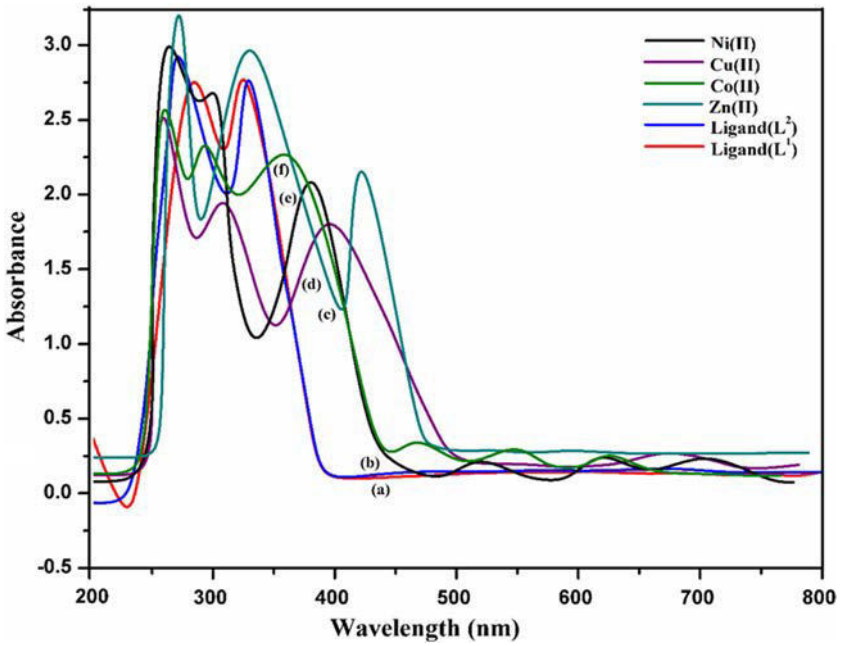

FIGURE 1 UV–Vis spectra of: (a) Schiff base (**L1**); (b) L2; (c) Zn (II); (d) Cu (II); (e) Ni (II); and (f) Co (II) complexes in 10^{-3} M dimethylsulfoxide (DMSO) solution

complex was found to be 1.90 B.M., which lies within the normal range for octahedral Cu (II) complexes. The electronic absorption spectrum of **C2** shows bands at 460, 550 and 630 nm that are assigned to $^4T_{1g}(F) \rightarrow {}^4T_{1g}(P)$, $^4T_{1g}(F) \rightarrow {}^4A_{2g}(F)$ and $^4T_{1g}(F) \rightarrow {}^4T_{2g}(F)$, respectively. The band at 382 nm corresponds to ligand to metal charge transfer band.[27] The magnetic moment of complex (**C2**) was found to be 4.90 B.M. The absorption bands and the magnetic moment suggested an octahedral geometry around the Co (II) ion. The absorption spectrum of **C3** displayed three absorption bands at 521, 634 and 705 nm, which may be attributed to $^3A_{2g} \rightarrow {}^3T_{1g}(P)$, $^3A_{2g} \rightarrow {}^3T_{1g}(F)$ and $^3A_{2g} \rightarrow {}^3T_{2g}$ transitions, respectively.[28] The spectrum also displayed a band at 398 nm, which may be assigned to ligand to metal charge transfer. The magnetic moment observed for complex **C3** was found to be 3.7 B.M. The absorption spectra and magnetic moment reveal that there is an octahedral geometry around the Ni (II) ion. In **C4** the absorption band found at 424 nm may be attributed to the ligand to metal charge transfer with zero magnetic moment. Due to the diamagnetic nature of complex **C4**, no d-d bands were observed. An octahedral geometry has been proposed for the complex **C4**.

4.2 | FT-IR spectra

The IR spectra of the complexes were compared with those of the free Schiff base ligands (**L1** and **L2**) to verify the coordination sites that may be involved in chelation. In complexes, the position or intensity of the peaks obtained for ligands are expected to change upon chelation. The characteristic peaks are given in Section 2.2. The sharp band observed at 1602 cm^{-1} in the spectrum of free Schiff base ligand (**L1**) was assigned to υ (CH=N) stretching vibrations. In Schiff base ligand (**L2**), the υ(CH=N) stretching vibration was found at 1610 cm^{-1}. In the spectra of metal complexes, the υ(CH=N) stretching vibrations of azomethine were shifted to lower wavenumbers, which revealed the participation of the azomethine nitrogen in coordination. The participation of deprotonated phenolic OH in complexation was verified by the blue shift of υ(C-O) stretching band, present at 1286 cm^{-1} in the free ligand **L2**, which shifted to higher wavenumbers by 4–16 cm^{-1} in complexes. The IR spectrum of the **L2** ligand displayed a broad band at 3152 cm^{-1}, which could be assigned to the phenolic OH group.

In complexes (**C1–C4**), the broad bands present at 3490–3497 cm^{-1} might be attributed to the stretching frequencies of the υ(OH) of coordinated water molecules present in these complexes. In Schiff base ligand **L2** and complexes, the bands present at 1256–1263 cm^{-1} were assigned to C-O-C stretching vibrations. In complexes **C1–C4**, new bands are found in the regions 556–570 cm^{-1}, which were attributed to υ(M-O) stretching vibrations, and the bands present at 448–475 cm^{-1} in complexes have been ascribed to υ(M-N) of the azomethine mode. Therefore, from the IR spectra data it was revealed that the ligand (**L1**) behaves as a bidentate ligand with NN donor sites coordinating to the metal ions through

azomethine N atoms. The ligand (**L2**) also behaves as a bidentate ligand with NO donor sites coordinating to metal ions through azomethine N and phenolic O atoms. The IR spectra of the Schiff base ligands (**L1** and **L2**) and complex **C3** as an example is shown in Figure 2, and the spectra of complexes (**C1**, **C2** and **C4**) are given in the supplementary data.

4.3 | ^{1}H-NMR and ^{13}C-NMR spectra

The ^{1}H-NMR spectral data of the Schiff base ligands (**L1**, **L2**) and **C4** complex were recorded in DMSO-d_6 for the interpretation of number and nature of protons relative to TMS with chemical shifts given in ppm. The ^{1}H-NMR spectra of the Schiff bases (**L1** and **L2**) displayed singlet signals at 8.65 and 9.59 ppm, respectively, attributed to the protons of azomethine nitrogen (CH=N), which confirmed the formation of Schiff base ligands. In **C4** complex, a shift of electron density from ligands to metal ion has been detected. The signal for the azomethine protons is slightly deshielded and appeared at 8.72 and 9.60 ppm, and this downfield shift confirms the coordination of azomethine nitrogen with the Zn (II) metal ion (Figure 3). In **L1**, the two sharp singlets at 3.73 and 3.05 ppm are ascribed to active methylene protons (-CH_2 and -N-$(CH_3)_4$), respectively. The ^{1}H-NMR spectra of **L2** exhibited a sharp singlet at 4.29 ppm attributed to methylene protons (-OCH_2). The Ph-OH proton of **L2** appeared as a singlet at 13.15 ppm.[29] In **C4** complex, the Ph-OH proton signal was found absent confirming the complexation through phenolic oxygen. In **C4** complex, a new signal has been found at 3.48 ppm due to the presence of coordinated H_2O protons. The aromatic protons in **C4** complex appeared as a set of multiplets in the region of 6.69–7.89 ppm. The positions of the main signals in the ^{1}H-NMR and ^{13}C-NMR are stated in the Experimental section. The attained ^{13}C values of **C4** complex were compared with the corresponding ligands and were in good agreement with the proposed structure of the **C4** complex. In Schiff base ligands (**L1** and **L2**), the azomethine carbon atoms were observed at 161.70 and 155.80 ppm, which were shifted to 162.30 and 156.85 ppm in **C4** complex, respectively. The paramagnetic **C1**, **C2** and **C3** complexes did not show fine NMR spectra and were therefore not included in this study. The ^{1}H-NMR of Schiff base ligands and ^{13}C-NMR of **L1**, **L2** and **C4** are shown in the supplementary data.

4.4 | Mass spectra

The mass spectra of the Schiff base ligands (**L1**, **L2**) and complexes (**C1–C4**) are characterized by moderate to high

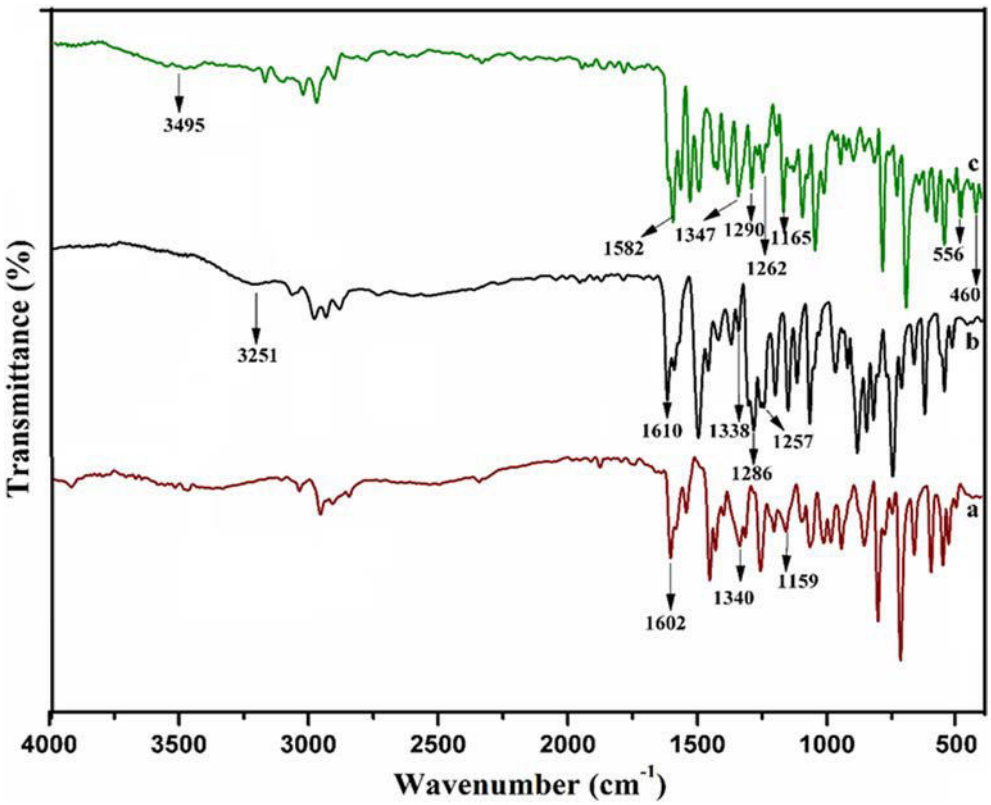

FIGURE 2 Fourier transform-infrared (FT-IR) spectra of: (a) Schiff base (**L1**); (b) Schiff base (**L2**); and (c) Ni (II) complex (**C3**)

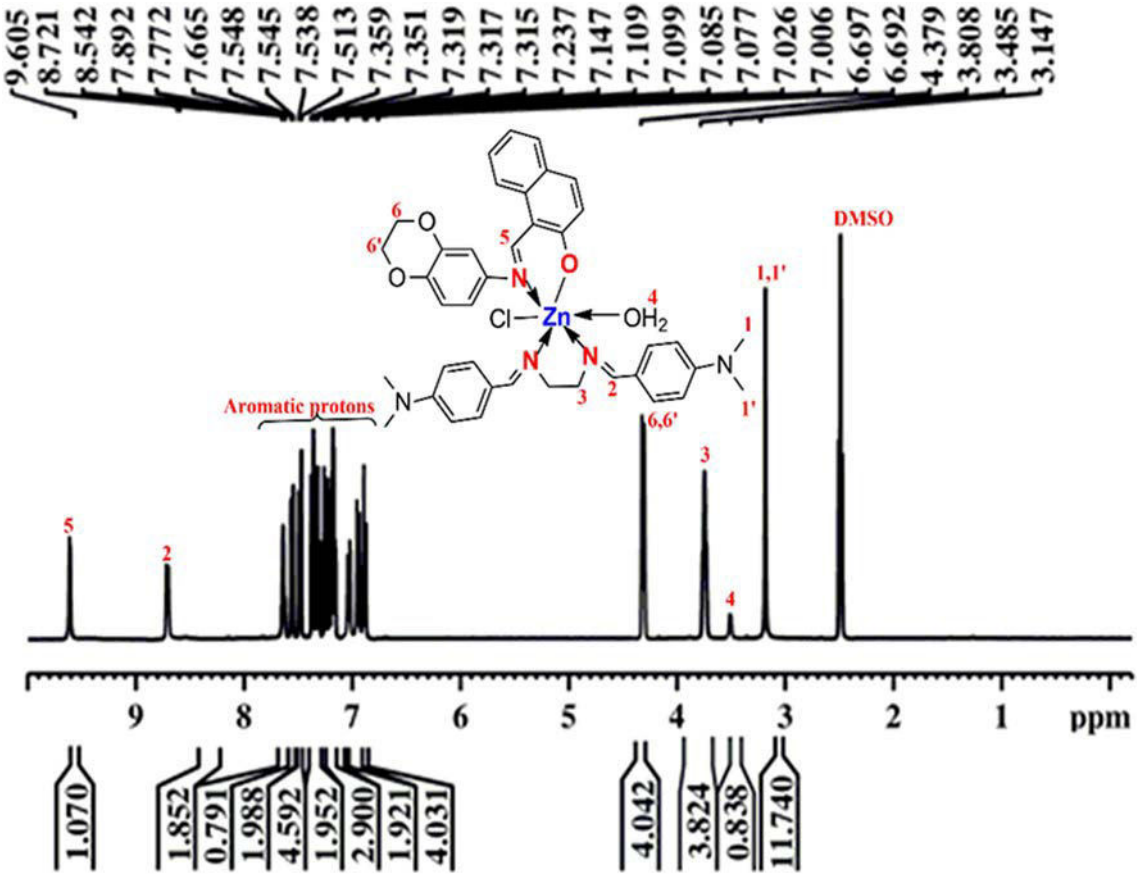

FIGURE 3 ^{1}H-NMR spectrum of **C4** complex in dimethylsulfoxide (DMSO)-d_6

relative intensity molecular ion peaks. It is noticeable that the molecular ion peaks are in good agreement with the suggested empirical formula of the compounds. The mass spectra $[M + H]^+$of Schiff base ligand (**L1**) showed the molecular ion peak at m/z 323.2, and the mass spectra $[M + Na]^+$ of **L2** showed the molecular ion peak at m/z 328.0. The mass spectra $[M + H]^+$ of metal complexes (**C1**, **C2**, **C3** and **C4**) showed molecular ion peaks at 742.3, 739.3, 738.8 and 743.7, respectively. The mass spectra of the synthesized compounds are given in the supplementary data.

4.5 | Powder X-ray diffraction studies

All the efforts failed to grow single crystals of synthesized compounds suitable for single X-ray crystallography. So, X-ray powder diffraction studies of the compounds were carried out to get more details about their structure. The powder XRD of the compounds were carried out in the range 10-80^{o} (θ) at a wavelength of 1.54 Å. The XRD pattern indicates that the ligands (**L1**, **L2**) and complexes (**C1**, **C2**, **C4**) have well-defined crystalline patterns with various degrees of crystallinity. The XRD pattern of **L1**, **L2** and complex **C1** is shown in Figure 4. In complex **C3**, the trend of curves decreases from maximum to minimum intensity indicating its amorphous nature. Some new extra peaks were found in complexes as compared with ligand, signifying the coordination of ligand to metal ions. The XRD of ligand (**L1**) displayed reflecting peaks at 2θ scattering angles of 11.50, 14.30, 17.97, 23.92, 25.73 and 27.10. The **L2** exhibited reflecting peaks at 2θ scattering angles of 15.94, 19.62, 20.64, 23.78, 24.98 and 28.86, while complex **C1** exhibited reflecting peaks at 2θ scattering angles of 15.87, 17.10, 20.10, 20.42, 22.50, 25.10, 26.94 and 29.50 assigned to (100), (110), (111), (021), (111), (121), (102) and (022) crystal planes, respectively, characteristic of well-ordered monoclinic arrangement of Cu atoms (space group: P21/c, JCPDS: 72–0438). The complex **C2** displayed fine reflecting peaks at 2θ scattering angles of 15.03, 15.70, 17.38, 18.70, 23.15, 23.40, 25.70, 31.30 and 33.28 ascribed to (100), (001), (110), (111), (120), (021), (101), (131) and (202) crystal planes, respectively, characteristic of well-ordered monoclinic arrangement of Co atoms (space group: P21/m, JCPDS: 75–2160), whereas complex **C4** showed reflecting peaks at 2θ scattering angles of 11.35, 13.54, 15.12, 19.63, 20.43, 22.12 and 29.85 assigned to (010), (110), (111), (210), (211), (113) and (123) crystal planes, respectively,

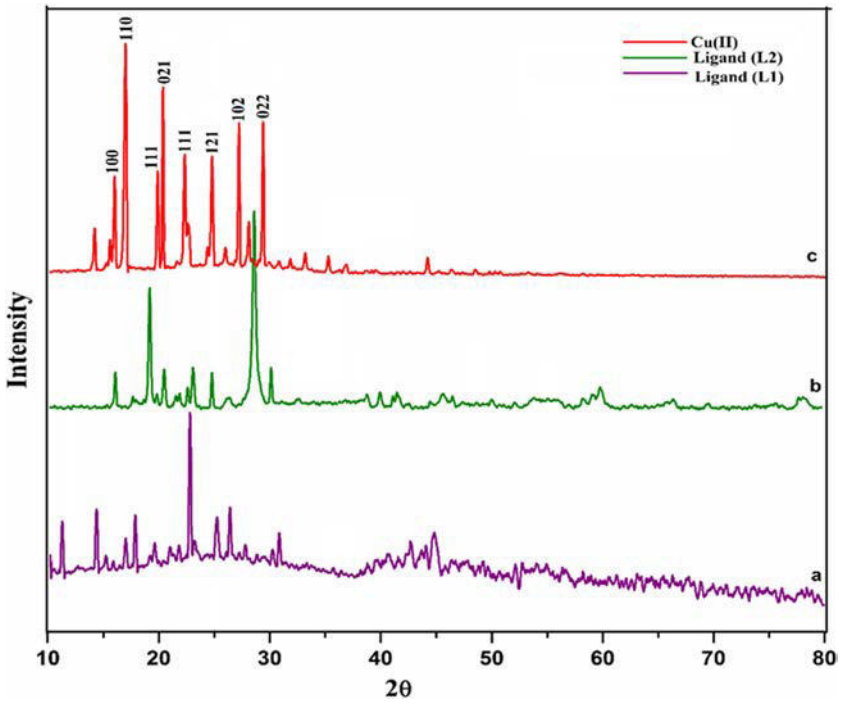

FIGURE 4 Powder X-ray diffraction (XRD) pattern of: (a) Schiff base ligand (**L1**); (b) **L2**; and (c) **C1** complex

characteristic of well-organized orthorhombic arrangement of Zn atoms (space group: $Pca2_1$, JCPDS: 76–0778). The detailed XRD parameters of the complexes are listed in Table S1.

The average crystallite size of the ligands (**L1** and **L2**) and the complexes (**C1**, **C2** and **C4**) was estimated using the Debye Scherrer's formula.[30]

$$D = 0.9\lambda / \beta\cos\theta$$

where constant 0.9 is the shape factor, D is the particle size, λ is the X-ray wavelength of CuKα radiation (1.5406 Å), θ is the Bragg diffraction angle and β is the full-width at half-maximum value of θ.[30] The average crystallite sizes of the ligands (**L1** and **L2**) and the complexes (**C1, C2** and **C4**) were found to be 30.79, 30.18, 39.87, 26.68 and 34.28 nm, respectively.

4.6 | Thermal analysis (TG and DTG)

The thermal analysis of the complexes (**C1–C4**) was studied by using thermogravimetric techniques (Thermal Gravimetric Analysis and Derivative Thermogravimetry) within a temperature range from room temperature to 1000°C at a heating rate of 10°C/min. As a representative case, the TG/DTG curve of **C1** is depicted in Figure 5. The TGA/DTG data of complexes are summarized in Table 2.

The thermal decomposition of **C1** occurs in three stages. The first stage proceeded with two degradation steps with the weight loss of 6% (calcd 7.18%) in the temperature range of 148–222°C with DTG peaks observed at 148 and 222°C. This weight loss is due to the simultaneous loss of coordinated water molecule and chlorine atom. The second stage continued with one degradation step with the weight loss of 40% (calcd 41.07%) in the temperature range of 230–490°C with DTG peak observed at 347°C. This weight loss is due to the loss of $C_{19}H_{15}NO_3$ fragment. The third stage occurred at the temperature range of 490–800°C with the weight loss of 42% (calcd 43.37%) due to the loss of $C_{20}H_{26}N_4$ fragment with DTG peak observed at 660°C. The overall weight loss observed in **C1** was found to be 88% (calcd 91.62%). The metallic Cu left as the residue has the observed weight of 10% against the calculated value of 11%.

Complex **C2** underwent degradation in three stages. The first stage occurred at the temperature range of 100–220°C with a weight loss of 6.50% (calcd 7.24%). The DTG peaks were observed at 142 and 220°C. This weight loss is due to the simultaneous loss of one coordinated water molecule and chlorine atom. The complex underwent further degradation at the temperature range of 220–480°C, with the loss of 40.50% (calcd 41.33) and the DTG peak was observed at 315°C. This weight loss is due to the loss of $C_{19}H_{15}NO_3$fragment. The third stage of degradation occurred at the temperature range of 480–880°C, with the loss of 42.40% (calcd 43.64%) and the DTG peak was observed at 674°C. This weight loss is due to the loss of $C_{20}H_{26}N_4$ fragment. The overall weight loss was found to be

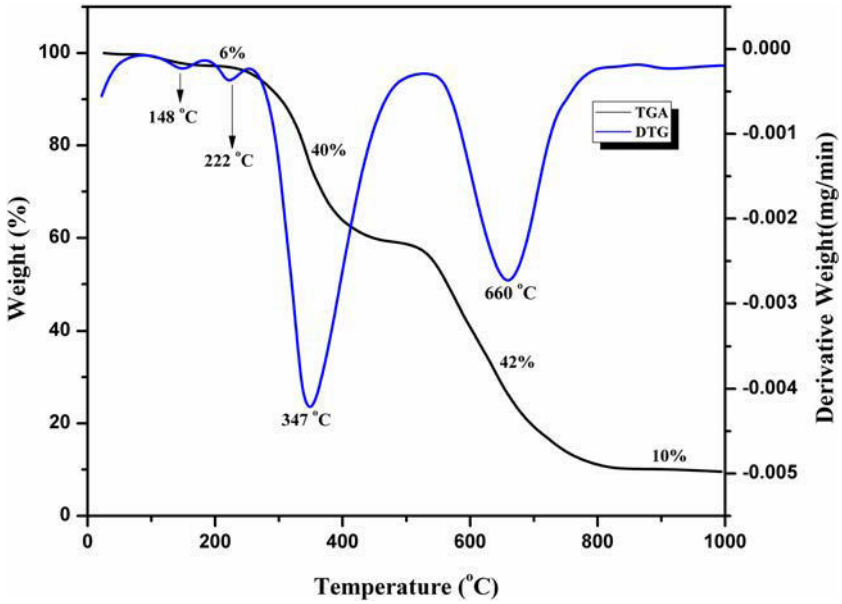

FIGURE 5 Thermogravimetric analysis (TGA) and DTG curves of complex **C1**

89.40% (calcd 92.21%). The metallic Co left as a residue has the observed weight of 10.60% against the calculated value of 7.79%.

The thermogram of **C3** showed degradation in three stages. The first degradation occurred at the temperature range of 100–240°C with the loss of 6% (calcd 7.22%), and the DTG peaks were observed at 130 and 229°C. This weight loss is due to the loss of one coordinated water molecule and chlorine atom. The second stage of degradation occurred at the temperature range of 240–500°C with the loss of 40% (calcd 41.37%) with the DTG peak observed at 376°C. This weight loss is due to the loss of $C_{19}H_{15}NO_3$ fragment. The third stage of degradation occurred at the temperature range of 500–920°C with the loss of 43% (calcd 43.8%), and the DTG peak was observed at 754°C. This weight loss is due to the loss of $C_{20}H_{26}N_4$ fragment. The total weight loss was found to be 89% (calcd 92.39%). The metallic Ni left as a residue has the observed weight of 11% against the calculated value of 7.61%.

The thermogram of **C4** showed the first stage of degradation due to the simultaneous loss of one coordinated water molecule and one chlorine atom at the temperature range of 100–250°C with the loss of 6% (calcd 7.18%). The DTG peaks were observed at 120 and 220°C. The complex underwent further degradation due to the loss of $C_{19}H_{15}NO_3$ fragment at the temperature range of 250–540°C with the loss of 41% (calcd 41.03%). The DTG peak was observed at 287°C. The third stage of degradation occurred due to the loss of $C_{20}H_{26}N_4$ fragment at the temperature range of 540–790°C with the loss of 43% (calcd 43.35%). The DTG peak was observed at 710°C. The overall weight loss was found to be 90% (calcd 91.56%). The metallic Zn left as a residue has the observed weight of 10% against the calculated value of 8.44%.

4.7 | Minimum inhibitory concentration and minimum fungicidal concentrations

The antifungal activity of all the newly synthesized ligands and their complexes was evaluated by determining their MIC and MFC values against 11 different *C. albicans* strains, including one laboratory standard strain, seven FLC-susceptible clinical strains and three FLC-resistant clinical strains. All the MIC results are summarized in Table 3. Evaluation of MIC depicts that among the two ligands and their four complexes, **C3** showed the highest inhibitory activity, while both ligands (**L1** and **L2**) showed the least inhibitory activity against all the tested strains. Based on the MIC values, the order of potency of the test compounds was **C3** > **C2** > **C1** > **C4** > **L1** ≥ **L2**. The median MIC values for **C3**, **C2**, **C1**, **C4**, **L1** and **L2** are 0.10, 0.40, 6.25, 12.5, 100 and 100, respectively. FLC was also tested, and the isolates with MIC values < 8 μg/mL for FLC were considered FLC-susceptible while the isolates with MIC ≥ 8 μg/mL were categorized as FLC-resistant, following the CLSI Interpretive Guidelines for *In vitro* Susceptibility Testing of *Candida* species.[31] Furthermore, all the test compounds were prepared to different concentrations using 1% DMSO, and therefore DMSO was used as negative vehicle control and was observed to have no inhibitory activity against any of the tested isolates. The MIC data revealed that the structural changes from ligand to its metal complexes produced the marked enhancement in their potency as antifungal agents.

The MFC is the lowest concentration of the test compounds that causes death of cells that can be observed on clear agar plates. Table 3 summarizes the MFC values of all the test compounds against 11 tested *C. albicans* isolates. Except two ligands (**L1**, **L2**), all the derivatives showed MFC values, depicting the fungicidal activity of newly synthesized compounds. The MFC values are generally two–fourfold higher than MIC values.

4.8 | Sterol quantitation

The antifungal effect of the tested compounds was rapid and lethal. The rapid irreversible action of the active complexes suggests that there may be a cellular target accessible to the compound externally. Therefore, we studied the effect of these active complexes on sterol biosynthesis. Figure 6 and Table S2 summarize the effect of these compounds on ergosterol biosynthesis in FLC-susceptible and -resistant *C. albicans* isolates at MIC and ½ MIC values of all the newly synthesized compounds. Sterol patterns were altered in a similar manner in FLC-susceptible and -resistant isolates when cells were treated with subinhibitory concentrations of the test compounds. These compounds completely blocked ergosterol synthesis at MIC values (Figure 6). As shown in Table S2, the decrease in total cellular ergosterol content for susceptible isolates ranged from 21% to 57% for cells grown in ½ MIC values to 62% to 93% for cells grown with MIC values of the test compounds. Similarly, for resistant isolates, the decrease in total cellular ergosterol content ranged from 28% to 63% when treated with ½ MIC, and 71% to 97% when treated with MIC values of the test compounds, respectively. As expected, the decrease in total cellular ergosterol content of susceptible cells treated with FLC was measured to be 96%. In contrast to this, resistant isolates only showed decline in ergosterol content by 37%.

Ergosterol and its biosynthesis pathway is an established drug target for different classes of antifungal drugs including that of azoles and polyenes. There are several studies reporting that the manipulation of this drug target is responsible for drug resistance in different fungal species including *C. albicans*. Our results clearly indicate that the resistant isolates used in this study are resistant due to the overexpression of ergosterol. The survival of these cells at ½ MIC values of the test compounds, where more than 50% ergosterol biosynthesis was inhibited, indicate that these *C. albicans* isolates belong to ergosterol-tolerant class. Due to the structural variability of these compounds, it is possible that they interact with different enzymes of the ergosterol pathway and thereby inhibit its biosynthesis. However, further in-depth studies are required to elucidate the actual binding of these compounds with the specific enzymes.

4.9 | Effect on membrane integrity

The effect of active compounds (**C1–C4**) on disruption of membrane integrity in *C. albicans* was studied using flow

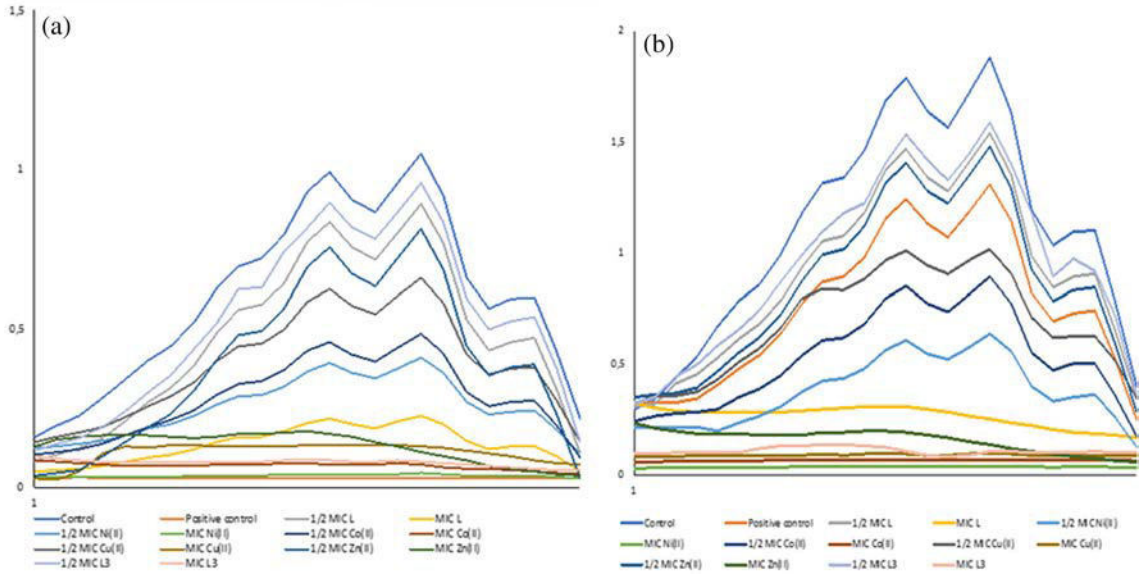

FIGURE 6 UV spectrophotometric sterol profiles of representative fluconazole(FLC)-susceptible (a) and FLC-resistant (b) *Candida albicans* isolates. Isolates were grown for 16 hr in Sabouraud Dextrose (SD) broth containing ½ minimum inhibitory concentration (MIC) and MIC values of two ligands and four derivatives. Sterols were extracted from cells, and spectral profiles in the range 240–300 nm were determined. Control represents untreated cells, while positive control represents cells treated with 2 μg/mL of FLC

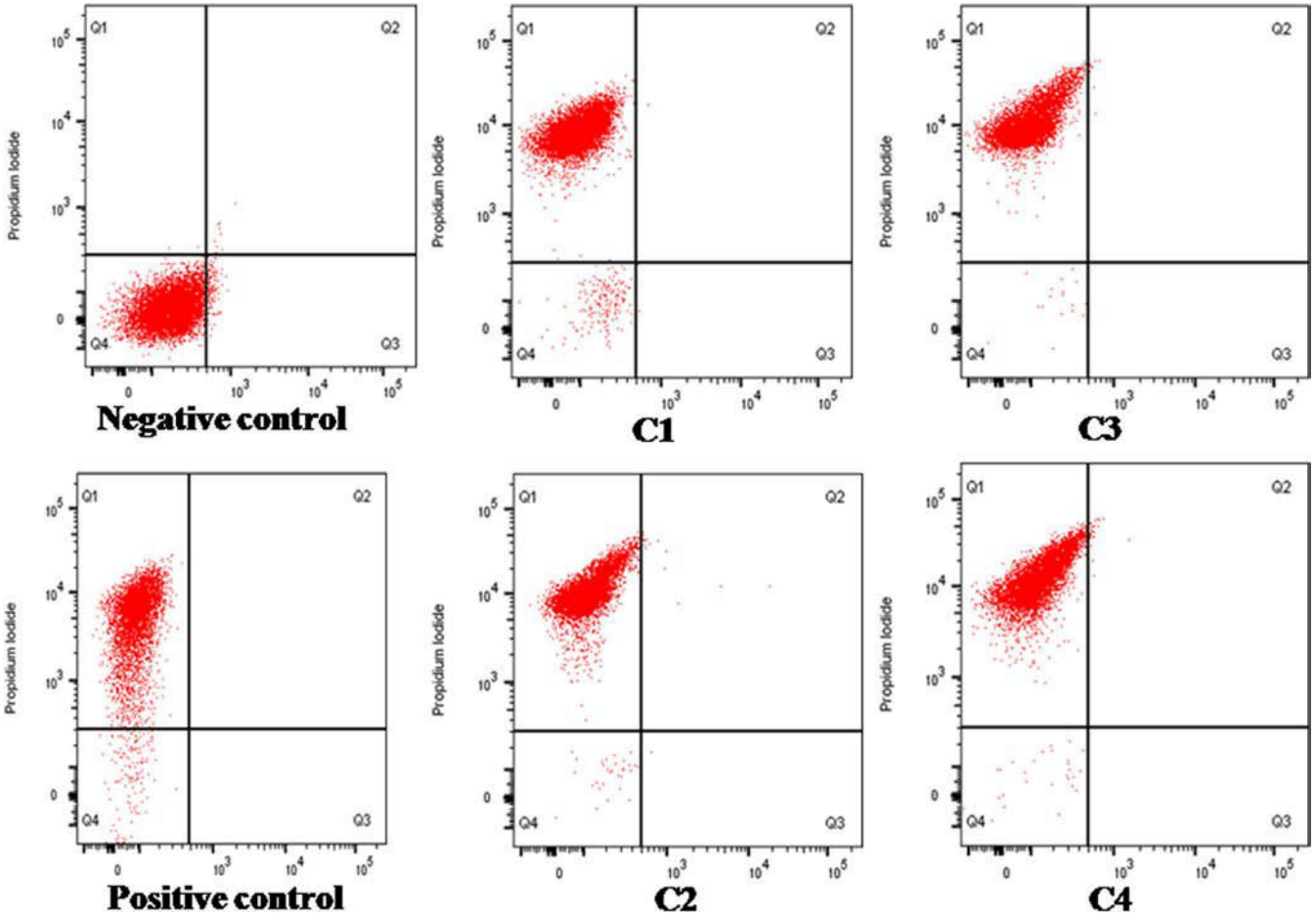

FIGURE 7 Sequence of density plots showing *Candida albicans* SC5314 cells analyzed by flow cytometry for the samples treated with minimum fungicidal concentrations (MFCs) of compounds **C1**, **C2**, **C3** and **C4**. Negative and positive controls are untreated and 2 μg/ml amphotericin B-treated cells, respectively. Density plots show relative fluorescence intensities of *Candida* cells marked with propidium iodide (PI) on the *y*-axis. The lower left quadrant (Q4) marked the morphologically intact live cells observed with higher relative fluorescence intensity, while the upper left grid (Q1) marked dead cells

cytometer. PI is the most commonly used fluorescent dye to study the effect of drugs on cell membranes. Live cells with integrated membranes will not allow PI to internalize the cells; however, dead cells with disintegrated membranes internalize PI, resulting in an increase in red fluorescence.[24] The PI penetration in *C. albicans* cells treated with MFC values of test compounds along with negative and positive controls are summarized in Figure 7. All the four tested compounds along with amphotericin B at MFC values showed >90% PI internalization, indicating that these compounds have a potential to disintegrate cell membranes at the higher concentrations similarly to that of amphotericin B.

The membrane damage in collaboration with the inhibition of ergosterol biosynthesis by these derivatives can contribute to membrane malfunctioning resulting in membrane depolarization, intracellular content leakage, disturbance in membrane permeability and ultimately cell death. The results in this study are in congruent with the previous findings where derivatives from natural products have been reported to disrupt fungal membrane integrity causing cell death.[24,32]

5 | CONCLUSIONS

In this study, some heteroleptic complexes derived from two Schiff base ligands, obtained from biologically important scaffolds were synthesized in a quest to find better antifungal therapeutic agents. With the help of spectral and other physical measurements, an octahedral geometry was assigned to the complexes **C2**, **C3** and **C4**, while a distorted octahedral geometry was assigned to the complex **C1**. The antifungal activity evaluation against susceptible and resistant *C. albicans* revealed that both the ligands have moderate activity, while derivative complexes have strong antifungal activity. Insight mechanisms revealed that these complexes disrupt cell membranes and also deplete ergosterol content. To conclude, this work suggests that these compounds could

be promising antifungal drugs, and also advocates the determination of optimal concentrations for clinical applications for the treatment and prevention of candidiasis. The excellence of these compounds demands more insight studies into all other possible mechanisms.

ACKNOWLEDGEMENTS

The author OAD is thankful to University Grants Commission (UGC), Government of India for financial assistance through Central University Ph.D. Students Fellowship. AA acknowledges financial support from University Research Committee Grant for 2019 - Friedel Sellschop Award (Grant No: AZMD019). The funders had no role in study design, data collection and analysis, decision to publish, or preparation of the manuscript.

CONFLICT OF INTEREST

The authors declare that they have no competing interests.

ORCID

Shabir Ahmad Lone https://orcid.org/0000-0003-1850-9625
Mohmmad Younus Wani https://orcid.org/0000-0002-1838-1337
Aijaz Ahmad https://orcid.org/0000-0003-2845-0727

REFERENCES

[1] M. E. Rodrigues, S. Silva, J. Azeredo, M. Henriques, *Crit. Rev. Microbiol.* **2016**, *42*, 594.
[2] F. L. Van De Veerdonk, M. G. Netea, L. A. Joosten, J. W. M. Van De Meer, B. J. Kullberg, *FEMS Microbiol. Rev.* **2010**, *34*, 1063.
[3] D. W. Denning, *Philos. Trans. R. Soc. B Biol. Sci.* **2016**, *371*. 20 150 468.
[4] M. A. Pfaller, D. J. Diekema, D. L. Gibbs, V. A. Newell, J. F. Meis, I. M. Gould, W. Fu, A. L. Colombo, E. Rodriguez-Noriega, *J. Clin. Microbiol.* **2007**, *45*, 1735.
[5] N. M. Revie, K. R. Iyer, N. Robbins, L. E. Cowen, *Curr. Opin. Microbiol.* **2018**, *45*, 70.
[6] N. Robbins, T. Caplan, L. E. Cowen, *Annu. Rev. Microbiol.* **2017**, *71*, 753.
[7] S. Wu, Y. Wang, N. Liu, G. Dong, C. Sheng, *J. Med. Chem.* **2017**, *60*, 2193.
[8] K. D. Mjos, C. Orvig, *Chem. Rev.* **2014**, *114*, 4540.
[9] Y. C. Ong, S. Roy, P. C. Andrews, G. Gasser, *Chem. Rev.* **2019**, *119*, 730.
[10] M. Zaki, F. Arjmand, S. Tabassum, *Inorgan. Chim. Acta* **2016**, *444*, 1.
[11] K. J. Kilpin, P. J. Dyson, *Chem. Sci.* **2013**, *4*, 1410.
[12] K. L. Haas, K. J. Franz, *Chem. Rev.* **2009**, *109*, 4921.
[13] L. J. Boerner, J. M. Zaleski, *Curr. Opin. Chem. Biol.* **2005**, *9*, 135.
[14] M. Shebl, *Spectrochim. Acta Part A Mol. Biomol. Spectrosc.* **2014**, *117*, 127.
[15] X. Liu, C. Manzur, N. Novoa, S. Celedón, D. Carrillo, J.-R. Hamon, *Coord. Chem. Rev.* **2018**, *357*, 144.
[16] K. Mancha Madha, P. Gurumoorthy, S. Arul Antony, N. Ramalakshmi, *J. Mol. Struct.* **2017**, *1143*, 478.
[17] M. A. Malik, O. A. Dar, P. Gull, M. Y. Wani, A. A. Hashmi, *Medchemcomm.* **2018**, *9*, 409.
[18] A. M. Asiri, S. A. Khan, H. M. Marwani, K. Sharma, *J. Photochem. Photobiol. B Biol.* **2013**, *120*, 82.
[19] M. Y. Nassar, H. M. Aly, M. E. Moustafa, E. A. Abdelrahman, *J. Inorg. Organomet. Polym. Mater.* **2017**, *27*, 1220.
[20] M. Y. Nassar, H. M. Aly, E. A. Abdelrahman, M. E. Moustafa, *J. Mol. Struct.* **2017**, *1143*, 462.
[21] W. H. Mahmoud, G. G. Mohamed, O. Y. El-Sayed, *Appl. Organomet. Chem.* **2018**, *32*, e4051.
[22] CLSI-Clinical and Laboratory Standards Institute Standards, Wayne, PA, USA, **2008**, 40.
[23] A. Ahmad, M. Y. Wani, A. Khan, N. Manzoor, J. Molepo, *PLoS ONE* **2015**, *10*, e0145053.
[24] A. Khan, A. Ahmad, F. Akhtar, S. Yousuf, I. Xess, L. A. Khan, N. Manzoor, *Res. Microbiol.* **2010**, *161*, 816.
[25] G. Ahumada, T. Roisnel, S. Kahlal, D. Carrillo, R. Córdova, J.-Y. Saillard, J.-R. Hamon, C. Manzur, *Inorgan. Chim. Acta* **2018**, *470*, 221.
[26] J. Devi, N. Batra, *Spectrochim. Acta Part A Mol. Biomol. Spectrosc.* **2015**, *135*, 710.
[27] M. M. Abo-Aly, A. M. Salem, M. A. Sayed, A. A. Abdel Aziz, *Spectrochim. Acta Part A Mol. Biomol. Spectrosc.* **2015**, *136*, 993.
[28] P. Gull, O. A. Dar, M. A. Malik, A. A. Hashmi, *Microb. Pathog.* **2016**, *100*, 237.
[29] J. H. Pandya, R. N. Jadeja, K. J. Ganatra, *J. Saudi Chem. Soc.* **2014**, *18*, 190.
[30] M. A. Estermann, W. I. F. David in: W. I. F. David, K. Shankland, B. Mccusker, Ch. Baerlocher(Eds.), Structure determination from powder diffraction data (SDPD), Oxford Science Publications, New York, **2002**.
[31] CLSI-Clinical and Laboratory Standards Institute, 2012 (Document M27-S4).
[32] D. G. Yun, D. G. Lee, *Biochim. Biophys. Acta, Biomembr.* **2017**, *1859*, 467.

SUPPORTING INFORMATION

Additional supporting information may be found online in the Supporting Information section at the end of the article.

How to cite this article: Dar OA, Lone SA, Malik MA, et al. Heteroleptic transition metal complexes of Schiff-base-derived ligands exert their antifungal activity by disrupting membrane integrity. *Appl Organometal Chem*. 2019;33:e5128. https://doi.org/10.1002/aoc.5128

RSC Advances

PAPER

View Article Online
View Journal | View Issue

Cite this: *RSC Adv.*, 2019, **9**, 15151

New transition metal complexes with a pendent indole ring: insights into the antifungal activity and mode of action†

Ovas Ahmad Dar,[a] Shabir Ahmad Lone,[b] Manzoor Ahmad Malik,[a] Mohmmad Younus Wani,[c] Aijaz Ahmad *[bd] and Athar Adil Hashmi*[a]

Received 7th April 2019
Accepted 30th April 2019

DOI: 10.1039/c9ra02600b

rsc.li/rsc-advances

Development of new chemotherapeutic agents to treat multidrug-resistant fungal infections to augment the current treatment options is a must. In this direction, a series of mixed ligand complexes was synthesized from a Schiff base (**L**) obtained by the condensation of 2-hydroxynapthaldehyde and tryptamine, and 1,10-phenanthroline (1,10-phen) as a secondary ligand. Based on spectral characterization and physical measurements an octahedral geometry was assigned to [Co(phen)LClH_2O] (**C2**), [Ni(phen)LClH_2O](**C3**), and [Zn(phen)LClH_2O](**C4**) complexes while a distorted octahedral geometry was assigned to the [Cu(phen)LClH_2O](**C1**) complex. All the synthesized compounds were tested for antifungal activity against 11 *Candida albicans* isolates, including fluconazole (FLC) resistant isolates, by determining minimum inhibitory concentrations and studying growth curves. MIC results suggest that all the newly synthesized compounds have potent antifungal activity at varying levels. The rapid action of these compounds on fungal cells suggested a membrane-located target for their action.

1. Introduction

The emergence of drug resistance to almost all of the currently used antifungal medication necessitates the development of new treatment modalities and strategies.[1,2] Fungal diseases kill more than 1.5 million and affect over a billion people worldwide.[3,4] Among the various modalities that are being pursued, development of metallodrugs seems to be worthy; owing to the multiple pathways that a metallodrug could target to curb drug resistance.[5–7] A metal complex usually shows better efficacy compared to the ligand or the metal ion alone, by sometimes, the ligands protecting or stabilizing the otherwise reactive metal ion or the metal undergoing redox events which enhances the overall efficacy of the complex and sometimes the metal and the ligand(s) are mutually responsible for the biological activity of the complex.[8] Studies of the coordination chemistry of transition metal ions with several types of ligands have made big strides by the recent advancements in the fields of bioinorganic chemistry and medicine.[9] Due to their astonishing structural properties and varied denticities, Schiff bases have received considerable attention for many years and these properties have resulted in their wide application in the clinical, biological, analytical and pharmaceutical fields.[10–13] The coordination of transition metals to these scaffolds increases their biological activities and lowers the cytotoxicity of both metal and the ligand.[14–16] Schiff base metal complexes are gaining considerable attention due to their potential antifungal, antitumor and antibacterial activities.[17–20] Use of labile and auxiliary ligands like 1,10-phenenthroline, 2,2-bipyridyl, imidazole, and pyridine, on the other hand, have been demonstrated to show interesting biological profile with excellent antibacterial, antitumor, antiviral and antifungal activities already reported.[21–25] A good number of mixed ligand complexes containing 1,10-phenanthroline as a ligand are identified as potential chemotherapeutic agents and have received much attention in the field of medicine.[26–29]

In view of the promising biological activities of these scaffolds our main intention was to explore whether the incorporation of these important scaffolds in one complex would result in potentiation of activities and therefore would give a new strategy for the development of chemotherapeutic agents. Finding rare instances of literature about the tryptamine based Schiff base ligands and their mixed ligand complexes with 1,10-phenenthroline, bearing an indole ring pendent, we report the synthesis, characterization and antifungal activity of the ligand and its metal complexes. Insight studies into the mechanism of action were done by studying their effect on H^+-ATPase pump,

[a]*Department of Chemistry, Jamia Millia Islamia, New Delhi 110025, India. E-mail: aah_ch@yahoo.co.in*

[b]*Clinical Microbiology and Infectious Diseases, School of Pathology, Faculty of Health Sciences, University of the Witwatersrand, Johannesburg, 2193, South Africa. E-mail: aijaz.ahmad@wits.ac.za*

[c]*Chemistry Department, Faculty of Science, University of Jeddah, P. O. Box 80327, Jeddah 21589, Kingdom of Saudi Arabia*

[d]*Infection Control, Charlotte Maxeke Johannesburg Academic Hospital, National Health Laboratory Service, Johannesburg, 2193, South Africa*

† Electronic supplementary information (ESI) available. See DOI: 10.1039/c9ra02600b

a promising target to develop new antifungal drugs because of its important role in fungal cell physiology to maintain electrochemical proton gradient which in turn is important for nutrient uptake. In addition, this enzyme also plays a crucial role to regulate intracellular pH and maintains cell growth. The enzyme has also been reported to play role in the pathogenicity of *Candida* by regulating the pathogenicity markers such as morphological transition and secretion of hydrolytic enzymes.

2. Experimental

2.1 Materials and methods

All the reagents and chemicals used for the synthesis were of analytical grade and were purchased from commercial sources. They were used as received without further purification. Tryptamine and 2-hydroxynepthaldehyde were purchased from Sigma Aldrich. 1,10-Phenanthroline and metal chlorides were purchased from Merck.

Microanalyses (C, H and N) was carried out with FlashEA 1112 elemental analyzer (Thermo Scientific). The molar conductance at room temperature were measured on a Syntronics type 302 conductivity bridge equilibrated at 25 ± 0.01 °C. For conductivity measurements one millimolar solutions in DMSO were prepared. Electrothermal melting point apparatus was used to determine the melting point of the synthesized compounds. FT-IR spectra of the synthesized compounds were recorded using KBr pellets on a Perkin-Elmer 283 spectrophotometer. For ^{1}H NMR and ^{13}C NMR measurements Brucker WH 300 (200 MHz) and Brucker WH 270 (67.93 MHz) were used using $CDCl_3$ or DMSO-d_6 as a solvent and trimethylsilane as an internal standard. ESI-MS (AB-Sciex 2000, Applied Biosystem) was used to record mass spectra of the synthesized ligand and complexes.

2.2 Synthesis

2.2.1 Synthesis of Schiff base ligand (L). The Schiff base ligand, (*E*)-1-(((2-(1*H*-indol-3-yl)ethyl)imino)methyl)naphthalen-2-ol (**L**) was synthesized from the condensation reaction of 2-hydroxynepthaldehyde (0.86 g, 5 mmol) and tryptamine (0.8 g, 5 mmol) in ethanol (15 mL) at room temperature for 3 h. The reaction was monitored by taking TLC at regular intervals. The reaction mixture was kept overnight at room temperature and the bright yellow solid product formed was filtered, washed with least amount of ethanol and diethyl ether several times and then dried *in vacuo* over $CaCl_2$ for further use.

Color (yellow) yield: 82%. mp 192 °C; elemental anal. calc. for $C_{21}H_{18}N_2O$: C, 80.23; H, 5.77; N; 8.91; found: C, 79.57; H, 5.69; N, 9.46; IR (KBr Pellet, cm^{-1}): 1618 ν(–CH=N–), 3152 ν(OH), 1264 ν(C–O), 3334 ν(NH), ^{1}H NMR ($CDCl_3$, δ, ppm) 8.25 (s, 1H, NH), 8.42 (s, 1H, CH=N), 14.2 (s, 1H, OH), 3.18 (t, 2H, CCH_2), 3.89 (t, 2H, NCH_2), 6.86–7.65 (m, 11H, ArH). ^{13}C NMR ($CDCl_3$, δ, ppm): 171.22 (C–O), 163.44 (C=N), 58.25 (C–N), 27.37 (CH_2–C), 111.99–138 (Ar C's), mass spectrum (ESI) $[M + H]^+$ = 315.0.

2.2.2 Synthesis of mixed ligand complexes (C1–C4). All the complexes were prepared by the general procedure as shown in Scheme 1. To an ethanolic solution of the Schiff base (0.62 g, 2 mmol) was added an ethanolic solution of $[M(Cl)_2 \cdot nH_2O]$ (2 mmol) dropwise and then triethylamine (280 μL) with constant stirring. A few minutes later an ethanolic solution of 1,10-phen (0.36 g, 2 mmol) was added dropwise. The reaction mixture was refluxed for 4–6 h. The resultant product formed was washed several times with ethanol and diethyl ether, and then dried in vacuum over fused calcium chloride.

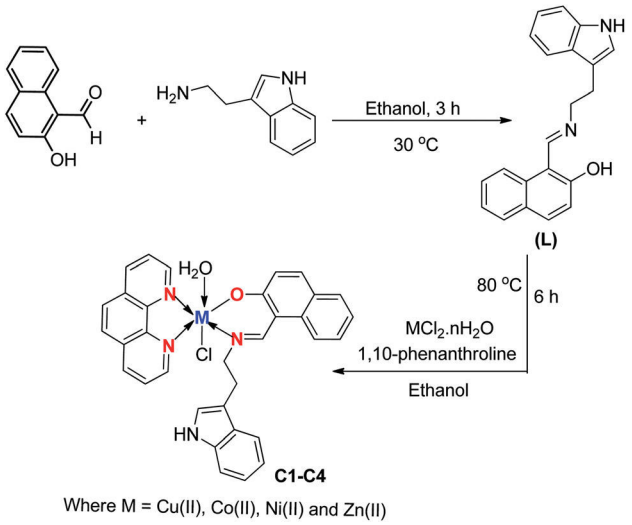

Scheme 1 Synthesis of Schiff base (L) and mixed ligand complexes (C1–C4).

2.2.2.1 [Cu(phen)LClH$_2$O] (C1). Color (yellow green) yield: 68%; mp: 252 °C; elemental anal. calc. for ($C_{33}H_{27}ClCuN_4O_2$): C, 64.91; H, 4.46; N, 9.18; found: C, 64.72; H, 4.87; N, 9.28; IR (KBr pellet, cm^{-1}): 1582 ν(CH=N), 1289 ν(C–O_{phenol}), 1178 ν(C–$N_{1,10\text{-}phen}$), 3310 ν(N–H), 735 δ(C=$N_{1,10\text{-}phen}$), 3505 ν(OH), 520 ν(Cu–O), 478 ν(Cu–N). Mass spectrum (ESI) $[M + H]^+$ = 609.5.

2.2.2.2 [Co(phen)LClH$_2$O](C2). Color (brown) yield: 65%. mp: 242 °C; elemental anal. calc. for [$C_{33}H_{27}ClCoN_4O_2$]: C, 65.41; H, 4.49; N, 9.25; found: C, 65.20; H, 4.37; N, 9.18; IR (KBr pellet, cm^{-1}): 1585 ν(CH=N), 1289 ν(C–O_{phenol}), 1170 ν(C–$N_{1,10\text{-}phen}$), 3320 ν(N–H), 728 δ(C=$N_{1,10\text{-}phen}$), 3510 ν(OH), 527 ν(Co–O), 476 ν(Co–N). Mass spectrum (ESI) $[M + H]^+$ = 605.9.

2.2.2.3 [Ni(phen)LClH$_2$O](C3). Color (reddish brown) yield: 69%; mp: 220 °C; elemental anal. calc. for [$C_{33}H_{27}ClN_4NiO_2$]: C, 65.43; H, 4.49; N, 9.25; found: C, 65.39; H, 4.52; N, 9.17; IR (KBr pellet, cm^{-1}): 1585 ν(CH=N), 1286 ν(C–O_{phenol}), 1178 ν(C–$N_{1,10\text{-}phen}$), 3304 ν(N–H),3508 ν(OH), 730 δ(C=$N_{1,10\text{-}phen}$), 524 ν(Ni–O), 478 ν(Ni–N). Mass spectrum (ESI) $[M + H]^+$ = 605.5.

2.2.2.4 [Zn(phen)LClH$_2$O](C4). Color (beige) yield: 70%; mp: 222 °C; elemental anal. calc. for [$C_{33}H_{27}ClN_4O_2Zn$]: C, 64.71; H, 4.43; N, 9.15; found: C, 64.52; H, 4.88; N, 9.10; IR (KBr pellet, cm^{-1}): 1590 ν(CH=N), 1288 ν(C–O_{phenol}), 1176 ν(C–$N_{1,10\text{-}phen}$), 3312 ν(N–H), 729 δ(C=$N_{1,10\text{-}phen}$), 3507 ν(OH), 530 ν(Zn–O), 480 ν(Zn–N).^{1}H NMR (DMSO-d_6, δ, ppm), 10.75 (s, 1H, NH), 8.53 (s, 1H, CH=N), 8.39 (s, 2H, CH=$N_{1,10\text{-}phen}$), 3.30 (t, 2H, CCH_2), 3.92 (t, 2H, NCH_2), 3.57 (s, 2H, H_2O), 6.51–8.19 (m, 18H, ArH). ^{13}C NMR (DMSO-d_6, δ(ppm)): 172.26 (C–O), 164.10 (CH=N), 149.83 (CH=$N_{1,10\text{-}phen}$), 60.28 (N–CH_2), 28.06 (CH_2–C),

146.47 (C–N), 107.93–136.69 (Ar C's), mass spectrum (ESI) $[M + H]^+ = 611.4$.

2.3 Microbiological analysis

2.3.1 Strains, media and chemicals. All the strains used in this study are detailed in Table 2, which consist of eight fluconazole (FLC) susceptible including 1 laboratory strain (*C. albicans* SC5314 and 7 clinical isolates) and 3 FLC resistant clinical isolates. All the clinical *Candida* strains were collected from Charlotte Maxeke Johannesburg Academic Hospital, Johannesburg, South Africa and were stored in glycerol stocks at −80 °C in the department of Clinical Microbiology and Infectious Diseases. All the test strains were isolated from patients under the ethical clearance number M10102 obtained from the Human Research Ethics Committee, University of the Witwatersrand. Prior to experiments, *Candida* isolates were revived by plating on Sabouraud Dextrose (SD) Agar (Sigma Aldrich, USA), followed by growing single colonies in fresh SD broth. Fluconazole was purchased from Sigma Fluke (USA) and stock solution of 2 mg mL^{-1} was prepared in sterile distilled water. All other chemicals and media were purchased from Sigma Aldrich and Merck.

2.3.2 Antifungal susceptibility tests

2.3.2.1 Determination of minimum inhibitory concentrations. To determine the antifungal activity of the newly synthesized ligand (**L**) and its four mixed ligand complexes (**C1–C4**), Minimum Inhibitory Concentrations (MIC) were determined against tested FLC susceptible and FLC resistant *C. albicans* isolates by serial micro-broth dilution method following Clinical and Laboratory Standards Institute (CLSI) recommended guidelines M27-A3,[30] with modifications. Briefly, microtiter plates were prepared by adding 100 μL of SD broth into each of the wells followed by an addition of the test substance at a volume of 100 μL in the first column with an initial concentration of 1000 μg mL^{-1}. The test compounds were serially diluted to yield a final concentration of 250, 125, 62.5, 31.25, 16, 8, 4, 2, 1, 0.5, 0.25 and 0.12 μg mL^{-1}. The positive control FLC (2000 μg mL^{-1}) and the negative vehicle control (1% DMSO) were also included in every set of experiments. Media and culture controls were included to confirm the sterility and viability, respectively. Following serial dilution, test organisms with an approximate final inoculum size of 1×10^6 colony forming units (CFU) per mL, were then added to each well, at a volume of 100 μL. The microtiter plates were sealed and incubated under 37 °C for 24 h. After incubation, 400 μg mL^{-1} of *p*-iodonitrotetrazolium violet solution (INT) was added to each well (40 μL). Viable micro-organisms interact with INT to create a colour change from clear to a red-purple colour. Thus, the lowest dilution with no colour change was considered as the MIC for that test compound. All the results were calculated as a mean of the experiments done in duplicate and all the results were expressed in μg mL^{-1}.

2.3.2.2 Growth studies. To further confirm the antifungal activity of the test compounds, growth curve studies were performed as described previously.[31] Prior to the experiment, all *Candida* species were sub-cultured and 50 μL (1×10^6 CFU mL^{-1}) were added to 50 mL SD broth. To test the effect of the compounds under study, MIC and $\frac{1}{2}$MIC of these compounds were added to the respective tubes. All the tubes including control (no test compound) were incubated at 37 °C with agitation. At a pre-determined time (0, 2, 4, 6, and 24 h), 2 mL aliquots were taken and growth was followed turbidometrically at 595 nm using Shimadzu UV-1800 spectrophotometer. Optical density was recorded for each concentration against time in hours. The growth rate is equivalent to the slope of log(optical density) *versus* time during the exponential phase. Average growth rate of untreated *versus* treated *C. albicans* were represented as line charts.

2.3.3 Proton efflux measurements. For insight mechanism of antifungal action of the tested compounds, activity of plasma membrane H^+-ATPase pump of different *C. albicans* strains was determined by monitoring the acidity of external medium by measuring the pH, as described earlier.[32] Briefly, one laboratory strain along with one FLC susceptible and one FLC resistant isolates were grown in SD media and incubated at 37 °C until the cells reach mid-log phase (6–8 h). After incubation cells were harvested by centrifugation and washed twice with sterile distilled water. 100 mg of wet weighed cells were then suspended in 5 mL of buffer containing 0.1 M KCl and 0.1 M $CaCl_2$. Immediately after the addition of cells, initial pH of the suspension was set at pH 7.0 using either 0.01 M NaOH or HCl. For the next 10 minutes, the pH of the solution was kept at 7.0 using 0.01 M NaOH and the volume of the 0.01 M NaOH consumed was calculated. To determine the effect of test compounds, 100 μL of the different stock compounds were added to achieve desired MIC values in the buffer and pH was kept constant at 7.0 and the volume of 0.01 M NaOH consumed was calculated. For glucose stimulation experiments, 100 μL of glucose was added to achieve a final concentration of 5 mM to both treated and untreated sets. The rate of proton efflux will be calculated using the formula:

$$\text{Rate of } H^+ \text{ efflux} = \frac{\text{volume of NaOH} \times 10^{-11} \text{ mol}}{\text{mg cells} \times \text{time}}$$

2.3.4 Measurements of intracellular pH (pHi). To further confirm the effect of test compounds on H^+ ATPase pump, pHi of *C. albicans* strains was measured as described previously.[32] pHi was quantified to determine whether the cells with dysfunctional H^+-ATPase activity maintains the internal pH of 6.5–6.9 as compared to cells with functional H^+ ATPase activity. 0.1 g of mid-log phase grown *C. albicans* cells were suspended in 5 mL solution containing 0.1 M KCl and 0.1 mM $CaCl_2$. To check the effect all the test compounds were separately added into the suspension at their respective MIC values and pH was adjusted to 7.0 using either 0.01 M NaOH or HCl. The suspensions were then incubated at 37 °C for 30 minutes with constant shaking at 200 rpm. After incubation pH was again set to 7.0 and 20 μM nystatin was added to all the cell suspensions followed by re-incubation at 37 °C for 1 h. After incubation, the change in pH level of the cell suspensions were measured and the value of the external pH at which nystatin permeabilization induced no further shift was taken as an estimate of pHi. In every set of

experiment untreated cells were included as negative control and pHi was measured directly from the suspensions in triplicates and the mean of the pH recorded was used as the final pHi.

3. Results and discussion

3.1 Chemistry

The mixed ligand complexes with an indole pendent were prepared by reacting equimolar amounts of the ligand, obtained by condensation of tryptamine with 2-hydroxynapthaldehyde and the corresponding metal salts, and 1,10-phenanthroline in presence of triethylamine. All the resulting metal complexes were neutral, colored, air stable and remarkably soluble in DMF and DMSO. The ligand and metal complexes were analyzed using various physico-chemical properties like melting point, yield, color, elemental analysis and conductivity measurements as reported in Table 1. The molar conductivity of the complexes was carried out using DMSO (10^{-3}M) at room temperature. The results obtained were in the range of 18–27 Ω^{-1} cm^2 m^{-1} which indicated their non-electrolytic nature. All the compounds were thoroughly characterized using various spectral techniques like FT-IR, NMR and mass spectrometry. The analytical data of the ligand and metal complexes were in good agreement with their proposed formula. The ESI MS of the Schiff base ligand (**L**) and complexes (**C1–C4**) in MeOH were recorded and found in good agreement with the calculated *m*/*z* values (Fig. S1–S5†). The FT-IR spectrum of the Schiff base ligand (**L**) displayed a strong band at 1618 cm^{-1} corresponding to ν(CH=N) of azomethine group. In complexes the azomethine (–CH=N–) band got shifted to lower frequencies due to the withdrawal of electron density from the nitrogen atom indicating the coordination of CH=N group to metal ions (Fig. 1).[33] The band present in Schiff base (**L**) at 3152 cm^{-1} attributed to –OH stretching vibrations was absent in complexes due to deprotonation upon complexation.[34] In complexes (**C1–C4**) the broad band at 3505–3510 cm^{-1} was attributed to ν(OH) of the coordinated water present in these complexes.[18] In 1,10-phenanthroline the band at 1633 cm^{-1}corresponds to pyridyl nitrogen stretching vibration and in complexes this band was shifted to lower frequencies which clearly indicate the coordination of two nitrogen atoms to metal ions upon complexation. The low frequency region of the spectra in complexes showed the presence of new bands in the region of 476–480 cm^{-1}and 520–530 cm^{-1}assigned to ν(M–N) and ν(M–O) stretching vibrations respectively (Fig. S6–S8†).[35] In addition, further evidence for the formation of Schiff base (**L**) and **C4** complex was obtained from the NMR spectra. The attained ^{1}H and ^{13}C NMR values of **C4** complex were compared with the corresponding ligand and were in good agreement with the proposed structure of the **C4** complex. The ^{1}H and ^{13}C NMR spectra of the ligand and **C4** complex have been given in ESI.† Complexes **C1**, **C2** and **C3** did not furnish good and presentable NMR spectra due to the paramagnetic nature of the complexes.

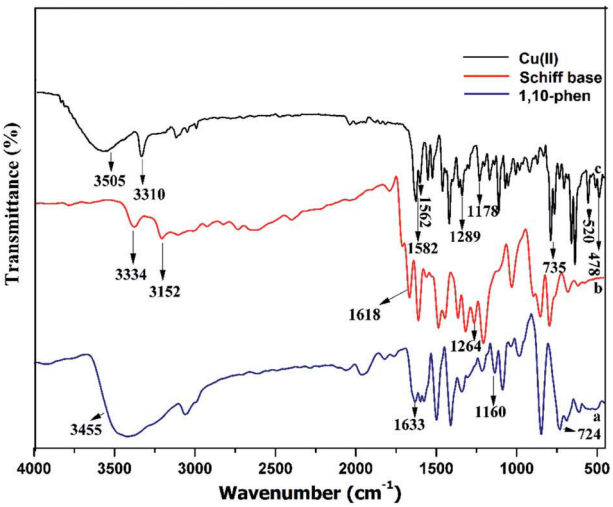

Fig. 1 FT-IR spectra of (a) 1,10-phenanthroline, (b) Schiff base (L) and (c) Cu(II) complex (**C1**).

3.2 Biological studies

3.2.1 Minimum inhibitory concentration. The antifungal activity of the ligand (**L**) and its metal complexes (**C1–C4**), **C4** was evaluated by determining their MIC values. All the MIC results are summarized in Table 2. Evaluation of MIC depicts that among the ligand (**L**) and its four complexes (**C1–C4**), **C3** showed highest inhibitory activity while as **L** showed the least inhibitory activity against all the tested strains. The MIC values for **C3** ranges from 1–0.25 μg mL^{-1} while as for L these values range from 125–500 μg mL^{-1}. Based on the MIC values, order of potency of the test compounds was **C3** > **C2** > **C1** ≥ **C4** > **L**. Isolates having an MIC values < 8 μg mL^{-1} for FLC were considered FLC susceptible while as the isolates having MIC ≥ 8 μg mL^{-1} were categorized as FLC resistant, following the CLSI Interpretive Guidelines for *In vitro* Susceptibility Testing of

Table 1 Physico-chemical properties of ligand (L) and complexes (**C1–C4**)

Compound	Color	Mol. formula	Mol. wt	(*m*/*z*) ratio	Yield (%)	Λ_m (Ω^{-1} cm^2 mol^{-1})	Mp (°C)
L	Yellow	$C_{21}H_{17}N_2O$	313	315	82	—	192
C1	Yellow green	$[C_{33}H_{27}ClCuN_4O_2]$	609.1	609.5	68	27	252
C2	Brown	$[C_{33}H_{27}ClCoN_4O_2]$	605.1	605.9	65	19	242
C3	Reddish brown	$[C_{33}H_{27}ClN_4NiO_2]$	604.1	605.5	69	18	220
C4	Beige	$[C_{33}H_{27}ClN_4O_2Zn]$	610.1	611.4	70	20	222

Table 2 Minimum inhibitory concentrations (μg mL^{-1}) of the ligand (L) and its complexes (C1–C4) against FLC susceptible and resistant *C. albicans* isolates

		Minimum inhibitory concentrations (μg mL^{-1})					
Strains		L	C1	C2	C3	C4	FLC
C. albicans SC5314		250	62.5	1	0.25	62.5	0.25
FLC susceptible strains	4175	500	250	0.50	0.50	250	0.12
	4179	500	250	2	0.50	250	0.25
	4180	250	62.5	2	0.50	125	0.25
	4251	125	125	1	0.25	125	0.25
	4554	500	250	2	0.50	250	0.25
	4563	125	62.5	0.50	0.25	62.5	0.25
	4576	250	250	2	0.50	250	0.25
FLC resistant strains	4085	250	125	4	0.5	125	16
	4122	500	250	8	1	250	32
	4135	500	250	8	0.5	250	32

Candida species.[36] Furthermore, all the test compounds were prepared to different concentrations using 1% DMSO and therefore DMSO was used as negative vehicle control and was observed to have no inhibitory activity against any of the tested isolates. The MIC data revealed that the structural changes from ligand to its metal complexes resulted in marked enhancement in their potency as antifungal agents.

3.2.2 Growth curve analysis. To further support the MIC results and to study the influence of the test compounds on *C. albicans*, cells of strain SC5314, 4175 and 4085 were grown in presence of MIC and $\frac{1}{2}$MIC values of all the test compounds and growth curves were determined. All the untreated control cells depict normal growth pattern, with a lag phase of 4 hours, exponential phase of 8–10 hours before attaining the stationary phase. At $\frac{1}{2}$MIC values, test compounds resulted in the reduction of cell growth at varying levels without being fungicidal (Fig. 2). However, at MIC values of these compounds, almost complete growth inhibition was observed which can be represented by a flat line in comparison to the control (Fig. 2). It was also observed at sub-MIC values of these compounds; log phase has been delayed by 2 to 4 hours. As expected, FLC at a concentration of 2 μg mL^{-1} drastically inhibited growth in both the tested FLC susceptible isolates while as in FLC resistant isolate, growth has been suppressed but not inhibited.

3.2.3 Proton efflux measurements. Varying MIC values of these test compounds encouraged us to determine their mode of antifungal action. Schiff base compounds and their metal complexes are known to interact with the proteins and nucleic acids.[37,38] In addition, quick antifungal action of these compounds suggests that there may be a cellular target(s) accessible to the compound externally. With this background, we tested the activity of *C. albicans* strains for their ability to pump intracellular protons to the external medium in the presence of all the tested compounds under study. Table S1† gives relative rates of H^+-efflux by *C. albicans* strains in presence of the ligand (L) and complexes (C1–C4) at their respective MIC values. H^+-efflux inhibition in standard *C. albicans* SC5314 strain, with respect to control, ranges from 26–67% in absence of glucose, whereas these figures range from 15–51% when lab strain was treated with compounds in presence of glucose. In

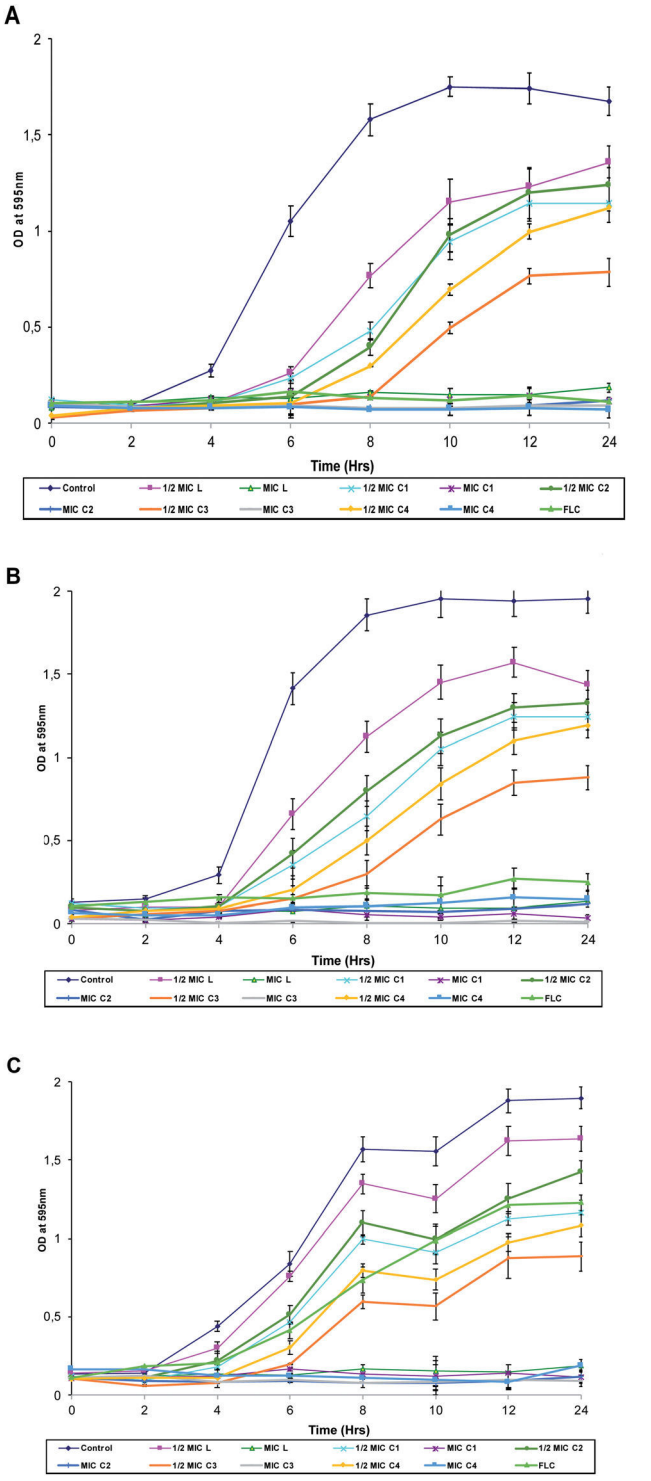

Fig. 2 Effect of Schiff base ligand (L) and its metal complexes (C1, C2, C3 and C4) at their MIC and $\frac{1}{2}$MIC values against *C. albicans* SC5314 (A), *C. albicans* 4175 (B) and *C. albicans* 4085 (C). Growth curves between absorbance at 595 nm and time (h) showed complete growth inhibition at MIC values of these compounds.

clinical strains, H^+-efflux inhibition ranged from 19–72% and 11–67% in absence and presence of glucose, respectively. Interestingly, 5 mM glucose stimulated H^+-efflux in all the strains by 2-fold, however all the test compounds inhibited this efflux with varying degrees. It can be presumed that the enzyme may exist in a different conformational state in presence and absence of glucose. The H^+-efflux results directly correlate with the antifungal activities of these test compounds with most prominent H^+-efflux inhibitory activity shown by **C3** complex where as **L** showed the least inhibition of H^+-efflux. Interestingly FLC at 2 μg mL^{-1} showed least inhibition on H^+-efflux by either of the *C. albicans* species tested. FLC is known to interact with the sterol components of the membrane, however, have no significant effect on H^+-ATPase pump. These results confirmed that interaction of any compound with plasma membrane is insufficient to inhibit the activity of the H^+-ATPase pump and therefore the compounds under study may be directly binding to this pump and thereby inhibiting the H^+-efflux from *Candida* cells. The H^+ translocating ATPase mediated fungicidal effects of the metal complexes under study suggest that plasma membrane H^+-ATPase targeting compounds could be developed as cell surface antifungal targets. The higher antifungal efficacy of the **C3** complex compared to the otherwise structurally similar complexes **C1**, **C2** and **C4** could be due to the difference in the redox potential of the metal ions or it could be due to the difference in the exchange of the co-ligands or binding with the biological target. Rapidity of action, low MIC values, and lethal effect demands more insight studies into all other possible mechanisms of these metal complexes.

3.2.4 Measurement of intracellular pH. The pHi of *Candida* cells is maintained between 6.0–7.5 by plasma membrane H^+-ATPase activity. The pHi of FLC susceptible and FLC resistant *C. albicans* strains was measured following the exposure to test compounds at MIC. All the test compounds decreased pHi of *C. albicans* cells compared to the untreated cells at varying levels (Fig. 3). As expected, untreated control cells maintain the pHi of 6.45 (FLC susceptible) and 6.87 (FLC resistant). In treated cells, pHi sharply decreased from 6.30–6.081 in FLC susceptible strains whereas these figures decreased from 6.66–6.186 in FLC resistant strains. The pHi in FLC resistant cells are comparatively acidic than FLC susceptible cells, however, the tested compounds declined pHi in both the types of cells. The decrease in pHi post treatment with the tested compounds further confirmed that these compounds target plasma membrane H^+-ATPase pump rather than disturbing electron transport chain and other V-type proton pumps. However, further studies are required to prove these claims.

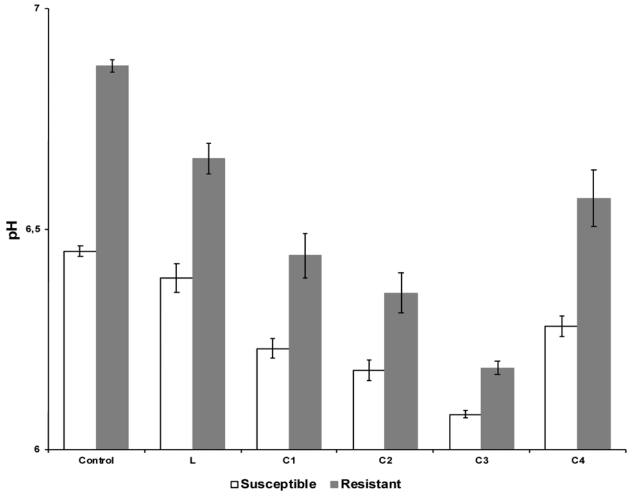

Fig. 3 Intracellular pH of FLC susceptible and resistant strains treated with the test compounds at MIC values. The pH of treated cells decreased towards a neutral pH in comparison to untreated control cells.

4. Conclusions

A series of metal complexes obtained from a Schiff base bidentate ligand and 1,10-phenenthroline as a co-ligand was obtained, structurally characterized and evaluated for their antifungal potential. Based on various physical and spectroscopic techniques octahedral geometry was assigned to **C2**, **C3** and **C4** complexes while as distorted octahedral geometry was assigned to **C1** complex. Evaluation of the antifungal potential against both resistant and susceptible *Candida albicans* showed that these complexes have a great potential to lead as antifungal agents; **C3** being the most active against the resistant strains. The collection of results presented herein are especially useful in antifungal drug development targeting proton pumping ATPase pump. The results of this study revealed that these complexes have a targeted activity, although, other modes of action cannot be ruled out because metal complexes are known to target multiple pathways to evade drug resistance.

Conflicts of interest

The authors declare that they have no competing interests.

Acknowledgements

The author OAD is thankful to University Grants Commission (UGC), Government of India for financial assistance through Central University PhD Students Fellowship. AA acknowledges financial support from University Research Committee Grant for 2019 – Friedel Sellschop Award (Grant No: AZMD019).

References

1 N. Wiederhold, *Infect. Drug Resist.*, 2017, **10**, 249–259.
2 M. C. Fisher, N. J. Hawkins, D. Sanglard and S. J. Gurr, *Science*, 2018, **360**, 739–742.
3 D. W. Denning, *Philos. Trans. R. Soc., B*, 2016, **371**, 20150468.
4 M. A. Pfaller, D. J. Diekema, D. L. Gibbs, V. A. Newell, J. F. Meis, I. M. Gould, W. Fu, A. L. Colombo and E. Rodriguez-Noriega, *J. Clin. Microbiol.*, 2007, **45**, 1735–1745.
5 K. D. Mjos and C. Orvig, *Chem. Rev.*, 2014, **114**, 4540–4563.
6 Y. C. Ong, S. Roy, P. C. Andrews and G. Gasser, *Chem. Rev.*, 2019, **119**, 730–796.

7 M. Zaki, F. Arjmand and S. Tabassum, *Inorg. Chim. Acta*, 2016, **444**, 1–22.
8 K. J. Kilpin and P. J. Dyson, *Chem. Sci.*, 2013, **4**, 1410.
9 S. A. Hosseini-Yazdi, P. Samadzadeh-Aghdam, A. Mirzaahmadi, A. A. Khandar, G. Mahmoudi, M. Ruck, T. Doert, S. S. Balula and L. Cunha-Silva, *Polyhedron*, 2014, **80**, 41–46.
10 L. Li, Q. Guo, J. Dong, T. Xu and J. Li, *J. Photochem. Photobiol., B*, 2013, **125**, 56–62.
11 N. Shahabadi, S. Kashanian and F. Darabi, *Eur. J. Med. Chem.*, 2010, **45**, 4239–4245.
12 S. Kathiresan, S. Mugesh, J. Annaraj and M. Murugan, *New J. Chem.*, 2017, **41**, 1267–1283.
13 A. Palanimurugan and A. Kulandaisamy, *J. Organomet. Chem.*, 2018, **861**, 263–274.
14 Z. Travnıicek, M. Malon, Z. Sindelar, K. Dolezal, J. Rolcík, V. Krystof, M. Strnad and J. Marek, *J. Inorg. Biochem.*, 2001, **84**, 23–32.
15 P. Tyagi, M. Tyagi, S. Agrawal, S. Chandra, H. Ojha and M. Pathak, *Spectrochim. Acta, Part A*, 2017, **171**, 246–257.
16 M. A. Malik, O. A. Dar, P. Gull, M. Y. Wani and A. A. Hashmi, *MedChemComm*, 2018, **9**, 409–436.
17 I. M. Mustafa, M. A. Hapipah, M. A. Abdulla and T. R. Ward, *Polyhedron*, 2009, **28**, 3993–3998.
18 A. A. S. Al-Hamdani and W. Al Zoubi, *Spectrochim. Acta, Part A*, 2015, **137**, 75–89.
19 M. Ibrahim, H. Ali, M. Abdullah and P. Hassandarvish, *Molecules*, 2012, **17**, 12449–12459.
20 J. Ki, A. Mukherjee, S. Rangasamy, B. Purushothaman and J. M. Song, *RSC Adv.*, 2016, **6**, 57530–57539.
21 C. M. Sharaby, M. F. Amine and A. A. Hamed, *J. Mol. Struct.*, 2017, **1134**, 208–216.
22 J. Dutta, S. Datta, D. Kumar Seth and S. Bhattacharya, *RSC Adv.*, 2012, **2**, 11751.
23 Z. A. Siddiqi, M. Khalid, S. Kumar, M. Shahid and S. Noor, *Eur. J. Med. Chem.*, 2010, **45**, 264–269.
24 Y. Prashanthi, K. Kiranmai, Ira, S. K. kumar, V. kumar Chityala and Shivaraj, *Bioinorg. Chem. Appl.*, 2012, **2012**, 1–8.
25 M. Aljahdali and A. A. EL-Sherif, *Inorg. Chim. Acta*, 2013, **407**, 58–68.
26 S. I. Mostafa, *Transition Met. Chem.*, 2007, **32**, 769–775.
27 H. F. Abd El-Halim, G. G. Mohamed and E. A. M. Khalil, *J. Mol. Struct.*, 2017, **1146**, 153–163.
28 W. H. Mahmoud, G. G. Mohamed and S. Y. A. Mohamedin, *J. Therm. Anal. Calorim.*, 2017, **130**, 2167–2184.
29 S. Baskaran, M. Murali Krishnan and M. N. Arumugham, *Inorg. Nano-Met. Chem.*, 2017, **47**, 269–277.
30 CLSI, *Clinical and Laboratory Standards Institute Reference method for broth dilution antifungal susceptibility testing of yeast, Approved Standard M27-A3*, Wayne, PA, USA, 2008, p. 40.
31 A. Khan, A. Ahmad, N. Manzoor and L. A. Khan, *Nat. Prod. Commun.*, 2010, **5**, 345–349.
32 A. Ahmad, A. Khan, S. Yousuf, L. A. Khan and N. Manzoor, *Fitoterapia*, 2010, **81**, 1157–1162.
33 M. A. Malik, M. K. Raza, O. A. Dar, Amadudin, M. Abid, M. Y. Wani, A. S. Al-Bogami and A. A. Hashmi, *Bioorg. Chem.*, 2019, **87**, 773–782.
34 M. M. Abo-Aly, A. M. Salem, M. A. Sayed and A. A. Abdel Aziz, *Spectrochim. Acta, Part A*, 2015, **136**, 993–1000.
35 W. H. Mahmoud, N. F. Mahmoud and G. G. Mohamed, *J. Organomet. Chem.*, 2017, **848**, 288–301.
36 Y. Jia and J. Li, *Chem. Rev.*, 2015, **115**, 1597–1621.
37 Clinical and Laboratory Standards Institute (CLSI), *Reference method for broth dilution antifungal susceptibility testing of yeasts*, Wayne, 2012, document M27-S4.
38 Z. Shokohi-pour, H. Chiniforoshan, A. A. Momtazi-borojeni and B. Notash, *J. Photochem. Photobiol., B*, 2016, **162**, 34–44.

Medicinal Chemistry, **2019**, *15*, 648-658

RESEARCH ARTICLE

Efficacy of Novel Schiff base Derivatives as Antifungal Compounds in Combination with Approved Drugs Against *Candida Albicans*

Manzoor Ahmad Malik[1], Shabir Ahmad Lone[2], Parveez Gull[1], Ovas Ahmad Dar[1], Mohmmad Younus Wani[3], Aijaz Ahmad[2,4,*] and Athar Adil Hashmi[1,*]

[1]*Department of Chemistry, Jamia Millia Islamia (Central University), New Delhi-110025, India,* [2]*Clinical Microbiology and Infectious Diseases, School of Pathology, Faculty of Health Sciences, University of the Witwatersrand, Johannesburg, 2193, South Africa,* [3]*Chemistry Department, Faculty of Science, University of Jeddah, P.O. Box 80327, Jeddah 21589, Kingdom of Saudi Arabia,* [4]*Infection Control, Charlotte Maxeke Johannesburg Academic Hospital, National Health Laboratory Service, Johannesburg, 2193, South Africa*

Abstract: ***Background*:** The increasing incidence of fungal infections, especially caused by *Candida albicans*, and their increasing drug resistance has drastically increased in recent years. Therefore, not only new drugs but also alternative treatment strategies are promptly required.

***Methods*:** We previously reported on the synergistic interaction of some azole and non-azole compounds with fluconazole for combination antifungal therapy. In this study, we synthesized some non-azole Schiff-base derivatives and evaluated their antifungal activity profile alone and in combination with the most commonly used antifungal drugs- fluconazole (FLC) and amphotericin B (AmB) against four drug susceptible, three FLC resistant and three AmB resistant clinically isolated *Candida albicans* strains. To further analyze the mechanism of antifungal action of these compounds, we quantified total sterol contents in FLC-susceptible and resistant *C. albicans* isolates.

***Results*:** A pyrimidine ring-containing derivative **SB5** showed the most potent antifungal activity against all the tested strains. After combining these compounds with FLC and AmB, 76% combinations were either synergistic or additive while as the rest of the combinations were indifferent. Interestingly, none of the combinations was antagonistic, either with FLC or AmB. Results interpreted from fractional inhibitory concentration index (FICI) and isobolograms revealed 4-10-fold reduction in MIC values for synergistic combinations. These compounds also inhibit ergosterol biosynthesis in a concentration-dependent manner, supported by the results from docking studies.

***Conclusion*:** The results of the studies conducted advocate the potential of these compounds as new antifungal drugs. However, further studies are required to understand the other mechanisms and *in vivo* efficacy and toxicity of these compounds.

ARTICLE HISTORY

Received: June 06, 2018
Revised: November 15, 2018
Accepted: November 15, 2018

DOI:
10.2174/1573406415666181203115957

Keywords: *Candida albicans*, Schiff base compounds, synergy, ergosterol biosynthesis, molecular docking, Infectious diseases.

1. INTRODUCTION

Infectious diseases incited by bacteria and fungi have become an important cause of morbidity and mortality worldwide [1]. Imprudent use and overuse of current antimicrobial drugs have resulted in the development of drug-resistant strains over the past decades [2]. Microbial resistance is a distressing feature that has led to the reduction in the efficiency of treatments. So, researchers are inspired in designing improved drugs that can overawe this exigency and offer augmented performance than the known drugs [3].

Several antifungal drugs belonging to polyenes, pyrimidines, azoles and echinocandins are being used to remove this looming medicinal concern [4]. Despite their effectiveness, the development of multidrug resistance among certain fungal strains and severe toxicity has challenged to find effective treatments and strategies for these infections [5]. At this point combination therapy proves to be a promising strategy to eliminate this problem as it offers potential benefits like a broad spectrum of efficacy, greater potency than the drugs used in monotherapy, improved safety and tolerability, and reduction in the number of resistant organisms [6]. Combination therapy tends to maximize the effectiveness of known drugs and other substances combined with antifungal drugs, without any antagonist mode of action, in order to reduce clinical failure [7]. The rationale for combination therapy is to maximize antifungal effects by attacking

*Address correspondence to these authors at the Department of Chemistry, Jamia Millia Islamia (Central University), New Delhi-110025, India; Tel: +91986523358: E-mail: aah_ch@yahoo.co.in and Department of Clinical Microbiology & Infectious Diseases, University of the Witwatersrand, Johannesburg, 2193, South Africa; Tel: +27 11 717 2515; E-mail: Aijaz.Ahmad@wits.ac.za

1875-6638/19 $58.00+.00

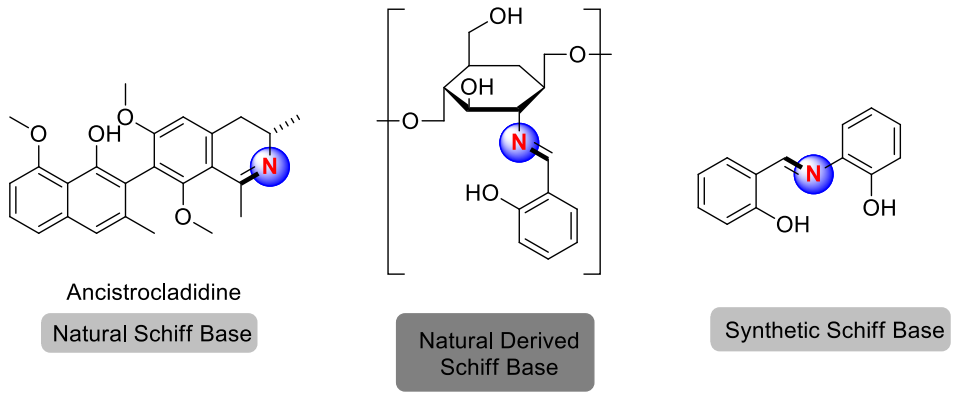

Fig. (1). Chemical structures of natural, naturally derived and synthetic Schiff bases.

different fungal targets at the same time with additive or synergistic effects, but some combinations offer good results when using the same target [8]. Combination antifungal therapy for invasive fungal infections is receiving growing attention [9-12] and considering our previous work [13-16] it is our premise that combining a new antifungal agent with a known antifungal drug, with different or a similar mechanism of action, would represent a novel therapeutic approach which could circumvent the multi-drug resistance problem.

In our previous studies, we reported some non-azole compounds showing synergy with azole drug fluconazole [13-17]. In this study, we synthesized some new Schiff base derivatives because of their versatile chelating properties. Typically, Schiff base, a condensation product is a nitrogen analogue of aldehyde or ketone in which the carbonyl group (-C=O) has been swapped by an imine or azomethine (-C=N-) group under specific conditions [18, 19]. The azomethine functional group imparts significant bioactivity as it is involved in the formation of intramolecular hydrogen bonding with some active sites in cell structures. Similarly, the lone pair of electrons in the sp^2 hybridized orbitals of azomethine nitrogen is another reason for their efficient chemical reactivity [20-23]. Such an azomethine functional group is present in various natural and synthetic compounds Fig. (**1**) [24]. A large number of reports revealed that Schiff base compounds are promising source of lead structures in designing biologically active molecules [25].

Several Schiff bases have been prepared and broadly exploited considering their inescapable properties like synthetic flexibility and medicinal efficiency [26]. Hydroxy-substituted Schiff bases are utilized as essential materials for the preparation of many medications due to their robust antibacterial, antifungal, antiviral, antitumor and anticancer properties [19, 27-29]. Recently, Schiff bases have been reported to mimic various biological systems and act as good metal chelators [30]. The synthesized Schiff bases are endowed with two donating (N, O) sites that could easily chelate with the metal atoms. When such bidentate compounds are administered as drugs, they could chelate with the metal atoms of essential enzymes of a microorganism and hence stop their proliferation.

The drugs used at present to treat *Candida* infections include the polyenes and azoles, both of which target ergosterol or its biosynthesis. The *Candida* ergosterol biosynthesis pathway is a major target of antifungal drugs, and mutations that affect the pathway contribute to drug resistance [31]. Azole antifungals inhibit lanosterol 14-alpha-demethylase, the product of the ERG11 gene allylamines, such as terbinafine, inhibit squalene epoxidase (the ERG1 gene product) and the polyene amphotericin B binds to ergosterol in the cell membrane [32]. We studied the effect of the test compounds on ergosterol biosynthesis by quantifying total intracellular sterols and performed docking studies of the active compound on lanosterol 14-alpha-demethylase to establish the possible mechanism of action.

Since none of the current antifungal agents has all the characteristics of an ideal antifungal agent [33] and discovery rate of new antifungal drugs is declining, we believe this approach has the potential to discover new antifungal agents as potentiators to be used in combination therapy treatment of invasive fungal diseases.

2. RESULTS AND DISCUSSION

2.1. Chemistry

A series of Schiff base compounds were prepared by simple condensation of an appropriate substituted aromatic amine with 2-hydroxynaphthaldehyde as shown in Scheme **1**. All the compounds were prepared in high yields and checked by TLC for their purity. The synthesis was carried out by refluxing the reaction mixture with a catalytic amount of glacial acetic acid. After successful synthesis, structural characterization of the Schiff base compounds was reported and then screened for their biological properties. Spectroscopic studies, namely IR, ^{1}H NMR and ESI-MS confirmed the proposed structures of the compounds.

The IR spectral data of the Schiff bases (**SB1-SB7**) proved to be an important probe in elucidating the structure of the compounds. The appearance of the bands in the region 1604-1621 cm^{-1}, 2811-3065 cm^{-1}, 3165-3359 cm^{-1}, 3567-3734 cm^{-1}can be assigned to the azomethinic (C=N) stretching vibration, C-H stretching vibrations, N-H stretching vibrations and to -OH stretching vibrations, respectively [34, 35]. The absence of the -OH peaks in all the Schiff bases except **SB5** confirms that the compounds exhibit keto-enol tautomerism (Fig. **2**) and predominate in the keto-amine form [36]. The mass spectra confirmed the expected molecular weights of the respective compounds. ^{1}H NMR proved to

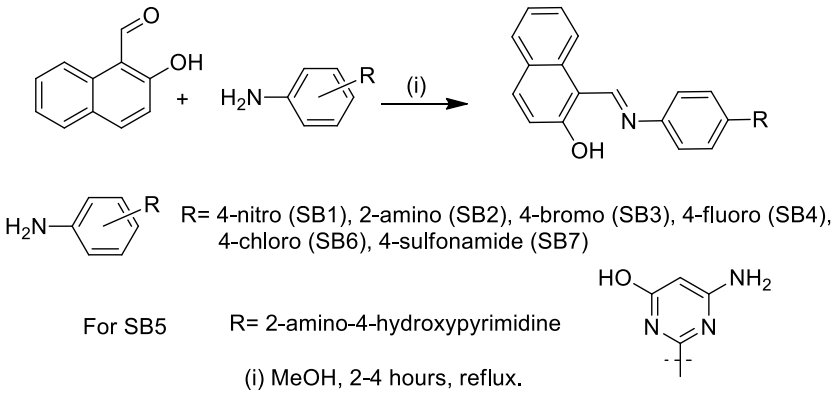

Scheme 1. Synthesis of the compounds **SB1-SB7**.

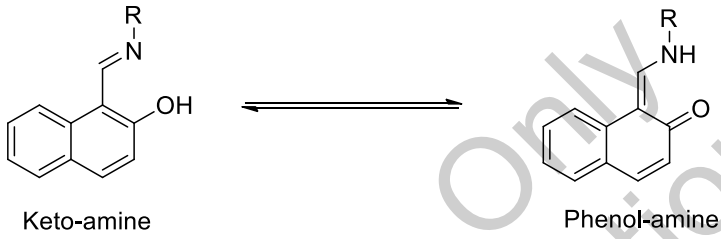

Fig. (2). Tautomerism in Schiff base compounds.

be an important evidence for the formation of Schiff base compounds. Signal assignments are made on the basis of chemical shifts and intensity patterns. In all the compounds, peaks around the region 9.3-9.5 ppm were observed and assigned to the proton of the azomethinic group. All the compounds show peaks at ca. 14-15 ppm, attributed to -NH/-OH protons. Chemical shift values for the aromatic ring protons were observed in the region 7.0-8.3 ppm [37].

2.2. Biological Evaluation

2.2.1. Minimum Inhibitory Concentration (MIC)

Microbroth dilution assay results revealed that all the test compounds showed a potent antifungal activity against different susceptible and resistant *C. albicans* isolates at varying degrees. The results for all the test compounds vary from 6 to 1250 µg/mL and are detailed in (Table **1**). On the basis of median MIC values against all the *C. albicans* strains, the order of potency of the tested compounds was **SB5>SB1≥SB2>SB7>SB6>SB3≥SB4**. Based on the MIC values, highest antifungal activity was shown by **SB5** against the drug-susceptible (median MIC of 9 µg/mL), FLC resistant strains (median MIC of 25 µg/mL) and AmB resistant strains (median MIC of 100 µg/mL). Comparatively AmB resistant isolates showed less potent antifungal activity than FLC resistant and susceptible *C. albicans* isolates. The reason for the disparity in activity could be related to the difference in the structures of the compounds. Presence and position of different electron withdrawing and electron donating groups on the phenyl ring at the imine nitrogen had a marked effect on the activity of the compounds where electron withdrawing nitro group at position-4 showed some reasonable activity, followed by electron donating amine group at position-2 of the phenyl ring. Benzenesulfonamide showed some activity whereas all the electron withdrawing and ring activating –Cl, -Br and –F groups at position-4 did not show any appreciable activity possibly due to the movement of electron density towards the ring and unavailability of the lone pair of electrons for any interaction with the target. The replacement of the substituted phenyl ring with a substituted pyrimidine ring in **SB5** resulted in 4-10-fold enhancement of the activity of the compound. This could be attributed to the different nature of the ring and availability of electrons on –OH and -NH_2 substituents, which resulted in some interactions with the target and hence its enhanced activity compared to the other analogues.

2.2.2. Combination Interaction with Fluconazole and AmB

More often the required concentration of the drugs to inhibit or suppress the fungal growth *in vivo* is higher than the maximum peak concentration the drug can achieve in serum, which results in failures for clinical use. Therefore, to reduce the required drug concentrations we studied the combination interaction of all these synthesized derivatives with two commonly used antifungal drugs (FLC and AmB) by determining FICI. The mean FICI values for all the tested compounds and FLC against all the clinical susceptible strains ranged from 0.087 to 3.496, whereas for fluconazole resistant strains mean FICI values were 0.072 to 2.054 (Table **2**). These results for the combination of test compounds and AmB against susceptible strains range from 0.218 to 1.641 and against AmB resistant strains ranges from 0.065 to 2.021. Out of 98 combinations for all the compounds against seven tested strains, 39% (n=38) showed synergy while as 37% (n=36) showed additive, 24% (n=24) showed indifferent interactions; however, no antagonistic interaction was observed for any of the tested compounds. Compared to clinical susceptible strains, which showed 34% synergy, drug resistant strains showed more synergy (66%). Of all the seven tested compounds, **SB5** showed synergism with both FLC as well as with AmB against drug susceptible and resistant strains; which advocates that if this compound

Table 1. Minimum inhibitory concentrations (µg/mL) of compounds SB1-SB7 against different drug susceptible and resistant *C. albicans* isolates. Fluconazole and amphoterecin B were used as positive controls.

Compounds	Median (range) MIC (µg/mL)		
	Drug Susceptible Strains (n=4)	FLC Resistant Strains (n=3)	AmB Resistant Strains (n=3)
SB1	34,5 (23-46)	94 (94-188)	375 (375-750)
SB2	46 (23-46)	188 (94-188)	750 (375-750)
SB3	160 (160-320)	625 (312-1250)	1250 (625-1250)
SB4	160 (80-320)	625 (312-625)	625 (625-1250)
SB5	9 (6-24)	25 (12-100)	100 (50-200)
SB6	117 (78-312)	624 (312-624)	156 (156-312)
SB7	60 (40-160)	156 (23-46)	312 (156-624)
AmB	0,75 (0.25-1)	NT	31 (39-312)
FLC	4 (2-8)	250 (125-250)	NT

NT = not tested

Table 2. Fractional inhibitory concentration index of compounds SB1-SB7with fluconazole and amphotericin B.

Combination 1:1	Fractional Inhibitory Concentration Index (FICI) for *C. albicans*							
	FLC (susceptible strains including ATCC90028) (n=4)		FLC (resistant strains) (n=3)		AmB (susceptible strains including ATCC90028) (n=4)		AmB (resistant strains) (n=3)	
	Mean±SD	INT	Mean±SD	INT	Mean±SD	INT	Mean±SD	INT
SB1 + Drug	0.81±0.11	ADD	0.49±0.15	SYN	0.65±0.23	ADD	0.51±0.01	ADD
SB2 + Drug	1.46±0.51	IND	0.54±0.12	ADD	1.29±0.46	IND	1.52±0.59	IND
SB3 + Drug	0.48±0.17	SYN	0.13±0.01	SYN	0.67±0.57	ADD	0.22±0.07	SYN
SB4 + Drug	1.68±0.47	IND	0.35±0.19	SYN	0.84±0.01	ADD	0.56±0.34	ADD
SB5 + Drug	0.21±0.21	SYN	0.13±0.07	SYN	0.24±0.02	SYN	0.15±0.09	SYN
SB6 + Drug	1.02±0.67	IND	0.23±0.06	SYN	1.08±0.64	IND	0.38±0.15	SYN
SB7 + Drug	1.54±1.69	IND	1.12±0.74	IND	1.01±0.33	IND	1.26±0.51	IND

INT: interpretation; SYN: synergy; ADD: additive; IND: indifferent

is developed into therapeutic agent, it will be effective against multidrug resistant strains of *C. albicans*. It is also interesting to observe that in all synergistic combinations there was a 4 to 10-fold reduction in the MIC values of the test antibiotics. Combination therapy has already been reported to treat different pathogens and is highly useful to lower down the mortality rates compared to monotherapy [38]. In addition, combination therapies are recommended not only to reduce drug resistance but also may help reverse the prevalence of infections due to highly resistant organism. In this study, we also identified and confirmed that the combination of Schiff base compounds and known antibiotics have border-spectrum antifungal activity.

2.2.3. Varied Ratio Combinations

To further confirm the synergistic combinations observed in 1:1 ratio and to observe the realistic formulations, nine different ratio combinations of the test compounds with FLC and AmB were done with one susceptible, one FLC resistant and one AmB resistant strain. To interpret the results from the FIC values of different combinations, isobolograms were constructed as detailed in materials and methods above. As expected all the combinations in different ratios either showed synergy or additive effect (Fig. **3**). None of the combinations falls in the indifferent or antagonistic periphery. The best ratio showing significant synergistic interaction in the isobolograms is 5:4 of the tested compounds and drugs

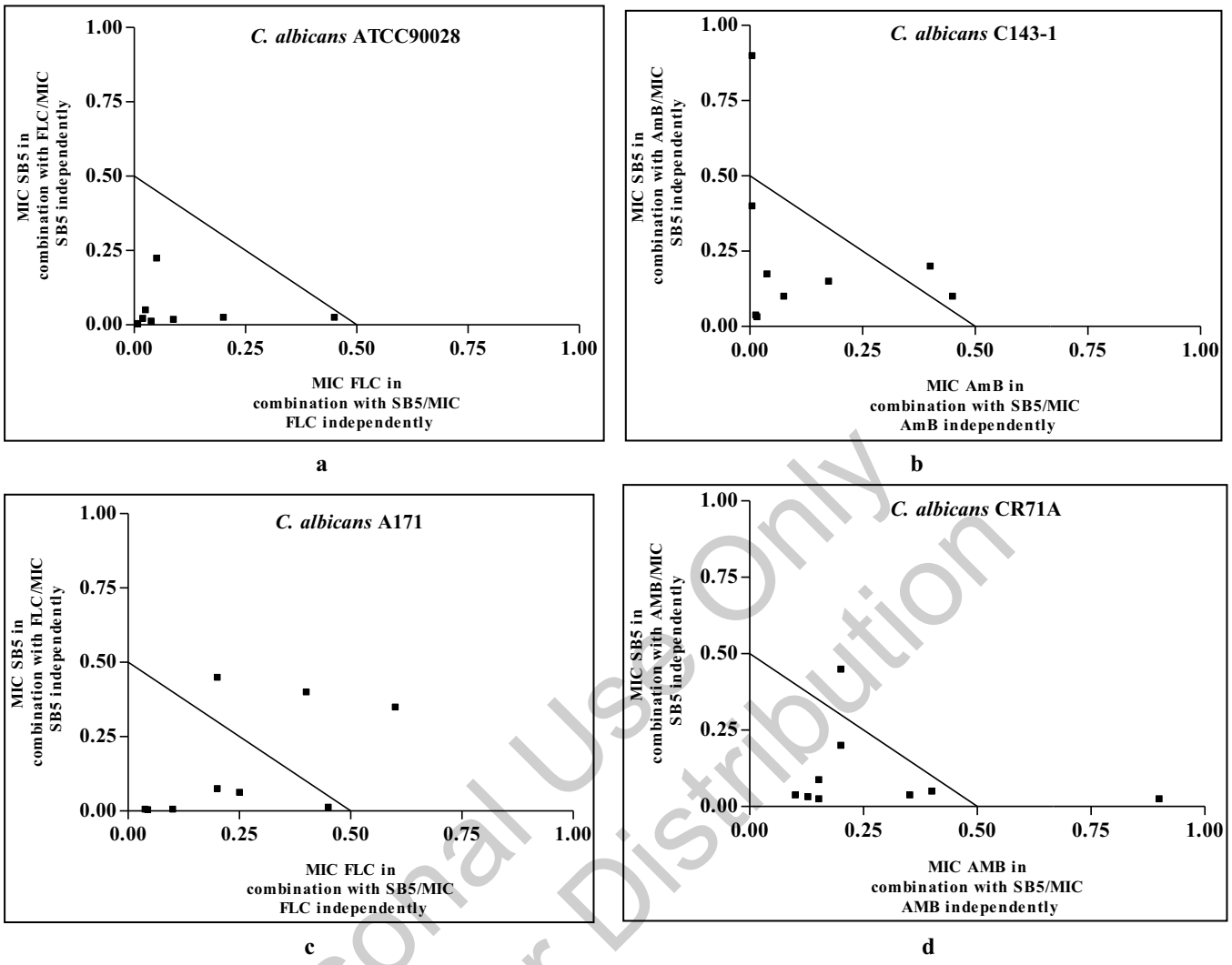

Fig. (3). Representative isobolograms for the synergistic interactions in nine different ratios of **SB5** with FLC against 90028 (**A**); SB5 with AmB against C143-1 (**B**); SB5 with FLC against A171 (**C**); and SB5 with AmB against CR71A (**D**).

respectively. The combinations of **SB5** and FLC against *C. albicans* ATCC90028 showed synergistic interactions for seven out of nine ratios studied. When the same combination was assayed against AmB resistant strain *C. albicans* CR71A; only four out of nine ratios showed synergy, while five of the ratios exhibited additive effects.

2.2.4. Effect on Ergosterol Biosynthesis

Multiple functions of ergosterol and its biosynthesis pathway proteins govern its importance in the survival and pathogenicity of *C. albicans.* Azole antifungal class is known to inhibit the activity of sterol 14α-demethylase and ergosterol production. In this study, we determined the effect of Schiff base derivatives on ergosterol biosynthesis by quantifying the total intracellular sterols in control and compound treated cells. Fig. **4**(**A** and **B**), respectively, represented the effect of the Schiff base compounds on FLC susceptible *C. albicans*ATCC90028 and FLC resistant *C. albicans* A71 at MIC and ½MIC values. In drug susceptible cells, 10-85% decrease in ergosterol content was observed when cells were treated with ½ MIC values of the test compounds while as 85-97% decrease in ergosterol content was observed when treated with MIC values of these compounds. These figures range from 12-84% and 35-88% when drug resistant cells were treated with ½ MIC and MIC values of the test compounds respectively. As expected, FLC at a concentration of 8 µg/mL showed an inhibition of ergosterol biosynthesis by 100% and 11% in FLC susceptible and FLC resistant cells, respectively.

As the test *C. albicans* isolates were able to persist despite possessing negligible or very low amounts of ergosterol, as was found in species treated with sub-MIC values of Schiff base compounds, these results provide further evidence that these isolates belong to ergosterol tolerant class as reported earlier [6]. Results in this study are in congruent with the previous finding by Capobianco *et al.,* where they reported a non-azole based inhibitor of ergosterol biosynthesis in *C. albicans* by inhibiting 14α-demethylase of ergosterol biosynthesis pathway [39].

2.2.5. Molecular Docking Studies

To gain insight into the possible mechanism of action and binding interactions, the most active compounds (**SB5**) were docked into the active site of cytochrome P450 lanosterol

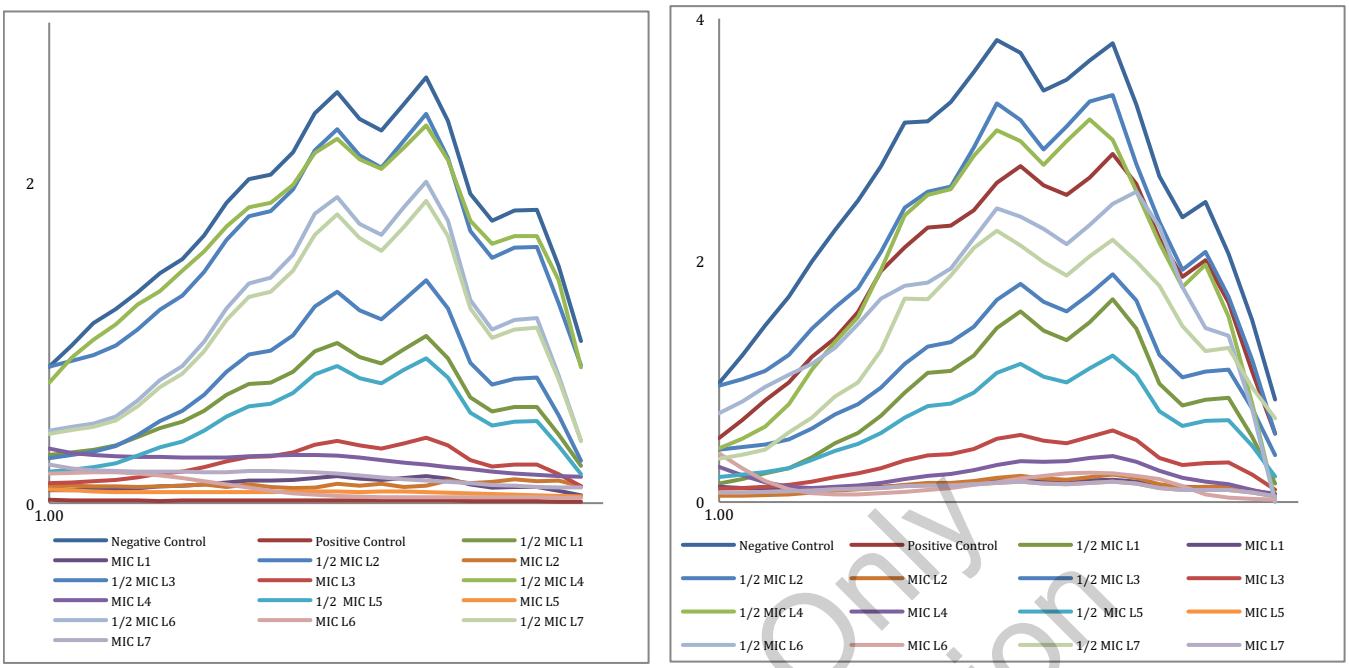

a **b**

Fig. (4). Effect of the tested compounds on ergosterol levels in FLC susceptible *C. albicans* ATCC90028 (**A**) and FLC resistant *C. albicans*A71 (**B**) at MIC and sub-MIC values. FLC represents the positive control.

14α-demethylase of *C. albicans* using autodock 4.2 and autodock vina software package. The active site pocket consists of amino acid residues ILE304, MET306, GLY307, GLY308, GLN309, THR311, SER312, PRO375, HIS377, SER378, ARG381, HID468, PRO462, PHE463, GLY464, HIS468, ARG469, CYS470, ILE471, GLY472, GLU473, PHE475, SER507, MET508 and Heme. Binding affinity values of the docked active compounds **SB5** was found to be -12.8 kcal mol^{-1} (Table **3**). The more negative the relative binding energy, the more potent the binding of drug to protein. The docking result indicated that synthesized compounds were held in the active pocket by forming combination of hydrogen bonds, hydrophobic bonds and van der Waals interactions with the enzyme. The –OH and NH_2 substituents on the pyrimidine ring of the molecule formed hydrogen bonds with PRO375, HIS377, SER378, and MET508 amino acid residues of the protein. On the basis of activity data and docking results, it was found that the active compound had the potential to inhibit 14a-demethylase of *C. albicans* and therefore can be considered as a lead structure for further optimization. An idea for further optimization of the designed molecules can be generated from the fact that all the molecules have the same basic ring skeleton, which differs only in the presence of different substituted phenyl rings on the imine nitrogen (–C=N-Ph). Compounds having a 4-nitrophenyl (SB1), 4-aminophenyl (SB2), 4-bromophenyl (SB3), 4-florophenyl (SB4), 4-chlorophenyl (SB6) and benzenesulfonamide (SB7), on the imine nitrogen didn't show any appreciable antifungal activity. Presence of 2-amino-4-hydroxy pyrimidine ring at the same position resulted in the enhancement of activity due to the interaction with the target enzyme as evidenced by docking studies (Fig. **5**) and ergosterol biosynthesis inhibition (Fig. **4**). The structure of this compound needs to be further optimized by placing different substituted heteroaromatic rings on the imine nitrogen to enhance the activity.

Table 3. Binding affinity value and other parameters of the docked compound SB5.

Compound	Binding Affinity (kcal/mol)	H-Bonding Interaction with Nearest Residues	H-Bonds
SB5	-12.8	PRO375, HIS377, SER378, MET508	4

Another theoretically possible mechanism of action of the active pyrimidine containing compound **SB5** could be due to its chelation with some metallo-enzyme involved in the ergosterol biosynthesis cycle; Schiff-base ligands are strong chelators and could be used as competitors in binding to the metallo-enzymes present in the form of Zinc cluster proteins which are characterized by the presence of a highly conserved Zn (II)2Cys6 zinc finger required for DNA recognition. Interestingly, this motif is only found in fungi. Given the emergence of fungi that show resistance to cytotoxic compounds, zinc cluster proteins may constitute new targets for antifungal drugs. For instance, a drug disrupting the zinc finger of Upc2p could be effective when used in combination with other compounds such as azoles. These propositions, however, demand further studies, which are currently underway in our laboratories.

3. MATERIALS AND METHODS

3.1. Chemistry

All starting materials and solvents used in this work were of analytical grade and used as purchased from Sigma Al-

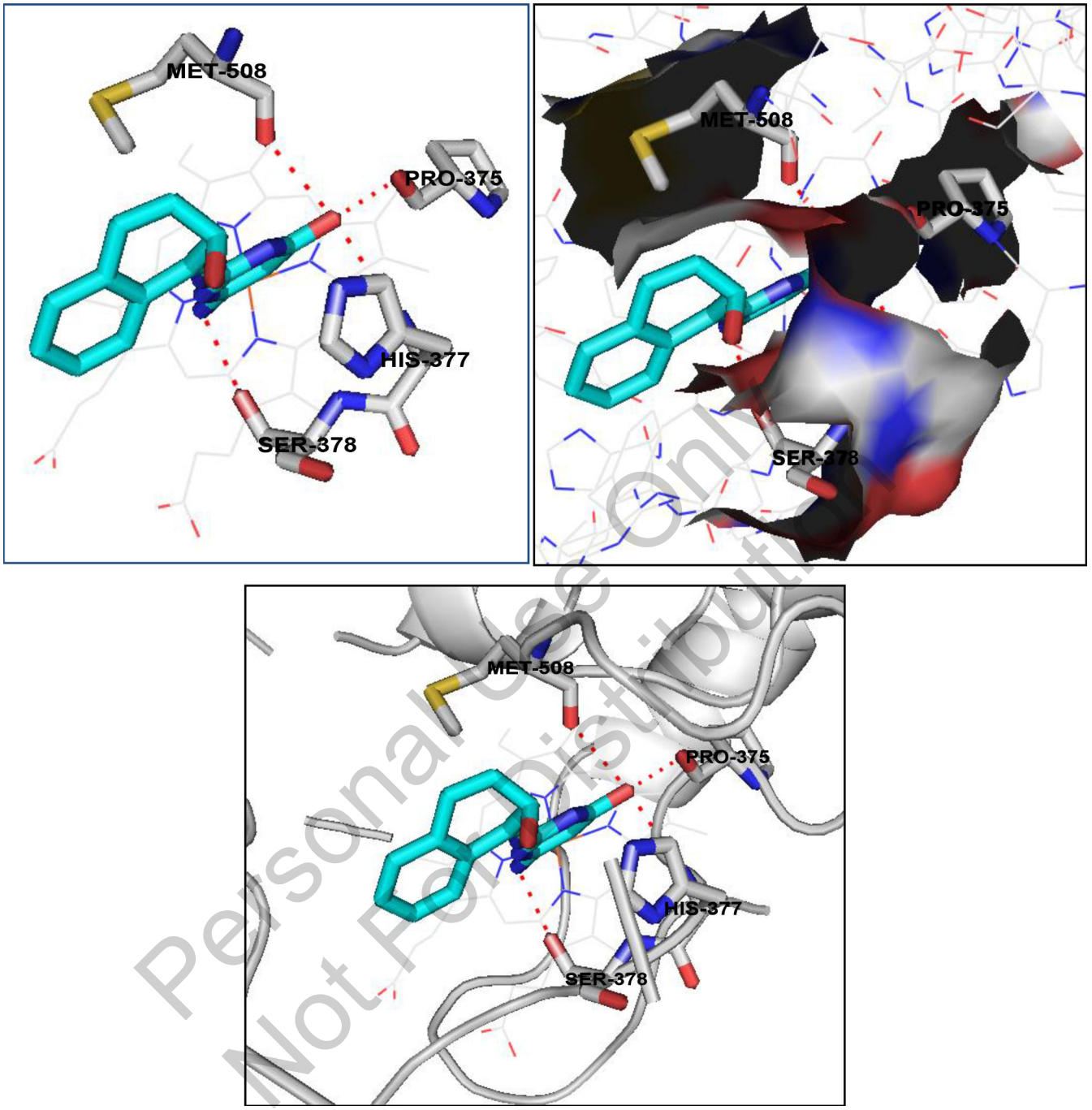

Fig. (5). Docking poses of the most active compound **(SB5**) into the active site pocket of cytochrome P450 lanosterol 14a-demethylase of *C. Albicans,* showing hydrogen bonding interactions with different amino acid residues inside the protein cavity. These poses were generated using PyMOL.

drich Chemical Company without further purification. Organic solvents of analytical purity were supplied by commercial sources and used as received. Elemental analyses (C, H, and N) was performed on a Flash EA1112 microanalyzer. The FT-IR spectra were recorded in a Nicolet-360 FT-IR spectrometer as KBr pellets in the 4000–400 cm^{-1} region. ESI-MS was determined on Applied Biosystem (ABSCIEX-2000 Triple quad) spectrometer. The ^{1}H NMR spectra were recorded on Bruker Avance III HD (500MHz) spectrometer in $CDCl_3$-d_6 with Me_4Si (Tetramethylsilane) as the internal standard.

3.2. Synthetic Procedures

3.2.1. 1-(((4-nitrophenyl)imino)methyl)naphthalen-2-ol (SB1)

An ethanol (20 mL) solution of *p*-nitroaniline (1.381 g, 0.01 mol) was added dropwise to an ethanol (20 mL) solution of 2-hydroxynaphthaldehyde (1.721 g, 0.01 mol) with stirring. The reaction was carried out in the presence of a few drops of glacial acetic acid. Then, the reaction mixture was refluxed for 4 hours with vigorous stirring and subsequently

cooled to room temperature resulting in the formation of the microcrystalline product. The product was collected by vacuum filtration, washed with cold ethanol and diethyl ether, and dried in air (Scheme S1).Yield: (79%). Colour: Maroon, ^{1}H NMR ($CDCl_3$, 500MHz): δ = 7.14 (d,1H, Ar-H), 7.39 (t, 1H, Ar-H), 7.45- 8.36 (m, 8H, Ar-H), 9.41 (s,1H, CH=N), 14.89 (d, 1H, N-H).^{13}C NMR (DMSO-d_6, 75 MHz) δ(ppm):172.5 (C=N), 156.9 (C-N), 150.2 (C-O), 145.2, 138.8, 133.6, 129.6, 128.9, 127.3, 125.7, 124.5, 122.7, 121.6, 121.2, 109.6; FTIR (ν_{max}cm^{-1}): 1614.65, 2913.36, 3065.12, 1325.76, 1284.93, 1095.38, 956.26, 828.46 cm^{-1}; ESI-MS (positive ion mode): m/z 293.2 $[M+H]^+$, calculated 292.08;CHN analysis for $[C_{17}H_{12}N_2O_3]$ calculated: C, 69.86; H, 4.14; N, 9.58: Found: C, 69.79; H, 4.17; N; 9.53.

3.2.2. 1-(((2-aminophenyl)imino)methyl)naphthalen-2-ol (SB2)

The Schiff base (SB2) was synthesized by a similar procedure like that adopted for SB1but with a slight modification that o-phenylenediamine was used in place of p-nitroaniline. Yield: (85%). Colour: Orange,^{1}H NMR ($CDCl_3$, 500MHz): δ = 3.50 (2H, -NH_2), 7.16-8.14 (m, 10H, Ar-H), 9.45 (s,1H, CH=N), 15.05(d, 1H, N-H);^{13}C NMR (DMSO-d_6, 75 MHz) δ(ppm):169.0 (C=N), 157.8 (C-N), 138.9 (C-O), 137.2, 133.4, 129.4, 128.6, 127.8, 127.3, 124.1, 121.9, 121.1, 120.2, 109.7;FTIR (ν_{max}cm^{-1}): 1610.33, 2930.30, 3031.76, 3359.09, 1471.53, 1538.29, 1244.37 ESI-MS (positive ion mode): m/z 263.5 $[M+H]^+$, 264.9 $[M+2H]^+$, calculated 263.31 for $[M+H]^+$;CHN analysis for $[C_{17}H_{14}N_2O]$ calculated: C, 77.84; H, 5.38; N, 10.68; Found: C, 77.53; H, 4.98; N; 10.43.

3.2.3. 1-(((4-bromophenyl)imino)methyl)naphthalene-2-ol (SB3)

The Schiff base (SB3) was synthesized by a similar procedure like that adopted for SB1 but with a slight modification that p-bromoaniline was used in place of p-nitroaniline. Yield: (83%). Colour: Yellow; ^{1}H NMR ($CDCl_3$, 500MHz):δ = 7.12-8.13(m, 10H, Ar-H), 9.37 (s,1H, CH=N), 15.23 (d, 1H, N-H); ^{13}C NMR (DMSO-d_6, 75 MHz) δ(ppm):170.0 (C=N), 157.0 (C-N), 144.2 (C-O), 137.4, 133.5, 132.8, 129.4, 128.6, 127.2, 124.1, 123.3, 122.2, 120.9, 119.4, 109.1;FTIR (ν_{max}cm^{-1}): 1605.73, 3021.80, 1473.93, 1312.96, 663.02 ESI-MS (positive ion mode): m/z 327.9 $[M+2H]^+$, calculated 327.01;CHN analysis for $[C_{17}H_{12}BrNO]$ calculated: C, 62.60; H, 3.71; N, 4.29; Found: C, 62.59; H, 3.47; N; 4.33.

3.2.4. 1-(((4-fluorophenyl)imino)methyl)naphthalene-2-ol (SB4)

The Schiff base (SB4) was synthesized by a similar procedure like that adopted for SB1 but with a slight modification that p-fluoroaniline was used in place of p-nitroaniline. Yield: (81%); R_f = 0.25 (*n*-hexane–AcOEt 7:3); ^{1}H NMR ($CDCl_3$, 500MHz):δ(ppm): = 7.11-8.14 (m, 10H, Ar-H), 9.36 (s,1H, CH=N), 15.24 (d, 1H, N-H); ^{13}C NMR (DMSO-d_6, 75 MHz) δ(ppm): 169.0 (C=N), 162.3 (C-N), 159.9 (C-O), 157.2, 141.7, 136.9, 133.4, 128.4, 127.2, 123.9, 123.2, 123.1, 121.8, 120.9, 116.8, 109.1; FTIR (ν_{max}cm^{-1}): 1609.43, 3046.80, 1415.19, 1218.50, 1090.24 ESI-MS (positive ion mode): m/z 266.2 $[M+H]^+$, calculated 266.09;CHN analysis for $[C_{17}H_{12}FNO]$calculated: C, 76.97; H, 4.56; N, 5.28. Found: C, 76.88; H, 4.47; N; 5.31.

3.2.5. 6-amino-2-(((2-hydroxynaphthalene-1-yl)methylene-) amino)pyrimidine-4-ol(SB5)

The Schiff base (SB5) was synthesized by a similar procedure like that adopted for SB1 but with a slight modification that 2,6-diaminopyrimidine-4-ol was used in place of p-nitroaniline. Yield: (75%). Colour: Brown,^{1}H NMR ($CDCl_3$, 500MHz): δ = 5.09 (2H, -NH_2), 6.61-8.64(m, 7H, Ar-H), 9.57(s,1H, CH=N), 10.83 (s, 1H, -OH), 14.32 (d, 1H, N-H); ^{13}C NMR (DMSO-d_6, 75 MHz) δ(ppm): 169.2 (C=N), 160.3 (C-N), 158.5 (C-O), 157.0, 141.2, 136.7, 133.1, 128.5, 127.0, 123.4, 123.0, 122.9, 121.1, 120.4, 116.2, 109.2; FTIR (ν_{max}cm^{-1}): 1615.64, 3598.97, 3329.07, 3056.47, 1266.25 ESI-MS (positive ion mode): m/z 282.9 ($[M+H]^+$, calculated 282.10;CHN analysis for $[C_{15}H_{12}N_4O_2]$ calculated: C, 64.28; H, 4.32; N, 19.99; Found: C, 64.19; H, 4.55; N; 19.63.

3.2.6. 1-(((4-chlorophenyl)imino)methyl)naphthalene-2-ol (SB6)

The Schiff base (SB6) was synthesized by a similar procedure like that adopted for SB1 but with a slight modification that p-chloroaniline was used in place of p-nitroaniline. Yield: (82%). Colour: Yellow,^{1}H NMR ($CDCl_3$, 500MHz):δ = 7.12-8.13 (m, 10H, Ar-H), 9.36 (s,1H, CH=N), 15.30 (s, 1H, N-H); ^{13}C NMR (DMSO-d_6, 75 MHz) δ(ppm): 170.3 (C=N), 157.5 (C-O), 144.8 (C-S), 137.5, 133.4, 132.6, 129.5, 128.0, 127.1, 124.3, 123.5, 122.6, 120.8, 119.1, 109.4; FTIR (ν_{max}cm^{-1}): 1604.87, 3022.91, 1477.06, 1218.50, 1147.63, 817.59, 742.57 ESI-MS (positive ion mode): m/z 282.1$[M+H]^+$, calculated 282.10;CHN analysis for $[C_{17}H_{12}ClNO]$calculated: C, 72.47; H, 4.29; N, 4.97; Found: C, 72.43; H, 4.27; N; 4.65.

3.2.7. 4-(((2-hydroxynaphthalene-1-yl)methylene)amino)-benzenesulfonamide (SB7)

The Schiff base (SB7) was synthesized by a similar procedure like that adopted for SB1 but with a slight modification that sulphanilamide was used in place of p-nitroaniline. Yield: (79%). Colour: Yellow,^{1}H NMR ($CDCl_3$, 500MHz):δ = 2.09 (2H, -NH_2), 7.12-8.13 (m, 10H, Ar-H), 9.54 (s,1H, CH=N), 14.30 (d, 1H, N-H); ^{13}C NMR (DMSO-d_6, 75 MHz) δ(ppm): 169.8 (C=N azomethine), 165.3 (C=N, Ar), 164.5 (C=N, Ar), 157.3 (C-O), 144.8 (C-S), 137.5, 133.5, 132.8, 129.2, 128.2, 127.3, 124.5, 123.5, 122.4, 120.5, 109.8, 82.5;FTIR (ν_{max}cm^{-1}): 1621.31, 3734.54, 3282.45, 3013.84, 1346.49, 1136.18, 965.28, 898.53 ESI-MS (positive ion mode): m/z 327.3 ($[M+H]^+$, calculated 327.07);CHN analysis for $[C_{17}H_{14}N_2O_3S]$ calculated: C, 62.56; H, 4.32; N, 8.58; Found: C, 62.53; H, 4.27; N; 8.42.

3.3. Microbiological Analysis

3.3.1. Strains, Media and Chemicals

In this study, along with one laboratory strain (*Candida albicans* ATCC90028), three drug susceptibles (C178-1, C143-1, C193-1), three fluconazole resistants (A171, N21, CR34B) and three amphotericin B resistants (CR71A, CR73, CR79) clinical strains of *C. albicans* were used. Clinical *Candida* strains were isolated from either HIV positive pa-

tients or patients with other immunocompromised conditions that were attending clinics at the Charlotte Maxeke Johannesburg Academic Hospital, Johannesburg, South Africa. All the strains were grown and maintained on Sabouraud Dextrose (SD) Agar and prior to experiments, cells were grown in fresh SD broth. Ethical clearance was obtained from the Human Research Ethics Committee, University of the Witwatersrand. Fluconazole was purchased from Sigma Fluke (USA) and a stock solution of 2 mg/ml was prepared in sterile distilled water while as 250 µg/mL solution of amphotericin B (AmB) was purchased from Bristol-Myers Squibb (Pty) Ltd. All other chemicals and media were purchased from Sigma Aldrich and Merck.

3.3.2. Antifungal Activity

3.3.2.1. Minimum Inhibitory Concentrations

Minimum inhibitory concentrations (MIC) of all the newly synthesized Schiff base compounds against all the tested *C. albicans* were determined using the Clinical and Laboratory Standards Institute (CLSI) guidelines recommended broth microdilution method M27-A3 [40]. Briefly, a 96 well microtiter plate was prepared by adding 0.1 ml of fresh SD broth. To the first row, 0.1 ml of test compounds in varying concentrations (SB1 and SB2 = 6 mg/mL; SB3 and SB4 = 10 mg/mL; SB5 = 26 mg/mL; SB6 = 5 mg/ml; SB7 = 20 mg/mL) were added in triplicate and serially diluted. For comparison, positive controls (FLC and AmB = 2 mg/mL) were included along with a negative (1% DMSO), media and culture controls in every set of experiments. All the experiments were done in duplicate and all the results were expressed in µg/mL.

3.3.2.2. Combination Index

All the seven synthesized compounds were tested for combination interaction with FLC and AmB by determining the Fractional Inhibitory Concentration Index (FICI), following the method described previously [15]. In each combination set, test compounds and drugs were added into a well in 1:1 ratio. Interactions were assessed on the basis of zero-interaction theory of Loewe additivity and FICI values were calculated as follows:

$$\text{FICI} = \text{FICa} + \text{FICb} = \frac{\text{MICa in combination}}{\text{MICa tested alone}} + \frac{\text{MICb in combination}}{\text{MICb tested alone}}$$

Where MICa is the MIC of the Schiff base derivativesandMICbis the MIC of drug (FLC or AmB). Interpretations of FICI values were done as synergy when ≤0.5, additive between 0.5 and 1.0, indifferent between 1.0 and 4.0 and antagonistic when FICI values were >4.0 [41].

3.3.2.3. Isobologram Analysis

For graphical analysis of the synergistic interactions between the synthesised compounds and drugs in 1:1 ratios, nine different ratio combinations (9:1; 8:2; 7:3; 6:4; 5:5; 4:6; 3:7; 2:8; and 1:9) were done and for all the combinations MICs were determined. For all these combinations, isobolograms were constructed using GraphPad Prism version 5-software as described previously [15]. All the data points were assessed and interpreted as synergistic (below or on the 0.5:0.5 lines), or additive.

3.3.2.4. Sterol Quantification Assay

To determine the effect of the Schiff base derivatives on ergosterol biosynthesis, total intracellular sterols were quantified in one FLC susceptible and one FLC resistant *C. albicans* isolates. For extraction of total intracellular sterols in the control and treated *C. albicans* cells, alcoholic KOH method was employed as described previously [17]. Briefly, FLC susceptible *C. albicans*ATCC90028 and FLC resistant *C. albicans* A71 were grown in 50 ml of SDB with MIC and ½ MIC of all the seven Schiff base compounds and incubated for 18 h. After incubation, cells were harvested, weighed and treated with 25% alcoholic potassium hydroxide solution and incubated in an 85ºC water bath for 1h. Sterols were then extracted by the addition of distilled water and n-heptane by scanning the n-heptane layer spectrophotometrically between 230 and 300 nm using Shimadzu Lab Solution Spectrophotometer. In every set of experiment, an untreated negative control and 8 µg/mL of FLC treated positive control was included. The ergosterol content was calculated by the following equation:

% ergosterol + % 24(28) DHE = $[(A_{281.5}/290) \times F]$/pellet weight

% 24(28) DHE = $[(A_{230}/518) \times F]$/pellet weight

% ergosterol = [% ergosterol + % 24(28) DHE] − % 24(28) DHE

Where F is dilution factor and 290 and 518 are the E values (in percentages per centimetre) determined for crystalline ergosterol and 24(28) DHE, respectively. The experiment was performed in triplicate and results are represented as mean ± SD.

3.3.2.5. Docking

Homology modeling and active site prediction was done as reported by us previously **[**14, 15]. Docking of the active compound **SB5**, into the lanosterol 14a-demethylase (CYP51) modeled protein was done by using`Autodock vina [42]. The detailed procedure is given in the supporting information.

CONCLUSION

In this study, seven Schiff base compounds were synthesized and the bioassay results showed that these compounds possess moderate to high antifungal activity against drug susceptible and drug resistant *C. albicans* isolates. Compound **SB5** was the most potent antifungal compound with median MIC of 9-100 µg/mL. In addition, all these compounds showed synergistic, additive or indifferent combination interaction with FLC and AmB, resulting in 4-10-fold increase of antifungal activity. Varied ratio combinations showed that 5:4 of the tested compounds and drugs combination showed most potent synergy. The investigation of the mechanism of antifungal action by sterol quantification and molecular docking studies indicated that these com-

pounds target ergosterol biosynthesis pathway by interacting with important amino acid residues of cytochrome P450 lanosterol 14α-demethylase. Structure-activity relationship studies showed that the presence of substituted pyrimidine ring on the azomethine nitrogen drastically enhances its antifungal potential compared to the non-pyrimidine analogues. The structure of the active compound could be further optimized by installing different electron withdrawing and electron releasing substituents on the pyrimidine ring or another possibility is to replace the pyrimidine ring with other heteroaromatic rings to get the most suitable molecule for further *in vivo* studies, which could provide an alternative clinical application to treat drug resistant fungal species.

ETHICS APPROVAL AND CONSENT TO PARTICIPATE

This study was approved by the Human Research Ethics Committee of University of the Witwatersrand (Johannesburg, South Africa). *Candida albicans* used in this study were isolated from patients under the ethical clearance number M10102.

HUMAN AND ANIMAL RIGHTS

No Animals were used for studies that are base of this research. All humans research procedures were followed in strict accordance with the World Medical Association's "Declaration of Helsinki" as a statement of ethical principles (18th WMA General Assembly, Helsinki, Finland, June 1964).

CONSENT FOR PUBLICATION

All participants were provided written informed consent before participation.

AVAILABILITY OF DATA AND MATERIALS

Not applicable.

FUNDING

MAM is thankful to the University Grants Commission (UGC), Government of India for financial support through central university doctoral fellowship.

CONFLICT OF INTEREST

The authors declare no conflict of interest, financial or otherwise.

ACKNOWLEDGEMENTS

Declared none.

SUPPLEMENTARY DATA

Supplementary data associated with this article can be found in the online version.

REFERENCES

[1] Lindahl, J.F.; Grace, D. The consequences of human actions on risks for infectious diseases: A review. *Infect. Ecol. Epidemiol.*, **2015**, *5*(1), 30048.

[2] Zowalaty, M.E.; Ibrahim, N.A.; Salama, M., Shameli, K.; Usman, M.; Zainuddin, N. Synthesis, characterization, and antimicrobial properties of copper nanoparticles. *Int. J. Nanomedicine*, **2013**, *8*, 4467-4479.

[3] Devi, J.; Devi, S.; Kumar, A. Synthesis, antibacterial evaluation and QSAR analysis of Schiff base complexes derived from [2,2′-(ethylenedioxy)bis(ethylamine)] and aromatic aldehydes. *Med. Chem. Commun.*, **2016,** *7*(5), 932-947.

[4] Perlin, D.S.; Shor, E.; Zhao, Y. Update on antifungal drug resistance. *Curr. Clin. Microbiol. Rep.*, **2015**, *2*(2), 84-95.

[5] Shapiro, R.S.; Robbins, N.; Cowen, L.E. Regulatory circuitry governing fungal development, drug resistance, and disease. *Microbiol. Mol. Biol. Rev.*, **2011**, *75*(2), 213-267.

[6] Ahmad, A.; Wani, M.Y.; Patel, M.; Sobral, A.; Duse, A.; Aqlan, F.; Al-Bogami, A. Synergistic antifungal effect of cyclized chalcone derivatives and fluconazole against *Candida albicans*. *Med. Chem. Commun.*, **2017**, *8*(12), 2195-2207.

[7] Sanglard, D. Emerging threats in antifungal-resistant fungal pathogens. *Front. Med.*, **2016**, *3*(11), 1-10.

[8] Belanger, E.S.; Yang, E.; Forrest, G.N. Combination antifungal therapy: When, where, and why. *Curr. Clin. Microbiol. Rep.*, **2015**, *2*(2), 67-75.

[9] Carrillo-Muñoz, A.J.; Finquelievich, J.; Tur-Tur, C.; Eraso, E.; Jauregizar, N.; Quindós, G.; Giusiano, G. Combination antifungal therapy: A strategy for the management of invasive fungal infections. *Rev. Esp. Quimioter.*, **2014**, *27*(3), 141-158.

[10] Mukherjee, P.K.; Sheehan, D.J.; Hitchcock, C.A.; Ghannoum, M.A. Combination treatment of invasive fungal infections. *Clin. Microbiol. Rev.,* **2005**, *18*(1), 163-194.

[11] Spitzer, M.; Robbins, N.; Wright, G.D. Combinatorial strategies for combating invasive fungal infections. *Virulence,* **2017**, *8*(2), 169-185.

[12] Hatipoglu, N.; Hatipoglu, H. Combination antifungal therapy for invasive fungal infections in children and adults. *Expert. Rev. Anti. Infect. Ther.,* **2013**, *11*(5), 523-535.

[13] Wani, M.Y.; Ahmad, A.; Kumar, S.; Sobral, A.J. Flucytosine analogues obtained through Biginelli reaction as efficient combinative antifungal agents. *Microb. Pathog.,* **2017**, *9*(105), 57-62.

[14] Wani, M.Y.; Ahmad, A.; Shiekh, R.A.; Al-Ghamdi, K.J.; Sobral, A.J. Imidazole clubbed 1,3,4-oxadiazole derivatives as potential antifungal agents. *Bioorg. Med. Chem.,* **2015**, *23*(15), 4172-4180.

[15] Ahmad, A.; Wani, M.Y.; Khan, A.; Manzoor, N.; Molepo, J. Synergistic interactions of Eugenol-tosylate and its congeners with fluconazole against *Candida albicans*. *PLoS One,* **2015**, *10*(12), e0145053.

[16] Wani, M.Y.; Ahmad, A.; Malik, M.A.; Sobral, A.J. Mononuclear transition metal complexes containing iodo-imidazole ring endowed with potential anti-*Candida*activity. *Med. Chem. Res.,* **2016**, *25*(11), 2557-2566.

[17] Ahmad, A.; Khan, A.; Manzoor, N.; Khan, L.A. Evolution of ergosterol biosynthesis inhibitors as fungicidal against *Candida*. *Microb. Pathog*., **2010**, *48*(1), 35-41.

[18] Hameed, A.; Al-Rashida, M.; Uroos, M.; Abid Ali S.; Khan, K.M. Schiff bases in medicinal chemistry: A patent review (2010-2015). *Expert Opin. Ther. Pat.,* **2017**, *27*(1), 63-79.

[19] Lam, P.L.; Lee, K.K.H.; Kok, S.H.L.; Gambari, R.; Lam, K.H.; Ho, C.L.; Ma, X.; Lo, Y.H.; Wong, W.Y., Dong, Q.C.; Bian, Z.X.; Chui, C.H. Antifungal study of substituted 4-pyridylmethylene-4′-aniline Schiff bases. *RSC Adv.*, **2016**, *6*(106), 104575-104581.

[20] Malik, M.A.; Dar, O.A.; Gull, P.; Wani, M.Y.; Hashmi, A.A. Heterocyclic Schiff base transition metal complexes in antimicrobial and anticancer chemotherapy. *Medchemcomm,* **2018**, *9*, 409-436.

[21] Kajal, A.; Bala, S.; Kamboj, S.; Sharma, N.; Saini, V.; Schiff Bases: A versatile pharmacophore. *J. Catal.*, **2013**, *2013,* 1-14.

[22] Petrović, Z.D.; Đorović, J.; Simijonović, D.; Petrović V.P.; Marković, Z. Experimental and theoretical study of antioxidative properties of some salicylaldehyde and vanillic Schiff bases. *RSC Adv.*, **2015**, *5*(31), 24094-24100.

[23] El-Gamel, N.E.A. Coordination behaviour and biopotency of metal *NN*salen complexes**.** *RSC Adv.*, **2012**, *2*(13), 5870-5876.

[24] Da Silva, C.M.; da Silva, D.L.; Modolo, L.V.; Alves, R.B.; de Resende, M.A.; Martins, C.V.B.; de Fátima, Â. Schiff bases: A short review of their antimicrobial activities. *J. Adv. Res.*, **2011**, *2*(1), 1-8.

[25] Sztanke, K.; Maziarka, A.; Osinka A.; Sztanke, M. An insight into synthetic Schiff bases revealing antiproliferative activities *in vitro*. *Bioorg. Med. Chem.*, **2013**, *21*(13), 3648-3666.

[26] Dong, Y.W.; Fan, R.Q.; Wang, P.; Wei, L.G.; Wang, X.M.; Zhang, H.J.; Gao, S.; Yang, Y.L.; Wang, Y.L. Synthesis and characterization of substituted Schiff-base ligands and their d^{10} metal complexes: structure-induced luminescence tuning behaviors and applications in co-sensitized solar cells. *Dalt. Trans.*, **2015**, *44*, 5306-5322.

[27] Chen, W.; Ou, W.; Wang, L.; Hao, Y.; Cheng, J.; Li, J.; Liu, Y.N. Synthesis and biological evaluation of hydroxyl-substituted Schiff-bases containing ferrocenyl moieties. *Dalt. Trans.*, **2013**, *42*, 15678-15686.

[28] Yao, Y.H.; Li, J.; Yuan, L.F.; Zhang, Z.Q.; Zhang, F.X. Novel porphyrin-Schiff base conjugates: Synthesis, characterization and *in vitro* photodynamic activities. *RSC Adv.*, **2016**, *6*(51), 45681-45688.

[29] Al-Amiery, A.A.; Al-Majedy, Y.K.; Ibrahim, H.H.; Al-Tamimi, A.A. Antioxidant, antimicrobial, and theoretical studies of the thiosemicarbazone derivative Schiff base 2-(2-imino-1-methylimidazolidin-4-ylidene) hydrazinecarbothioamide (IMHC). *Org. Med. Chem. Lett.*, **2012**, *2*(1), 4.

[30] Nath, M.; Saini, P.K. Chemistry and applications of organotin(IV) complexes of Schiff bases. *Dalt. Trans.*, **2011**, *40*(27), 7077-7121.

[31] Li, X.; Houb, Y.; Yuec, L.; Liua, S.; Duc, J.; Sund, S. Potential targets for antifungal drug discovery based on growth and virulence in *Candida albicans*. *Antimicrob. Agents Chemother.,* **2015**, *59*(10), 5885-5891.

[32] Mahmoud, A.G.; Louis, B.R. Antifungal agents: Mode of action, mechanisms of resistance, and correlation of these mechanisms with bacterial resistance. *Clin. Microbiol. Rev.,* **1999**, *12*(4), 501-517.

[33] Wong, S.S.W.; Samaranayake, L.P.; Seneviratne, C.J. In pursuit of the ideal antifungal agent for Candida infections: High-throughput screening of small molecules. *Drug Discov. Today,* **2014**, *19*(11), 1721-1730.

[34] Gomathi, G.; Srinivasan, T.; Velmurugan, D.; Gopalakrishnan, R. A bluish-green emitting organic compound methyl 3-[(*E*)-(2-hydroxy-1-naphthyl) methylidene] carbazate: Spectroscopic, thermal, fluorescence, antimicrobial and molecular docking studies. *RSC Adv.*, **2015***, 5*(56), 44742-44748.

[35] Lian, W.J.; Wang, X.T.; Xie, C.Z.; Tian, H.; Song, X.Q.; Pan, H.T.; Qiao, X.; Xu, J.Y. Mixed-ligand copper(II) Schiff base complexes: The role of the co-ligand in DNA binding, DNA cleavage, protein binding and cytotoxicity. *Dalt. Trans.*, **2016**, *45*(22), 9073-9087.

[36] Martínez, R.F.; Ávalos, M.; Babiano, R.; Cintas, P.; Jiménez, J.L.; Light, M.E.; Palacios, J.C. Tautomerism in Schiff bases. The cases of 2-hydroxy-1-naphthaldehyde and 1-hydroxy-2-naphthaldehyde investigated in solution and the solid state. *Org. Biomol. Chem.*, **2011**, *9*(24), 8268-8275.

[37] Carreño, A.; Gacitúa, M.; Páez-Hernández, D.; Polanco, R.; Preite, M.; Fuentes, J.A.; Mora, G.C.; Chávez, I.; Arratia-Pérez, R. Spectral, theoretical characterization and antifungal properties of two phenol derivative Schiff bases with an intramolecular hydrogen bond. *New J. Chem.*, **2015**, *39*(10), 7822-7831.

[38] Sun, W.; Weingarten, R.A.; Xu, M.; Southall, N.; Dai, S.; Shinn, P.; Sanderson, P.E.; Williamson, P.R.; Frank, K.M.; Zheng, W. Rapid antimicrobial susceptibility test for identification of new therapeutics and drug combinations against multidrug-resistant bacteria. *Emerg. Microbes Infect.,* **2016**, *5*(11), e116.

[39] Capobianco, J.O.; Doran, C.C.; Goldman, R.C.; De, B. A non-azole inhibitor of lanosterol l4α-methy1 demethylase in *Candida albicans*. *J. Antimicrob. Chemother.,* **1992**, *30*, 781-90.

[40] CLSI - Clinical and Laboratory Standards Institute Reference method for broth dilution antifungal susceptibility testing of yeast, Approved Standard M27-A3, Clinical and Laboratory Standards Institute Standards, Wayne, PA, USA, **2008**, 40.

[41] Vuuren, S.V.; Viljoen, A. Plant-based antimicrobial studies-methods and approaches to study the interaction between natural products. *Planta Med.,* **2011**, *77*(11), 1168-1182.

[42] Trott, O.; Olson, A. J. Software news and update AutoDock Vina: Improving the speed and accuracy of docking with a new scoring function, efficient optimization, and multithreading. *J. Comput. Chem*., **2010**, *31*(2) 455-461.

Appendix 2: Ethics clearance

This study was approved by the Human Research Ethics committee of University of the Witwatersrand, Johannesburg, South Africa, and performed according to the guidelines outlined in the Helsinki Declaration. Existing stock cultures of *Candida albicans* used in this study were stored in the Department of Clinical Microbiology and Infectious Diseases, University of the Witwatersrand.

UNIVERSITY OF THE WITWATERSRAND, JOHANNESBURG	HUMAN RESEARCH ETHICS COMMITTEE (MEDICAL)

Office of the Deputy Vice-Chancellor (Research & Post Graduate Affairs)

TO: Mr SA Lone
School: Pathology
Department: Clinical Microbiology & Infectious Diseases
National Health Laboratory Service

E-mail: 1311748@students.wits.ac.za

CC: Supervisor: Ahmad A Dr <Aijaz.Ahmad@wits.ac.za>
and <HREC-Medical.ResearchOffice@wits.ac.za>

FROM: Iain Burns
Human Research Ethics Committee (Medical)
Tel: 011 717 1252

E-mail: Iain.Burns@wits.ac.za

DATE: 30/10/2019

REF: *R14/49*

PROTOCOL NO: W-CBP-191030-01 (This is your ethics application study reference number. Please quote this reference number in all correspondence relating to this study)

PROJECT TITLE: *Modulation of cell death and pathogenicity by eugenol tosylate congeners in Candida albicans (formerly W-CJ-170621-1)*

Please find attached the Ethics Waiver Certificate for the above project. I hope it goes well and that an article in a recognized publication comes out of it. This will reflect well on your professional standing and contribute to the Government funding of the University.

MSWorks2000/Iain0007/ClearScanWaiver.wps

UNIVERSITY OF THE
WITWATERSRAND,
JOHANNESBURG

HUMAN RESEARCH ETHICS COMMITTEE (MEDICAL)

30/10/2019

Ref: W-CBP-191030-01

TO WHOM IT MAY CONCERN:

Waiver: This certifies that the following research does not require clearance from the Human Research Ethics Committee (Medical).

Investigator: Mr SA Lone
Student No. (if appropriate): 1311748
Staff No. (if appropriate):

Supervisor: Ahmad A Dr

School: Pathology
Department: Clinical Microbiology & Infectious Diseases
National Health Laboratory Service

Project title: *Modulation of cell death and pathogenicity by eugenol tosylate congeners in Candida albicans (formerly W-CJ-170621-1)*

Reason: In vitro laboratory study.
No human participants will be involved in the study.

Dr CB Penny
Chairperson: Human Research Ethics Committee (Medical)

Research Office Secretariat:
Physical address: Phillip Tobias Building, 3rd Floor, Office 302, Corner York Road and Princess of Wales Terrace, Parktown, Johannesburg 2193.
Postal address: Private Bag 3, Wits 2050
Tel Nos. +27 (0)11-717-1234/2656/2700/1252
Office E-mail: HREC-Medical.ResearchOffice@wits.ac.za.
Website:http://www.wits.ac.za/research/about-our-research/ethics-and-research-integrity/